CONTRIBUTIONS OF HIPPOCAMPCAL AREA CA2 TO HIPPOCAMPAL OSCILLATORY NETWORKS

Logan Y. Brown

A dissertation submitted to the faculty at the University of North Carolina at Chapel Hill in partial fulfillment of the requirements for the degree of Doctor of Philosophy in the Neuroscience Curriculum.

Chapel Hill
2018

Approved by:

Paul B. Manis

Flavio Frohlich

Garret D. Stuber

Georgia M. Alexander

Serena M. Dudek

ABSTRACT

Logan Y. Brown: Contributions of Hippocampal Area CA2 to Hippocampal Oscillatory Networks
(Under the direction of Serena M. Dudek)

Complex cognitive abilities, such as memory, require synchronized neural activity across large populations of cells. The hippocampus is a region of the brain required for the formation of long term episodic memories, which is our memory for autobiographical information. The hippocampus itself consists of four sub-regions, the dentate gyrus (DG), CA1, CA2, and CA3, which can be viewed as functionally specialized processing hubs that uniquely contribute to memory formation based on their distinct molecular, synaptic, and anatomical properties. Only together; however, does the collective activity of all four sub-regions provide the neurobiological underpinnings necessary for a functional memory system.

One mechanism for the coordination of neural networks is synchronization through oscillations. Neuronal oscillations reflect waves of synchronous action potentials and their presence in the hippocampus is strongly associated with episodic learning and memory. Although much progress been made towards understanding how different frequencies of activity are generated and how they support hippocampal-based memory, relatively little is known about the role of CA2 in organizing oscillations. In this dissertation work, I use combinatorial electrophysiological and chemogenetic approaches to genetically target and manipulate CA2 principal cells to investigate their role in coordinating hippocampal oscillatory networks in awake, behaving mice.

In Chapter 2, I use Designer Receptors Exclusively Activated by Designer Drugs (DREADDs) to manipulate the endogenous G protein-coupled receptor (GPCR) signaling pathways in CA2 while animals explore a novel spatial environment. These experiments revealed that activation or inhibition of CA2 pyramidal cells through the endogenous Gq- and Gi-coupled pathways, respectively, is sufficient to bi-directionally modulate synchronized hippocampal activity in the slow gamma and beta frequency ranges.

In Chapter 3, I further dissect the role of CA2 in coordinating hippocampal oscillations by inhibiting CA2 pyramidal cells while animals investigate novel social stimuli and record from CA2's

primary output region, CA1. These experiments revealed that the oscillatory structure observed in CA1 is organized in a layer- and frequency-specific manner that depends causally on CA2 output. These findings provide evidence that CA2 is an integral processing node capable of coordinating the hippocampal oscillatory networks that support long term episodic memory.

ACKNOWLEDGEMENTS

First, I would like to thank the University of North Carolina at Chapel Hill and the Curriculum in Neuroscience for providing me with an outstanding environment for my graduate studies. Many faculty were involved with, and contributed to, my progress as a graduate student and I am eternally grateful for the support provided.

I would especially like to thank my academic advisor, Dr. Serena Dudek, for all her guidance and support throughout my dissertation work. It has been an incredible journey and I am deeply grateful for her mentorship. I would also like to thank all the current, and former, members of the Dudek lab for their support, training, and wealth of expertise. I am especially grateful for the mentorship and oversight of Dr. Georgia Alexander, whom without, none of the work presented here would have been possible. Beyond the Dudek Lab, I would also like to thank Dr.'s Flavio Frohlich and Paul Manis who have both served as invaluable resources throughout my graduate studies. I am both honored and humbled to have had the privilege to work with so many brilliant, talented, and dedicated scientists.

The ways our earliest mentors and teachers shape our lives cannot be overstated and I have been truly privileged to have had several exceptional mentors throughout my academic career. Dr.'s William McDaniel and Larry Lynch were both pivotal in my trajectory towards a doctoral degree and, more importantly, for inspiring in me a life-long curiosity and love of philosophy and science.

Finally, I would like to thank my family and friends for their unwavering love and support throughout all stages of my life. I surely would not have been able to overcome the many obstacles and challenges I faced over the last six years without their constant encouragement and belief in my ability to succeed. I am immeasurably grateful for the support of my mother and my father and their consistent belief that it would (one day) come to an end. Their wisdom has enriched my world and instilled in me the resilience and perseverance that were paramount to my success in this stage of life. My victory here reflects a culmination of effort by all of these people and many more. I thank you all.

TABLE OF CONTENTS

LIST OF FIGURES

LIST OF ABBREVIATIONS

AAV	Adeno-Associated Virus
ANOVA	Analysis of Variance
AMIGO2	Adhesion Molecule with Ig-like Domain 2
AVPR1B	Vasopressin 1B Receptor
BAC	Bacterial Artificial Chromosome
BGH-F	Bovine Growth Hormone-Forward primer
BP	Base Pairs
CA1	Cornu Ammonis 1
CA2	Cornu Ammonis 2
CA3	Cornu Ammonis 3
CNO	Clozapine-N-Oxide
DG	Dentate Gyrus
DIO	Doubled-floxed Inverted Open read
DREADD	Designer Receptors Exclusively Activated by Designer Drugs
EGFP	Enhanced Green Fluorescent Protein
ER	Estrogen Receptor
GABA	Gamma Amino Butyric Acid
GAD	Glutamate Decarboxylase
GIRK	G-protein Inward Rectifying potassium channel
GPCR	G-protein Coupled Receptor
HM3Dq	Human Muscarinic 3 DREADD-Gq receptor
HM4Di	Human Muscarinic 4 DREADD-Gi receptor
HSYN	Human-Synapsin
ICREERT2	Inducible Cre-Estrogen Receptor- Tamoxifen-inducible 2
IP	Intra-Peritoneal
IPSP	Inhibitory Post-Synaptic Potential
LFP	Local Field Potential

LTP	Long Term Potentiation
PBS	Phosphate Buffer Solution
PCR	Polymerase Chain Reaction
PLC	Phospholipase C
PSD	Power Spectral Density
PSP	Post-Synaptic Potential
SQ	Subcutaneous

CHAPTER 1. INTRODUCTION

1.1 The Hippocampus as an Episodic Memory Platform

In humans, the hippocampus serves as one part of an extended memory system residing in the medial temporal lobe of the brain. This distributed system encompasses several distinct regions including the hippocampus proper, the subiculum, and the entorhinal, perirhinal, and parahippocampal cortices (Anderson, 2007). The medial temporal lobe system is required for the encoding and consolidation of long term memories that take the form of facts and events, otherwise known as explicit or declarative memory (Squire, 1992). Explicit memory is one of two types of long-term memory in humans and refers to the conscious, intentional recollection of information, previous experiences, and concepts (Squire, 2004). Explicit memory can be further divided into two categories: episodic memory, which is our records for personal experiences, and semantic memory, which is our memory for factual information.

Episodic memory refers to our ability to recall autobiographical events and includes the times and places at which events occur, as well as other contextual information that can come to be associated with an event, such as who or what was present at a particular time and place (Tulving, 1984). In contrast, semantic memory refers to general world knowledge that we have accumulated throughout our lives that can be explicitly stated as facts (Squire, 1992). For example, semantic memory might contain information about what a cat is, whereas episodic memory might contain a specific memory of petting a particular cat. Episodic memory is strongly associated with the hippocampus proper, while semantic memory is thought to rely on the more extended hippocampal system located throughout the medial temporal lobe. Perhaps the most striking piece of evidence in support of the hippocampus's role in episodic memory comes from studies of the, now famous, neurological patient Henry Molaison, or H.M. for short. H.M. underwent bilateral resection of his hippocampi in an attempt to treat intractable epilepsy, but an unanticipated side effect of the surgery was that H.M. was left with severe anterograde, and partial retrograde, amnesia (Scoville & Milner, 1957). H.M. was unable to form new episodic memories for the rest of his life; however, he did retain memories for most of the events that occurred prior to the surgery. Decades of

research with patient H.M., and other clinical cases like his, have cemented the idea that the hippocampus is critical for episodic memory. At the same time, scientists have been utilizing molecular and electrophysiological tools in animal models to probe the biological mechanisms underlying episodic memory.

Much evidence for the spatial component of episodic memory comes from the discovery of place cells by O'Keefe and Dostrovsky in 1971 when they observed neurons in the rat hippocampus that selectively increased firing within a well-defined region of the animal's environment (O'Keefe & Dostrovsky, 1971). Almost fifty years later, the precise firing and spatial tuning properties of place cells have been extensively explored in a myriad of contexts and environments (Alexander et al., 2016; Lu, Igarashi, Witter, Moser, & Moser, 2015; Muller & Kubie, 1987; O'Keefe, Burgess, Donnett, Jeffery, & Maguire, 1998; D. M. Smith & Mizumori, 2006), leading to consensus that these cells, along with a few other classes of spatially selective cells, are responsible for generating the brain's spatial representations of its environment. Between human clinical studies and work in animal models, these two disparate lines of inquiry into the nature of hippocampal function have led to considerable debate over whether the primary function of the rodent hippocampus is spatial cognition or a more general episodic memory platform, as is the case in humans (Eichenbaum, Dudchenko, Wood, Shapiro, & Tanila, 1999; O'Keefe, 1999; Redish, 2001). Much recent work has focused on trying to bridge the disconnect between these two views, and consensus for the rodent hippocampus as a more general memory system incorporating both spatial and other episodic elements has grown in recent years (Eichenbaum & Cohen, 2014). Here, we present evidence in support of the view of the rodent hippocampus as a more general episodic memory platform capable of storing information about a variety of environmental stimuli, rather than one exclusively reserved for spatial representations.

1.2 Anatomical Characterization of the Rodent Hippocampus

The organization of the hippocampus is highly conserved across mammalian species (Strange, Witter, Lein, & Moser, 2014) and much of our knowledge about the organization and connectivity of circuits within the hippocampus comes from the pioneering work of early twentieth century neuroanatomists Ramon y Cajal and Lorente de No. As originally delineated by Lorente de No in 1934, the hippocampus contains four primary sub-regions: the dentate gyrus (DG) and cornu ammonis (CA)

fields one through three (CA1, CA2, and CA3) (Lorente de No, 1934) (**Figure 1.1**). Although there exist many hippocampal circuits, Ramon y Cajal established early on that the fields of the hippocampal formation are linked by a sequence of unique, and largely unidirectional, connections when he first described one important relay of synaptic transmission through the hippocampus, the tri-synaptic loop (Anderson, 2007). Later work by Andersen and colleagues provided an important extension of these early studies by proposing that the hippocampus is organized in parallel "lamellae," or small strips (Andersen, Bliss, & Skrede, 1971). The lamellar hypothesis of hippocampal function posited that excitatory activity travels from the entorhinal cortex, and through the hippocampus, within a series of parallel hippocampal "slices" or "lamellae". In this way, the temporal lobe interactions between the entorhinal cortex and the hippocampus were thought to be organized topographically, with different lamellae operating independently. Although later work by Amaral and colleagues ultimately found the lamellae hypothesis to be an incomplete description of hippocampal connectivity based on the observation that excitatory collaterals originating from CA3 dispersed over a much wider region than originally proposed (Amaral & Witter, 1989; Ishizuka, Weber, & Amaral, 1990), the lamellar hypothesis of the hippocampus's anatomical organization has had tremendous influence on the conceptualization of information processing in the hippocampus, and research today is still aimed at understanding how layer-specific interactions among subfields contribute to memory formation and retrieval.

The hippocampus is characterized by three to five strata depending on the region, but all CA fields exhibit the four following layers: stratum lacunosum-moleculare, radiatum, pyramidal, and oriens, while the CA3 and CA2 subfields also contain one additional layer known as the stratum lucidum (**Figure 1.1**). The principal cells of the CA fields are pyramidal cells, which are long-range, excitatory cells that interconnect the hippocampal subfields, as well as extend to extra-hippocampal targets, where they release glutamate. The somata of pyramidal cells are located in the pyramidal cell layer and possess apical dendrites that extend into the stratum radiatum and lacunosume-moleculare, and basal dendrites that extend into stratum oriens (Garcia-Lopez, Garcia-Marin, & Freire, 2006). These dendrite containing layers serve as the main input zone for excitatory synapses from upstream pyramidal cells. Pyramidal cells, in turn, send their axons to a diffuse range of intra- and extra-hippocampal targets depending on the subfield. In addition to the pyramidal cells, the hippocampus is also populated by an extensive and

diverse array of interneurons that primarily target local pyramidal cells, where they exert inhibition that contributes to the timing and organization of hippocampal activity (Klausberger & Somogyi, 2008).

Three major fiber systems are associated with input into and out of the hippocampus. The first is the angular bundle, which primarily carries fibers between the entorhinal cortex (EC) and the hippocampal fields (Anderson, 2007). The EC is a specialized region of cortex that serves as the primary interface between the hippocampus and the associational cortices of the neocortex (van Groen, Miettinen, & Kadish, 2003). The second is the fimbria-fornix pathway, through which the hippocampus is connected with the basal forebrain, hypothalamic, and brain stem regions. The third compromises the dorsal and ventral commissures, which connect the two hippocampi in each cerebral hemisphere. Here we will focus on a subset of pathways within the angular bundle, as this is main route taken by entorhinal cortex fibers projecting to the hippocampus, a key structure for the organization of hippocampal oscillations.

Although there exist many hippocampal circuits, the historically most studied pathway is the tri-synaptic loop. The tri-synaptic loop is one important relay of synaptic transmission residing within the angular bundle and begins with axons originating in EC layers II and III that terminate primarily in the DG, but to a lesser extent, also in CA3, CA2, and CA1 (Kohara et al., 2014; van Groen et al., 2003). On their way to the DG, EC axons traverse, or perforate, the subiculum and are thus referred to as the perforant path. The perforant path is the primary source of excitatory innervation for the hippocampus, and it is the first synaptic connection in the tri-synaptic loop. The principal cells of the DG, granule cells, in turn send their axons to the apical dendrites of CA3 pyramidal cells in stratum lucidum, a projection known as the mossy fiber pathway, which is the second synaptic connection in the tri-synaptic loop. From there, CA3 axons project to CA1, referred to as the Schaffer collaterals, which are the third and final synapse in the loop. Although the tri-synaptic loop has historically received the most attention within the hippocampal literature, many other hippocampal pathways exist. Despite being completely omitted from the classic loop, the CA2 subfield is deeply embedded within the hippocampus and participates in several unique circuits there. Beyond its connections with the neocortex, the fimbria-fornix fiber system provides the major conduit for subcortical afferent and efferent connections with the hippocampus. The hippocampus is interconnected with several regions via the fimbria-fornix including thalamic nuclei, septal nuclei, the supramamillary nucleus, raphe nuclei, and the locus coeruleus, among others (Anderson, 2007).

1.3 CA2- A Distinct Hippocampal Region

Episodic information is encoded and consolidated in the hippocampus through several parallel circuits and hippocampal area CA2 has become increasingly appreciated as a distinct region based on several unique synaptic (Chevaleyre & Siegelbaum, 2010; Zhao, Choi, Obrietan, & Dudek, 2007), molecular (Lein, Callaway, Albright, & Gage, 2005), and anatomical (Kohara et al., 2014) properties that suggest specific roles for CA2 hippocampal function. Previously believed to serve as a mere transition region between the CA3 and CA1 subfields, CA2 has now been shown to participate in several unique hippocampal circuits, receiving direct excitatory input from ECII and CA3 (Kohara et al., 2014), and from several subcortical nuclei, including the supramammillary and paraventricular nuclei (PVN) of the hypothalamus, as well as the medial septum and diagonal band of broca (Cui, Gerfen, & Young, 2013). In turn, CA2 axons primarily target the basal dendrites of ipsilateral CA1 located in stratum oriens, where its terminals account for approximately 20% of synapses, but also send a minor projection to CA1 dendrites in stratum radiatum, as well as recursive input onto itself (Lorente de No, 1934; Tamamaki, Abe, & Nojyo, 1988), and back-projections to CA3 (Shinohara et al., 2012; Tamamaki et al., 1988).

The hippocampus supports a cognitive map of space and in the rodent, the hippocampus is strongly associated with the spatial aspects of episodic memory due in large part to the presence of place cells, which are hippocampal pyramidal cells that selectively increase their firing rate within a well-defined region of the animal's environment. Only a subset of the place cells fire in any given environment; however, and when the animal is moved to a different environment, place cells undergo remapping (Muller & Kubie, 1987), enabling the hippocampus to form distinguishable representations of large numbers of experiences in a large number of environments, even when events take place at the same spatial coordinates (Lu et al., 2015). Place cells also encode and store non-spatial forms of information (Aronov, Nevers, & Tank, 2017; Eichenbaum, 2018); however, and although all hippocampal subfields exhibit place cells, CA2 place cells appear to be the least spatially tuned pyramidal cells (Lu et al., 2015; Mankin, Diehl, Sparks, Leutgeb, & Leutgeb, 2015), suggesting a shift to other cognitive processes. Interestingly, CA2 place fields remap upon exposure to novel or familiar conspecific animals while CA1 place fields do not (Alexander et al., 2016), and several lines of evidence now indicate that CA2 is uniquely situated to respond to environmental cues containing socially relevant information. These effects

may be mediated in part by vasopressinergic signaling, a peptide neurotransmitter derived from PVN neurons of the hypothalamus. The idea that vasopressin may be involved in the formation of memories containing socially relevant information is consistent with the fact that this neurotransmitter is involved in the regulation of social behaviors in many mammalian species (Insel, 2010).

In the rodent hippocampus, CA2 pyramidal cells exhibit a selective enrichment of mRNA for the vasopressin 1b receptor subtype (Avpr1b) (Young, Li, Wersinger, & Palkovits, 2006). Synaptic plasticity at the CA3 → CA2 Schaffer collateral synapses is also uniquely regulated relative to the CA3→ CA1 Schaffer collateral synapses, in that the CA2 synapses do not readily undergo high frequency stimulation-induced potentiation (Pagani et al., 2015). The ability of neurons to alter the strength of their synaptic connections has served as a candidate mechanism for a molecular correlate of memory storage (Bliss & Collingridge, 1993) since the discovery of long-term potentiation (LTP) in the early 1970's (Bliss & Lomo, 1973), which is one long lasting form of synaptic plasticity. Synaptic potentiation can be revealed at the CA3→CA2 synapses; however, with the use of certain neuromodulators, including an agonist for the Avpr1b subtype (Pagani et al., 2015). Of note, the Avpr1b is also coupled to the endogenous Gq-signaling pathway which we selectively target and manipulate in CA2 pyramidal cells in subsequently presented experiments, suggesting a link between vasopressin and our results demonstrating CA2's role in coordinating synchronous hippocampal activity. In addition to the molecular and synaptic evidence indicating a role for CA2 in social memory, several studies have genetically targeted and manipulated Avpr1b expressing cells in CA2 and measured changes in behavior. Genetic deletion of the Avpr1b impairs a variety of social behaviors while leaving other hippocampal dependent behaviors intact (Caldwell, Wersinger, & Young, 2008; Stevenson & Caldwell, 2012), and optogenetic stimulation of the vasopressin-containing axon fibers in CA2 can extend the duration of social memory (A. S. Smith, Williams Avram, Cymerblit-Sabba, Song, & Young, 2016). Additionally, Hitti and Siegelbaum showed that CA2 activity is required for intact social recognition memory by using a tetanus toxin light chain construct to permanently silence CA2 output which abolished memory for conspecifics while leaving other hippocampal dependent memories intact (Hitti & Siegelbaum, 2014).

Several features distinguish CA2 as a unique hippocampal subfield including its synaptic properties, molecular profile, anatomical connectivity, and spatial tuning properties. Although several studies have

demonstrated a role for CA2 in social memory via manipulation of the vasopressinergic system, in line with more traditional views of rodent hippocampal function, its participation in spatial cognition should also not be overlooked. Although much work has been done to identify the unique synaptic and molecular features that distinguish CA2, much less is known about the functional properties of CA2 neurons in vivo and how they might coordinate their activity with the rest of the hippocampus to integrate spatial and social cues into memory.

1.4 The Local Field Potential and Synchronization Through Oscillations

A microelectrode placed in neuronal tissue measures changes in voltage that originate from ionic currents flowing into and out of nearby cells. These transmembrane currents are driven by an imbalance of charge across neuronal membranes and, when measured in the extracellular space, are referred to as local field potentials (LFPs). Although the origin of the LFP can be complex, physically, it reflects the spatial summation of all electrical fields within recording range of the electrode. In neural tissue, this typically represents a mixture of fast activity generated by action potentials and slower activity generated by synaptic currents. After being low-pass filtered to remove the fast activity of action potentials, the LFP is thought to primarily reflect synaptic currents (Buzsaki, Anastassiou, & Koch, 2012), which are the same currents responsible for generating the post synaptic potentials. In signal processing, algorithms can be used to estimate the strength of different frequency components of a time-domain signal, referred to as the power spectrum. The LFP is such a time-domain signal that can be analyzed using spectral estimation methods because voltage fluctuations detected in the LFP frequently exhibit a periodic, or oscillatory, nature. These brain rhythms, or oscillations, are waves of neuronal activity that represent the synchronous activity of large groups of neurons, a process thought to be critical for cognitive operations which require coordinated activity of anatomically distributed cells, such as hippocampal based learning (Colgin & Moser, 2010; Fell & Axmacher, 2011).

Neurons organize their connections during development to form the circuits that provide the architectural framework for information flow through the brain, enabling one brain area to influence another; however, despite the relative stability of these anatomical connections post-development, neurons are capable of functionally coupling and uncoupling to one another (Buzsaki & Draguhn, 2004). One way in which neurons are thought to achieve this flexible coupling is by synchronization through

oscillations (Engel, Fries, & Singer, 2001; Jutras & Buffalo, 2010; Womelsdorf et al., 2007). At the single cell level, if a neuron receives input from multiple regions, each of which oscillate at distinct frequencies and/or phases relative to one another, the receiving neuron may tune into one of those input streams if excitably is modulated at the proper phase relative to the preferred input (Fries, 2005, 2015). In this way, synchronization of oscillatory phases is thought to influence the relative timing of action potentials between regions and, consequently, shape the flow of information through neural circuits. Accordingly, the power spectrum of the LFP recorded from neural tissue serves as one measure of neuronal synchrony in that network, and because currents that are synchronized in time sum to produce larger amplitude deflections, whereas asynchronous currents cancel out, increases in LFP power are thought to represent increases in synchronized input into the observed region.

1.5 Hippocampal Oscillations and Memory

In the hippocampus, the presence of oscillations is strongly correlated with episodic learning and memory (Colgin, 2016). Although a definitive explanation of how the hippocampus encodes and stores different types of memories is lacking, it is known that hippocampal based learning requires the association of information through several corticohippocampal and intrahippocampal pathways, including both long-range and local microcircuits (Basu & Siegelbaum, 2015). In the rodent hippocampus, three frequencies of activity dominate the LFP power spectrum during awake behavior: theta (~4-12 Hz), gamma (~25-100 Hz), and ripples (~100-300 Hz) (Buzsaki et al., 2003; Buzsaki, Leung, & Vanderwolf, 1983).

The theta frequency (4-12 Hz) is a large amplitude, highly regular oscillation that is easily detectable in all areas of the hippocampus whenever an animal engages in translational motion (Vanderwolf, 1969). In addition to a prominent increase in power during exploration, the theta oscillation is strongly linked to spatial processing due to its role in coordinating place cell firing, which is systematically related to the phase of the theta cycle (O'Keefe & Recce, 1993). As an animal moves through a place cell's receptive field, the place cell alters its action potential timing to occur at successively earlier points in each cycle of theta, a phenomenon known as theta phase precession (Skaggs, McNaughton, Wilson, & Barnes, 1996). In addition to its role in organizing spatial representations, the hippocampal theta oscillation has also been shown to serve a more general role in memory by organizing incoming sensory

information. Hippocampal theta oscillations transiently lock to the rhythmic neuronal activity that accompanies vibrissa-based sensation in rodents during the sensory-gathering epoch of a discrimination task (Kleinfeld, Deschenes, & Ulanovsky, 2016). To ensure that observed shifts in theta power are not merely a reflection of increased whisking requires controlling for spikes in theta power that co-occur with individual whisking motions. In our experiments, because we did not have a camera capable of tracking this behavior, we excluded the theta band from our experimental analysis in chapter 3 when subjects were allowed to investigate novel stimuli. Similar to the relationship between place cell firing and the theta cycle, the gamma oscillation also tends to occur during specific phases of the theta cycle (Leung, 1998; Scheffer-Teixeira et al., 2012; Schomburg et al., 2014; Shirvalkar, Rapp, & Shapiro, 2010), although there is currently disagreement about what that phase is (Colgin, 2015).

In contrast to the large amplitude, highly-regular activity of the theta band, the gamma frequency is a small-amplitude, transient oscillation that occurs in bursts throughout behavior (Colgin & Moser, 2010). Although historically thought to be a single, continuous frequency band spanning the entire ~25-100 Hz range, there is now evidence indicating that the gamma oscillation may correspond to two functionally distinct bands, including a slow (~25-55 Hz) and fast (~55-100 Hz) band (Colgin, 2015; Lasztoczi & Klausberger, 2014). In physiological situations, for a local network to become entrained to the gamma cycle, a network of interconnected, peri-somatically targeting, fast-spiking interneurons is required (Bartos, Vida, & Jonas, 2007; Buzsaki & Wang, 2012). Basket cells are a well-defined type of soma-inhibiting, GABA-releasing interneuron, so named because of their formation of peri-somatic 'baskets' around target cell somata (Bartos et al., 2007). In the hippocampus, a large subset of basket cells exhibit a fast-spiking action potential and express the calcium-binding protein parvalbumin and, although the function of parvalbumin is not fully understood, its expression represents a reliable marker for interneuron identification (Bartos et al., 2007). When such a network of interneurons is innervated, these cells synchronize their activity to generate the gamma rhythm. Although in vitro work and computational models have demonstrated that networks composed exclusively of interneurons (I-I networks) are capable of synchronizing activity in the gamma frequency range without contributions from pyramidal cells (Traub, Whittington, Stanford, & Jefferys, 1996), in physiological situations, excitation driving the network must arise from excitatory cells (E-I networks). This innervation can be generated either locally or from a

distal upstream region and does not have to be rhythmic itself (Bartos et al., 2002). When such a network of interneurons spike, synchronized IPSPs feedback onto pyramidal cell soma at the gamma frequency creating alternating periods of high & low inhibition which are thought to have several biophysical consequences for communication among participating neurons. Simultaneous paired intra- & extra-cellular recordings in vitro have determined that these IPSPs are the main electrophysiological event corresponding to the presence of hippocampal gamma oscillations in the LFP when recording in the pyramidal cell layer from actively spiking cells (Buzsaki & Wang, 2012). For this reason, gamma detected in the pyramidal cell layer serves as an electrophysiological signature for local network entrainment. In contrast, gamma oscillations recorded in synaptic layers are thought to represent excitatory input from distal upstream regions, which may or may not ultimately impact the timing of activity in the downstream network.

One prominent theory describing how gamma oscillations facilitate inter-regional communication is referred to as the communication through coherence (CTC) theory (Fries, 2005). When two separate networks that are each locally entrained to the gamma cycle interact, from the sending network's perspective, action potentials that are coordinated in time will result in larger EPSPs in the target dendritic domain of the receiving network, increasing the probability of depolarizing the receiving cells to threshold and generating an action potential. From the receiving network's perspective, each cell's membrane potential repeatedly moves closer to and away from action potential threshold, providing discrete windows in which appropriately timed inputs have an increased probability of inducing firing. If input is not appropriately timed; however, arriving during heightened inhibition, the input may be ignored. Cells will be most susceptible to excitatory drive that is timed to arrive during the fading inhibition part of the cycle. Accordingly, if the sending network is to exert the maximum impact possible on the receiving network, it should deliver coordinated bursts of spikes at every falling inhibition phase of the gamma cycle. This can occur only if the gamma phases in each region are synchronized. In this way, the efficacy of communication is thought to depend on the temporal coordination of the gamma phases in the upstream and downstream networks (Buzsaki & Schomburg, 2015; Fries, 2005, 2015; Fries, Nikolic, & Singer, 2007).

Rhythmic synchronization in the gamma frequency range is highly structured across brain areas, but the precise patterns of synchronization among layers and corresponding projections changes dynamically with stimulation and behavioral context (Buzsaki et al., 2003; Buzsaki et al., 1983). Accordingly, the particular benefits of this oscillation depend on the function of the brain system that supports it. The hippocampus has long been recognized to be critical for episodic memory and, because shifts in gamma synchrony have been observed to correlate with performance in memory-dependent tasks, it is thought to aid memory formation and retrieval (Montgomery & Buzsaki, 2007; J. Yamamoto, Suh, Takeuchi, & Tonegawa, 2014). Current theories suggest gamma oscillations may support memory through several distinct mechanisms including input selection, grouping cells into functional ensembles, facilitating inter-regional communication, and dynamic routing of information (Colgin & Moser, 2010). Although a comprehensive model explaining how gamma supports memory does not yet exist, the observation of increased gamma synchronization during active behaviors can still be viewed as a proxy for a coordinated pattern of neural activity that supports memory acquisition and retrieval. While an exhaustive list linking changes in gamma synchronization with specific stages and types of memory remains lacking, several studies have begun to build such a framework.

The Buszaki lab provided evidence that slow gamma synchronization supports memory retrieval using a delayed spatial alternation task in a modified T maze. The authors found that peak gamma power and coherence in the hippocampus occurred between CA3 and CA1 just prior to the subject entering the T junction of the maze, where a memory-based decision had to be made to select the previously unvisited maze arm (Montgomery & Buzsaki, 2007). The authors concluded that slow gamma oscillations may serve as a physiological mechanism by which CA3 output can coordinate CA1 activity to support retrieval of hippocampus-dependent memories. The Tonegawa lab demonstrated that transient bursts of fast gamma power between CA3 and CA1 during the retention period of a reward-based-spatial-working-memory task preceded an animal's correct choice, but not an incorrect one, suggesting that transient fast gamma synchrony contributes to successful execution of spatial working memory (J. Yamamoto et al., 2014). Additionally, the Colgin lab demonstrated that fast gamma rhythms promoted the encoding of novel object-place pairings (Zheng, Bieri, Hwaun, & Colgin, 2016) and the Eichenbaum lab showed that the strength of theta-gamma coupling increases during the learning of item-context associations (Tort,

Komorowski, Manns, Kopell, & Eichenbaum, 2009). Together, these studies illustrate that hippocampal networks, particularly at the CA3-CA1 interface, can be dynamically coupled by gamma oscillations according to the specific behavioral demands of a task. In addition to the progress that has been made toward understanding which frequencies of neuronal activity support distinct types of memory, the contributions of the different subfields to the generation and maintenance of these oscillations is also being explored. While all hippocampal sub-fields possess the cellular constituents required to exhibit gamma rhythmogenesis, gamma oscillations in vivo are not observed to occur spontaneously in all regions, but rather, are generated locally in some regions and propagate to others (Hajos & Paulsen, 2009).

One approach to probing the extent of involvement of a given region in the generation of gamma has been to disrupt the function of that region and observe how synchronization is altered. Such disruption-based methods have revealed that slow and fast gamma oscillations in CA1 rely on input from two distinct sources (Colgin et al., 2009). Fast gamma oscillations are prevalent in stratum lacunosum-moleculare of CA1 (Schomburg et al., 2014), co-occur with fast gamma oscillations in medial entorhinal cortex (MEC)(Colgin et al., 2009) and their power is reduced by lesions to the EC (Bragin et al., 1995). Slow gamma oscillations are prevalent in stratum radiatum (Schomburg et al., 2014), synchronize with slow gamma in CA3 (Colgin, 2015), and their power is reduced by lesions to CA3, leading to the conclusion that slow gamma oscillations in CA1 depend on CA3 Schaffer collateral input. Slow gamma oscillations are thought to originate locally within CA3 in part due to the presence of a recursive collateral system, a key morphological feature proposed to be required for spontaneous gamma rhythmogenesis in vivo (Hajos & Paulsen, 2009). Interestingly, complete silencing of CA3 synaptic output with tetanus toxin light chain does not abolish slow gamma oscillations, but causes a reduction in their magnitude by approximately 30% (Middleton & McHugh, 2016), suggesting another source of slow gamma oscillations may exist. Because slow gamma oscillations also become more prominent in CA1 upon EC lesioning (Bragin et al., 1995), slow and fast gamma oscillations have been proposed to compete for dominance over the hippocampal network in a time-sharing manner and, consequently, may differentially support memory formation and retrieval by dynamically routing incoming sensory information (Colgin, 2015; Colgin & Moser, 2010).

Prior studies have examined the single-unit firing properties of individual CA2 pyramidal cells in spatial and social contexts (Alexander et al., 2016; Mankin et al., 2015), as well as its role in sharp-wave ripple generation (Kay et al., 2016; Oliva, Fernandez-Ruiz, Buzsaki, & Berenyi, 2016), but none have examined the role of CA2 in the organization of gamma oscillations. Given that CA3 is recognized as a source of slow gamma oscillations in CA1, and CA1 also receives Schaffer collateral input from CA2 pyramidal cells (Kohara et al., 2014; Shinohara et al., 2012; Tamamaki et al., 1988), we asked whether hippocampal gamma oscillations also depend on CA2 output. Because studies of hippocampal gamma oscillations have historically focused on spatial memory, we first investigated the role of CA2 in coordinating oscillations during periods of running, a behavior during which physiological gamma power is elevated (Ahmed & Mehta, 2012; Chen, Resnik, McFarland, Sakmann, & Mehta, 2011). Here, we show that acute, reversible manipulation of CA2 pyramidal cells using excitatory and inhibitory DREADDs (hM3Dq and hM4Di, respectively) (Alexander et al., 2009; Armbruster, Li, Pausch, Herlitze, & Roth, 2007) bidirectionally modulates hippocampal slow gamma oscillations in awake, behaving mice.

1.6 Chemogenetic Tools for Manipulation of Discrete Neural Circuits

The neural circuits underlying memory are complex and involve anatomically distinct sub-regions composed of many different cell types. We have begun to untangle the contributions of one of these sub-regions, CA2, by employing electrophysiological recording techniques in combination with chemogenetic tools to selectively target and manipulate CA2 pyramidal cells in vivo and observe the effects on hippocampal synchrony as measured by oscillations detected in the LFP. Chemogenetics refers to the use of proteins that have been selectively modified to bind previously unassociated compounds (Roth, 2016). The most common chemogenetic tools used by neuroscientists are the Designer Receptors Exclusively Activated by Designer Drugs (DREADDs), which are modified G protein-coupled receptors (GPCRs) coupled to the canonical G alpha subunits (Gs, Gi, and Gq) (Armbruster et al., 2007). The first DREADD construct was a modified human muscarinic receptor that responded selectively to the inert ligand clozapine *n*-oxide (CNO) (Armbruster et al., 2007), and this is the system we have employed for our experiments.

DREADD technology allows for the modulation of discrete G protein-coupled signaling pathways which can result in a net inhibitory or excitatory effect on a cell by inducing changes in membrane

potential. Notably, these changes in cellular activity are downstream of the receptor manipulation (Alexander et al., 2009). Thus, while G protein-coupled DREADDs enable targeted manipulations at the level of the receptor, they require the presence of endogenous signaling pathways to induce changes in neuronal activity, suggesting that this form of cellular manipulation may have more relevance to physiological forms of activity relative to other tools, such as optogenetics. Initial assessments of the hM3Dq receptor revealed that bath application of CNO in acute slice preparation induced a depolarization of CA1 pyramidal neurons which, in turn, caused an increase in action potential firing, confirming that hM3Dq-mediated Gq stimulation increases action potential probability. This effect was blocked in the presence of a PLC inhibitor, indicating that the effects of hM3Dq relied on the canonical Gq-coupled signaling cascade (Alexander et al., 2009). The inhibitory effects of the Gi-coupled hM4Di, on the other hand, appear to rely on multiple classic signaling pathways. Hyperpolarization through hM4Di is mediated, in large part, through activation of the G protein inward rectifying potassium (GIRK) channels by the Gβγ subunit (Armbruster et al., 2007).

DREADDs can be delivered to target cells using viral vectors that encode DREADD constructs (Roth, 2016). Although DREADDs can be delivered indiscriminately to all cells in a given region, they are also amendable to use with the Cre/lox system. Because expression of the Cre recombinase enzyme can be regulated by cell-specific promoters, this system allows access to genetically defined cell populations which, when combined with DREADDs, provides a tool for remotely manipulating the activity of these populations. The Cre/lox system is a widely used, site-specific recombination system in which the enzyme Cre recombinase recognizes specific DNA base-pair sequences called lox sites (Carter, 2010). Lox sites are added to a transgene so that they flank a sequence of DNA on either side. Each lox site has an asymmetric sequence in the middle, providing the sequence with directionality, which is critical because Cre processes DNA based on the orientation of the lox sites. When DNA is located between two lox sites oriented in the same direction, Cre excises the DNA, whereas when it is located between two inverted sites, the sequence is also inverted. In this way, the Cre/lox system allows for complex rearrangement of DNA in transgenic organisms (Carter, 2010).

Temporal control over the Cre/lox system can be achieved by fusing the gene encoding Cre recombinase to a gene encoding a modified estrogen receptor (ER) (A. Yamamoto, Hen, & Dauer, 2001).

This modified ER is altered so that it no longer binds its endogenous ligand, estrogen, but instead, selectively binds the chemical tamoxifen, an estrogen agonist that can be administered peripherally. Because the ER is normally localized to the cytoplasm, a Cre protein that is fused to the ER will also remain localized to the cytoplasm until administration of tamoxifen. When tamoxifen binds the ER, the ER-Cre complex is able to translocate to the nucleus, allowing recombination and expression of the virally delivered construct. Here, we employed the inducible Cre-ER system to gain temporal control over recombination after discovering that our transgene selected for CA2 targeting, *Amigo2*, was expressed in off target cortical regions caused by mechanical damage incurred during cannula insertion for viral infusion. By employing the inducible-Cre-ER system, we were able to circumvent this problem by providing animals with an extended post-surgical recovery period which allowed the activity dependent regulation of *Amigo2* to cease prior to inducing recombination. This system allowed for selective expression of the Cre recombinase enzyme and DREADD constructs in CA2 pyramidal cells.

1.7 Figures

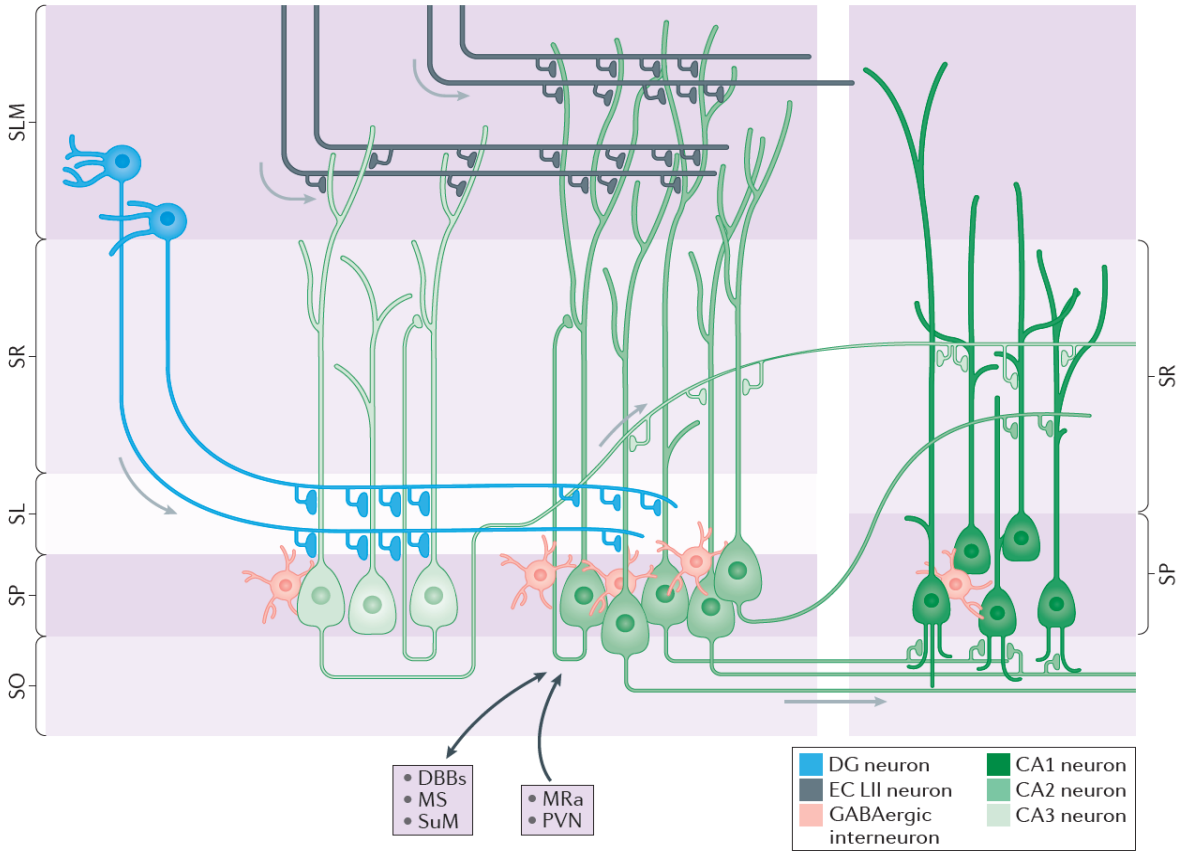

Figure 1.1: Anatomical Connectivity of Hippocampal Area CA2. CA2 pyramidal cells receive an array of intra- and extra-hippocampal inputs and, in turn, send the majority of their axon collaterals to the basal dendrites of CA1 pyramidal cells located in stratum oriens, but also to the apical dendrites located in stratum radiatum.

CHAPTER 2. CHEMOGENETIC MODULATION OF GQ- AND GI-COUPLED GPCR SIGNALING IN CA2 BI-DIRECTIONALLY MODULATES HIPPOCAMPAL SLOW GAMMA AND BETA OSCILLATIONS DURING RUNNING

2.1 Historical Context

Many cognitive operations require dynamic coordination of activity across anatomically distributed cells. Several mechanisms exist for this purpose, but one of the most studied is synchronization through oscillations (Buzsaki & Draguhn, 2004; Engel et al., 2001; Schomburg et al., 2014; Senior, Huxter, Allen, O'Neill, & Csicsvari, 2008; Vanderwolf, 1969). Because the hippocampus is critically involved in the encoding and storage of episodic memories, hippocampal oscillations are thought to support memory acquisition and consolidation.

The hippocampus propagates oscillations in three primary frequency bands: theta (~4-12 Hz), gamma (~25-100 Hz) and sharp-wave ripples (~100-300 Hz) (Buzsaki et al., 2003; Buzsaki et al., 1983). Prior studies have examined the role of CA2 in sharp-wave ripple generation (Kay et al., 2016; Oliva et al., 2016) and theta oscillations (Mankin et al., 2015), but none have examined the role of CA2 in the organization of gamma oscillations. The gamma oscillation is a small amplitude, transient rhythm that occurs in bursts throughout behavior and is hypothesized to temporally link anatomically distributed cells, grouping neurons into functional ensembles (Colgin & Moser, 2010). In the hippocampal CA1 subfield, fast and slow gamma oscillations have been shown to rely on input from two distinct sources, the EC and the CA3 subfield, respectively (Colgin et al., 2009). Fast gamma oscillations are prevalent in stratum lacunosum-moleculare of CA1 (Schomburg et al., 2014), co-occur with fast gamma oscillations in medial entorhinal cortex (MEC)(Colgin et al., 2009) and their power is reduced by lesions to the EC (Bragin et al., 1995). Slow gamma oscillations are prevalent in stratum radiatum (Schomburg et al., 2014), synchronize with slow gamma in CA3 (Colgin, 2015), and their power is reduced by lesions to CA3, leading to the conclusion that slow gamma oscillations depend on CA3 Schaffer collateral output. Slow gamma oscillations are believed to promote memory retrieval because the magnitude of slow gamma coupling to theta oscillations correlates with performance on learned behavioral tasks (Shirvalkar et al., 2010; Tort et

al., 2009). Interestingly, complete silencing of CA3 synaptic output with tetanus toxin light chain does not abolish slow gamma oscillations in the hippocampus, but causes a reduction in its magnitude by approximately 30% (Middleton & McHugh, 2016), suggesting another source of slow gamma oscillations may exist.

Given that CA3 Schaffer collaterals are recognized as a necessary source of innervation for generation of hippocampal slow gamma oscillations in CA1, that CA2 Schaffer collaterals also project to CA1 (Kohara et al., 2014; Shinohara et al., 2012; Tamamaki et al., 1988), and that CA2 exhibits several network features thought to be required for spontaneous gamma rhythmogenesis, we asked whether hippocampal slow gamma oscillations also depend on CA2 pyramidal cell output. Because prior studies examining gamma oscillations in the hippocampus in vivo have largely focused on spatial memory, we first investigated the role of CA2 in coordinating oscillations during periods of running, a behavior during which physiological gamma power is normally elevated (Ahmed & Mehta, 2012; Chen et al., 2011).

Although much progress has been made toward understanding which frequencies of neuronal activity support different types of memory, understanding the contributions of each hippocampal sub-region to the generation, and maintenance, of these oscillations is less well understood. In this chapter, we present evidence that targeted, reversible manipulation of CA2 pyramidal cells using excitatory and inhibitory DREADDs (hM3Dq and hM4Di, respectively) is sufficient to bidirectionally modulate hippocampal slow gamma and beta oscillations in awake, behaving mice. These findings provide support for the idea that CA2 is a unique hub capable of coordinating hippocampal neural synchronization through oscillations.

2.2 Methods

Mice: All animals (>8 weeks old) were maintained on a 12:12 light/dark cycle with *ad libitum* access to food and water. Both male and female mice were used. Mice were naïve to any treatment, procedure or testing at the beginning of experiments described here. Mice were group-housed until the time of electrode implantation, at which point they were singly housed. All procedures were approved by the NIEHS Animal Care and Use Committee and were in accordance with the National Institutes of Health guidelines for care and use of animals.

Generation of *Amigo2*-icreERT2 mice: The BAC clone RP23-288P18 was used to generate the *Amigo2*-icreERT2 mouse line. To recombine the cDNA encoding an icreERT2 fusion protein (Hainer et al., 2015) into the BAC, we constructed a targeting vector from which we derived a targeting fragment for recombineering. The targeting fragment consisted of a 243 bp homology region (A-Box) immediately upstream of the ATG in the *Amigo2* gene. The icreERT2 cassette was fused to the A-Box replacing the *Amigo2* ATG with the icre ATG preceded with a perfect KOZAK sequence. At the 3' end of the icreERT2 cassette a synthetic bovine growth hormone (BGH) polyadenylation signal was added after the STOP codon. For selection of recombined BACs, a flipase-site flanked neomycin resistance gene was incorporated into the targeting fragment following the icreERT2 cassette. Finally, the 3' end of the targeting fragment contained a 263 bp homology region (B-Box) starting downstream of the *Amigo2* ATG. Recombineering was performed according to a previously described protocol (E. C. Lee et al., 2001). In brief, the targeting fragment was electroporated into induced EL250 bacteria harboring the *Amigo2* BAC. Recombined colonies were selected on Chloramphenicol/Kanamycin plates and screened by colony PCR. The neo gene was removed from the recombined BAC by arabinose driven flipase expression. Recombined BACs without the neo marker were linearized by restriction enzyme digestion, gel purified and electro-eluted from the gel slice. After filter dialysis with a Millipore VSWP02500 filter, the BAC fragment concentration was adjusted to 1 ng/µl and microinjected into pronuclei of B6SJLF1 mouse oocytes (Taconic, North America). Six independent founder mice resulted, which were bred to *ROSA*-tdTomato indicator mice. Resulting offspring that genotyped positive for both Cre and tdTomato were treated with tamoxifen (Sigma, 100 mg/kg daily administration, IP, 7 days of treatment). At least one week following the final treatment with tamoxifen, mice were perfused with 4% paraformaldehyde and brains were sectioned and examined for tdTomato expression. Two lines showed adult expression of icreERT2 in CA2; one showed sparse expression in dentate gyrus and was not used in this study, another (line 1; *B6(SJL)-Tg(Amigo2-icre/ERT2)1Ehs*) showed selective expression in CA2 within hippocampus as well as expression in fasciola cinerea and hypothalamus, among other locations. Line 1 mice were used for electrophysiology and anatomy studies here and were bred to *ROSA*-tdTomato (described above), *GAD*-eGFP, or *GAD*-eGFP; *ROSA*-tdTomato mice for histological analysis. *Amigo2*-icreERT2 mice used in this study were backcrossed to C57Bl/6 7 generations. Genotyping of *Amigo2*-icreERT2 BAC transgenic

mice was done using the following primers: BGH-F (forward primer) 5'-CTT CTG AGG CGG AAA GAA CC-3' and dAmigo4 (reverse primer) 5'-AACTGCCCGTGGAGATGCTGG-3'. PCR protocol is 30 cycles of 94°C 30 sec., 60°C 30 sec., 72°C 30sec. PCR product is 600bp.

Viruses: All AAV viruses were produced by the Gene Therapy Center Vector Core at the University of North Carolina at Chapel Hill and had titers of $>10^{12}$ genome copies/mL. For chemogenetic manipulation using hM3Dq-mCherry, mice were unilaterally infused with 0.5 µl of AAV5-hsyn-hM3Dq-DIO-mCherry. For manipulation using hM4Di-mCherry, mice were bilaterally infused with 0.5 µl of AAV5-hsyn-DIO-hM4Di-mCherry into each hemisphere of the brain.

Stereotaxic virus infusions and tamoxifen treatment: For virus-infusion surgery, mice were anesthetized with ketamine (100 mg/kg, IP) and xylazine (7 mg/kg, IP), then placed in a stereotaxic apparatus while on a heated pad. Sedation was maintained at 1.5-2.0% isoflurane during surgery if animal regained reflex responses at any point throughout the procedure. Following 3 alternating swabs with betadine and 70% ethanol, an incision was made down the midline of the scalp, a burr hole was drilled above each target region and viruses were microinjected using a 1 µl Neuros Hamilton syringe at a rate of 100 nl/min. Following infusion, the needle was left in place for an additional 5-10 minutes to allow for diffusion of the virus before being slowly withdrawn. Injection coordinates for CA2 were (in mm: -2.30 AP, +/-2.50 ML, -1.90 DV from bregma). *Amigo2*-icreERT2 mice were infused unilaterally in the left hemisphere for the hM3Dq construct and bilaterally for hM4Di construct. The scalp was then sutured and animals were administered buprenorphine (0.1 mg/kg, SQ) for pain and returned to their cages. Two weeks following AAV infusion surgery, *Amigo2*-icreERT2 mice began daily tamoxifen treatments (100 mg/kg tamoxifen dissolved in warmed corn oil, IP) for a total of 7 days. At least one week following the last dose of tamoxifen, animals were euthanized and perfused with 4% paraformaldehyde for anatomical studies, or underwent electrode implantation for electrophysiology studies.

Electrode implantation: At least one week after the last tamoxifen treatment, mice used for in vivo electrophysiology experiments were implanted with custom built wire-bundle electrode arrays. Mice were anesthetized with ketamine (100 mg/kg, IP) and xylazine (7 mg/kg, IP), then placed in a stereotaxic apparatus while on a heated pad. Sedation was maintained at 1.5-2.0% isoflurane during surgery if animal regained reflex responses at any point throughout the procedure. Following 3 alternating swabs

with betadine and 70% ethanol, an incision was made down the midline of the scalp and the skull was cleaned and dried. One ground screw (positioned approximately 4 mm posterior and 2 mm lateral to Bregma over the right hemisphere) and four anchor screws were secured to the skull and electrode arrays were slowly lowered into drilled holes over the target brain region. Electrode wires were connected to a printed circuit board (San Francisco Circuits, San Mateo, CA), which was connected to a miniature connector (Omnetics Connector Corporation, Minneapolis, MN). Electrodes wires were composed of stainless steel (44 μm) with polyimide coating (Sandvik Group, Stockholm, Sweden). Wires were bundled using high performance medical tubing (Microlumen).

Neurophysiological data acquisition and behavioral tracking: Neural activity was transmitted via a 32-channel wireless 10× gain head stage (Triangle BioSystems International, Durham, NC) and was acquired using the Cerebus acquisition system (Blackrock Microsystems, Salt Lake City, UT). Continuous LFP data were band-pass filtered at 0.3–500 Hz and stored at 1,000 Hz. Neurophysiological recordings were referenced to a silver wire connected to a ground screw secured in the posterior parietal bone (approximately 4 mm posterior to Bregma, 2 mm lateral). For behavioral tracking we used two approaches. First, the wireless head stage was equipped with a light-emitting diode (for use with a color camera), and we also attached a piece of infrared reflective tape to the head stage (for use with an infrared camera). The X and Y coordinates in space of the light-emitting diode or infrared reflective tape were sampled at 30 Hz using the integrated Neuromotive Software (Blackrock Microsystems) and position data were stored with the neural data. These coordinates were used to calculate the subject's instantaneous velocity, which was then smoothed and periods of immobility extracted. To isolate periods of running, we analyzed behavioral videos offline using the behavioral tracking software suite Ethovision XT (Noldus, Wageningen, Netherlands). Samples in which the animal's smoothed instantaneous velocity exceeded a threshold of ≥ 7 cm/sec were collected and designated as periods of running.

Electrophysiology data analysis: The experimenters were blind to the genotype of animals at the time of data analysis. All neuronal data analyses were performed using Neuroexplorer software (Nex Technologies, TX) and Matlab (MathWorks, Inc., Natick, MA) with the Chronux toolbox for Matlab (http://chronux.org/, Cold Springs Harbor, Long Island, NY). Statistical analyses were performed using GraphPad Prism version 6. All hippocampal LFP measures were derived from an electrode channel

connected to a wire positioned in the cell body layer, as determined by the presence of ripples. Data collected during the 30 to 60 min time window following CNO administration were first divided into periods of running (>7 cm/sec) or resting (<0.5 cm/sec and limited to up to 20 sec once an animal has started moving <0.5 cm/sec). These LFP subsets were then z-scored to control for changes in overall signal amplitude (and, consequently, power) over the course of up to 2 weeks of recordings (in the case of hM3Dq animals in which multiple doses of CNO or vehicle were administered every 2 to 3 days). LFPs were then filtered using a zero-phase offset filter in the theta (5-10 Hz), beta (14-18 Hz), slow gamma (30-60 Hz) or fast gamma (65-100 Hz) range. The Chronux function mtspectrum, a multitaper spectral estimate, was used with 5 tapers, and resulting spectral values were smoothed. For all treatments, spectral measures were made during each of run and rest periods during the 30 to 60 minutes following treatment. Spectral density plots for each behavioral state, each treatment, and in each recording site were averaged across animals according to genotype and AAV infused. Plots shown in figures are measured in arbitrary units due to z-scoring of LFPs, as described above. Peak powers in each frequency range were collected to compare changes in peak theta, beta, low gamma or high gamma power according to treatment. Power values measured for each treatment were compared using appropriate statistical tests, listed in text, after data were checked for normal distributions and equal variance. As a consequence of z-scoring LFPs for periods of run and rest separately, theta power appears to be similar between the two states. However, measurement of spectral power without z-scoring LFPs for run and rest shows that theta power is higher during periods of running than during rest (see figure 2.4). We did not observe a difference in time spent running or in running speed during recordings for any of the treatments. For detection of ripples signals were denoised with an IIR notch filter at 60 and 180 Hz and filtered between 100 and 300 Hz with a 69-order FIR zero phase shift filter. Signals were then Hilbert transformed, and the absolute value envelopes were smoothed with a 50-msec window. Envelope amplitude deflections that exceeded 3 standard deviations from the mean amplitude (i.e., mean +3 standard deviations) for more than 30 msec were counted as ripple events.

Experimental paradigm: For experiments using hM3Dq-infused animals, baseline data was acquired for at least 20 minutes prior to treatment with either vehicle (10% DMSO in saline) or CNO (0.05-4 mg/kg CNO dissolved in DMSO to 50 mM and suspended in saline) and recording continued for an

additional 2 hours. For these experiments subjects could freely explore a custom-built, 5-sided (open top), black plexiglass open field arena (80 cm x 80 cm x 100 cm). Subjects always received vehicle for the first recording session and subsequently received increasing doses of CNO in three-day intervals. Room lights remained illuminated during data acquisition, but a curtain was placed around the open field chamber to minimize light exposure. For neurophysiology experiments using hM4Di-infused animals, subjects were administered either vehicle or CNO (5 mg/kg) and returned to their home cage for 30 minutes prior to the start of the experiment. For hM4Di experiments the room lights were turned off and red lights were illuminated following CNO or vehicle administration. Subjects were placed in the open field arena for recording just prior to the initiation of each experiment.

Histology and immunohistochemistry: Animals used for histology were euthanized with Fatal Plus (sodium pentobarbital, 50 mg/mL) and underwent transcardial perfusion with 4% paraformaldehyde. Brains were subsequently cryoprotected in 30% sucrose PBS for at least 72 hours and sectioned with either a cryostat or vibratome at 40µm. For immunohistochemistry, brain sections were rinsed in PBS, boiled in deionized water for 3 min, and blocked for at least 1 h in 3-5% normal goat serum/0.01% Tween 20 PBS. Sections were incubated in the following primary antibodies, which have previously been validated in mouse brain (Hitti & Siegelbaum, 2014; Kohara et al., 2014): rabbit anti-PCP4 (SCBT, sc-74186, 1:500), mouse anti-RGS14 (UC Davis, 75170, 1:250), rabbit anti-WFS1 (ProteinTech, 11558-1-AP, 1:250), rabbit anti-CaMKII alpha (Abcam, ab131468, 1:250), rat anti-mCherry (Life Technologies, M11217, 1:500- 1:1000). Antibodies were diluted in blocking solution and sections were incubated for 24 h. After several rinses in PBS/Tween, sections were incubated in secondary antibodies (Alexa goat anti-mouse 488 and Alexa goat anti-rabbit 568, Alexa Goat anti-rat 568, Invitrogen, 1:500) for 2 h. Finally, sections were washed in PBS/Tween and mounted under ProLong Gold Antifade fluorescence media with DAPI (Invitrogen). Images of whole-brain sections were acquired with a slide scanner using the Aperio Scanscope FL Scanner (Leica Biosystems Inc.). The slide scanner uses a monochrome TDI line-scan camera, with a PC-controlled mercury light source to capture high resolution, seamless digital fluorescent images. Images of hippocampi were acquired on a Zeiss 780 meta confocal microscope using a 40× oil-immersion lens.

Electrode localization: Upon completion of electrophysiology studies, mice were perfused with 4% paraformaldehyde. Heads with electrodes remaining implanted were then submerged in 4% paraformaldehyde for 24-48 h. Electrodes were carefully removed, brains were cryoprotected using 30% sucrose/PBS, and sectioned at 40 µm on a cryostat or vibratome. Slices were stained with cresyl violet for probe placement verification.

Sample size and group assignment: For all experiments, 35 *Amigo2*-icreERT2 mice (8 for histology, 29 for electrophysiology), 13 *Amigo2*-icreERT2; *ROSA*-tdTomato mice (all for histology), 3 *Amigo2*-icreERT2; *GAD*-eGFP; *ROSA*-tdTomato mice (all for histology) and 4 *Amigo2*-icreERT2; *GAD*-eGFP mice (all for histology) were used. No statistical tests were used to determine sample sizes *a priori*, but sample sizes for histological, electrophysiological and behavioral studies were similar to those used in the field and based on the expected variances from previous electrophysiological experiments. For electrophysiology studies, pairs of *Amigo2*-icreERT2+ and *Amigo2*-icreERT2- animals were randomly selected from individual litters and, whenever possible, mice from the same litter were split across treatments to minimize differences in age. No specific method of randomization was used to assign groups. Animals were housed with same-sex littermates following weaning but before genotyping. Genotype information was unknown at the time of selection for AAV infusion. Pre-established criteria for excluding mice or cells from analysis included 1) missed injections or lack of viral expression, 2) equipment failures during testing.

Statistical reporting: For each experiment presented within the results section and in figures, the number of replicates is presented as “N” when indicating the number of animals that were used for the experiment. Statistical tests used for each experiment are presented in the text. Statistical significance was based on a p-value of 0.05. All error bars in graphs represent standard error of the mean. Data are presented as means ± SEM. For comparisons with only two groups, p-values were calculated using two-tailed paired or unpaired t-tests as described in the figure legends, unless specified otherwise. In cases where the data were not normally distributed, a Mann-Whitney test was performed as indicated in figure legends. Comparisons across more than two groups were made using a repeated-measures, one-way Analysis of Variance (ANOVA) with Greenhouse-Geisser correction for unequal variance. A Tukey’s post-

test was performed following significance with an ANOVA. All data were analyzed with GraphPad Prism 6 software.

2.3 Results

2.3.1 *Amigo2*-icreERT2+ mice enable genetic access to CA2 pyramidal cells

To gain selective genetic access to molecularly-defined CA2 pyramidal cells, we generated a tamoxifen-inducible mouse line, *Amigo2*-icreERT2. When combined with a Cre-dependent tdTomato reporter mouse line (Madisen et al., 2010), we observed robust expression of tdTomato in CA2 of brain sections from *Amigo2-icreERT2*+; *ROSA*-tdTomato+/- mice treated with tamoxifen (**Figure 2.1 A**). Expression of tdTomato colocalized with the CA2 pyramidal cell marker, PCP4 (Kohara et al., 2014) (**Figure 2.1 B**), a marker of hippocampal pyramidal neurons, and CaMKIIα (**Figure 2.1 C**), a marker for glutamatergic cells, but did not colocalize with glutamic acid decarboxylase (GAD) (**Figure 2.1 D**), a marker for inhibitory neurons. Expression of tdTomato was present throughout the entire rostro-caudal extent of the hippocampus (**Figure 2.1 E**). Expression of tdTomato was also observed in extra-hippocampal brain structures and associated with vasculature. In control experiments, *Amigo2-icreERT2*+; *ROSA*-tdTomato+/- animals treated with corn oil (tamoxifen vehicle) showed no tdTomato expression. Because *Amigo2*-icreERT2+ mice expressed Cre selectively in CA2 pyramidal cells within the hippocampus, this line was suitable for use with Cre-dependent DREADDs. Infusion of 0.5 µl of AAVs encoding Cre-dependent hM3Dq (**Figure 2.2 A**) or hM4Di (**Figure 2.3 A**) with the neuron-specific human synapsin promoter into *Amigo2-icreERT2*+ mice allowed for selective expression of hM3Dq and hM4Di in CA2 pyramidal neurons without expression in fasciola cinerea, outside of the hippocampus, or in the vasculature, as detected by co-expression of hM3Dq with PCP4 (**Figure 2.2 A-B**) and hM4Di with RGS14 (**Figure 2.3 A-B**), both markers of CA2 pyramidal cells. Expression of hM3Dq also colocalized with the pyramidal cell marker CaMKIIα (**Figure 2.2 C**), but not with GAD in *GAD*-eGFP+; *Amigo2*-icreERT2+ mice (**Figure 2.2 D**). Expression of hM4Di also did not colocalize with WFS1, a marker for CA1 pyramidal cells (**Figure 2.3 C**). An infusion volume of 0.5 µl of per hemisphere resulted in expression that covered the entire rostro-caudal extent of CA2 for both the hM3Dq (**Figure 2.2 E**) and hM4Di (**Figure 2.3 E**) constructs. In control *Amigo2*-icreERT2- mice infused with hM3Dq or hM4Di, mCherry expression was absent. With genetic access to CA2 pyramidal cells gained, we could selectively modify activity of CA2

pyramidal neurons in vivo with excitatory or inhibitory DREADDs and measure the resulting effects on hippocampal activity and behavior. One major advantage offered by the DREADD technology is that modification of neuronal activity is transient and reversible, reducing the potential for compensatory circuit reorganization.

2.3.2 Acute chemogenetic activation of CA2 pyramidal cells induces hippocampal slow gamma oscillations and inhibits hippocampal beta oscillations

To determine how engagement of the Gq-coupled signaling pathway in CA2 pyramidal cells affects hippocampal oscillatory activity, we infused *Amigo2*-icreERT2+ and control *Amigo2*-icreERT2- mice unilaterally with a Cre-inducible hM3Dq construct (**Figure 2.2 A-D**), treated with tamoxifen, and implanted wire-bundle electrodes targeted to the pyramidal cell layer of CA2/proximal CA1 (**Figure 2.3 D**). For these experiments subjects could freely explore an open field arena of their own volition. Subjects were treated with various doses of CNO or vehicle and hippocampal LFPs were assessed for effects of CNO treatment using Fourier based spectral analysis, focusing on theta (5-10 Hz), beta (14-18 Hz), slow gamma (30-60 Hz), and fast gamma (65-100 Hz) frequency bands. As a first pass to assess the effects of CNO treatment in hM3Dq-infused animals, LFP spectrograms were generated for each dose level of CNO to examine how power varied with time in all frequencies ranging from 1-80 Hz. We found that CNO dose-dependently increased hippocampal oscillatory power in the slow gamma frequency range in *Amigo2*-icreERT2+ (**Figure 2.4 B**), but not in *Amigo2*-icreERT2- mice (**Figure 2.4 A**). To determine whether there was a state-dependent relationship between the animal's behavior and the frequency of hippocampal neuronal activity, we isolated behavioral epochs in which subjects were running or at rest, generated power spectral densities for the 1-100 Hz frequency range, and looked for state-specific shifts in oscillatory power. Power measurements were quantified 30 to 60 minutes following CNO administration. Power spectral densities are shown for *Amigo2*-icreERT2- (**Figure 2.5 A**) and *Amigo2*-icreERT2+ (**Figure 2.5 B**) mice. In *Amigo2*-icreERT2+ mice, CNO revealed a significant variation in theta power during running Friedman statistic=11.3; p=0.0234; results of *post hoc* tests not significant) (**Figure 2.5 C, left**) and periods of rest ($F(1.972, 13.81)=4.825$, $p=0.0261$, RM one-way ANOVA with Geisser-Greenhouse correction; results of *post hoc* tests not significant) (**Figure 2.5 C, right**). CNO also revealed a significant reduction in beta power during periods of rest ($F(1.408, 9.857)=10.07$, $p=0.0066$; RM one-way ANOVA with Geisser-Greenhouse correction; 0.5 mg/kg: $p=0.0486$; 1 mg/kg: $p=0.1240$; 2 mg/kg:

p=0.0545; 4 mg/kg: *p*=0.0133, Holm-Sidak *post hoc* test for multiple comparisons) (**Figure 2.5 D, right**); however, no significant differences were detected for periods of running (F(2.274, 15.91)=2.91, *p*=0.0784, RM one-way ANOVA with Geisser-Greenhouse correction) (**Figure 2.5 D, left**). CNO also caused a significant increase in slow gamma power during running for all doses tested (F(1.904, 13.33)=9.457, *p*=0.0030, RM one-way ANOVA with Geisser-Greenhouse correction; 0.5 mg/kg: *p*=0.0286; 1 mg/kg: *p*=0.0286; 2 mg/kg: *p*=0.0286; 4 mg/kg: *p*=0.0191, Holm-Sidak *post hoc* test for multiple comparisons) (**Figure 2.5 E, left**) and during periods of rest for all doses tested except at the 0.5 mg/kg level (F(2.306, 16.15)=32.2, *p*<0.0001, RM one-way ANOVA with Geisser-Greenhouse correction; 0.5 mg/kg: *p*=0.1008; 1 mg/kg: *p*=0.0161; 2 mg/kg: *p*=0.0002; 4 mg/kg: *p*=0.0004, Holm-Sidak *post hoc* test for multiple comparisons) (**Figure 2.5 E, right**)**.** Fast gamma power in *Amigo2*-icreERT2+ mice was not significantly affected by CNO treatment compared with vehicle during either running (F(1.384, 9.69)=2.288, *p*=0.1602, RM one-way ANOVA with Geisser-Greenhouse correction) (**Figure 2.5 F, left**) or periods of rest (F(1.286, 9.003)=4.775, *p*<0.0501, RM one-way ANOVA with Geisser-Greenhouse correction) **(Figure 2.5 F, right**). In contrast to the effects observed in *Amigo2*-icreERT2+ mice, no significant effects of CNO were observed in control *Amigo2*-icreERT2- mice during periods of running for the theta (F(1.782,5.347)=1.161, p=0.3734, RM one-way ANOVA with Greenhouse-Geisser), beta (F(1.61, 4.829)=0.8606, p=0.4547, RM one-way ANOVA with Greenhouse-Geisser), slow gamma (F(1.669, 5.006)=1.36, *p*=0.3281; RM one-way ANOVA with Greenhouse-Geisser correction), or fast gamma (F(1.895, 5.684)=0.5079, *p*=0.6175, RM one-way ANOVA with Geisser-Greenhouse correction) frequency bands (data not shown). CNO also revealed no significant effects in *Amigo2*-icreERT2- during periods of rest for the theta (F(1.335, 4.006)=1.072, p=0.3875, RM one-way ANOVA with Greenhouse-Geisser correction), beta (F(1.867, 5.600)=0.521, p=0.6086, RM one-way ANOVA with Greenhouse-Geisser correction), slow gamma (F(2.256, 6.769)=0.2001, *p*=0.8460; RM one-way ANOVA with Greenhouse-Geisser correction), or fast gamma (F(1.35, 4.051)=0.3676, *p*=0.6382, RM one-way ANOVA with Geisser-Greenhouse correction) frequency bands (data not shown).

2.3.3 Acute chemogenetic inhibition of CA2 pyramidal cells inhibits hippocampal slow gamma oscillations and induces hippocampal beta oscillations

Based on our finding that engagement of the Gq-coupled signaling pathway in CA2 pyramidal cells of hM3Dq-expressing mice increased synchronized neuronal activity in the slow gamma frequency range, we hypothesized that acute inhibition of CA2 pyramidal neurons through engagement of the Gi-coupled singling pathway would have the opposite effect: a reduction in slow gamma power during running, a behavior in which endogenous hippocampal gamma power is elevated. To test our hypothesis, we recorded LFPs from the pyramidal cell layer of *Amigo2*-icreERT2+ and control *Amigo2*-icreERT2- mice bilaterally infused with hM4Di, treated with tamoxifen, and implanted with wire bundle electrodes. Using the same type of analysis as for hM3Dq experiments, we compared LFPs filtered in the theta (5-10 Hz), beta (14-18 Hz), slow gamma (30-60 Hz), and fast gamma (65-100 Hz) frequency ranges during periods of running and resting 30-60 minutes following CNO (5 mg/kg) or vehicle administration. Power spectral densities are shown for *Amigo2*-icreERT2- (**Figure 2.6 A**) and *Amigo2*-icreERT2+ (**Figure 2.6 B**) mice. In contrast to the observed increases in theta power in *Amigo2*-icreERT2+ mice as a result of activating CA2 pyramidal cells, acute inhibition of CA2 with CNO did not affect theta power during running ($t(7)=0.7786$, $p=0.4617$, two-tailed paired t-test) (**Figure 2.6 C, left**) or periods of rest ($t(7)=2.214$, $p=0.0625$, two-tailed paired t-test) (**Figure 2.6 C, right**). Consistent with the observed increases in beta power following activation of CA2 pyramidal cells, inhibition of CA2 with CNO revealed a significant decrease in beta power during running ($t(7)=2.401$, $p=0.0474$, two-tailed paired t-test (**Figure 2.6 D, left**); however, no change was observed during periods of rest ($t(7)=0.7453$, $p=0.0625$, two-tailed paired t-test) (**Figure 2.6 D, right**). Consistent with our hypothesis, inhibition of CA2 with CNO revealed a significant reduction in slow gamma power during running ($t(7)=4.408$, $p=0.0031$, two-tailed paired t-test) (**Figure 2.6 E, left**); however, no change was observed during periods of rest ($t(7)=0.4522$, $p=0.6648$, two-tailed paired t-test) (**Figure 2.6 E, right**). Treatment with CNO did not significantly alter fast gamma power relative to vehicle during running ($t(7)=2.029$, $p=0.0821$, two-tailed paired t-test) (**Figure 2.6 F, left**) or periods of rest ($t(7)=0.172$, $p=0.8683$, two-tailed paired t-test) (**Figure 2.6 F, right**). In contrast to the effects observed in *Amigo2*-icreERT2+ mice, no significant effects of CNO were observed in control *Amigo2*-icreERT2- mice during periods of running for the theta ($t(4)=0.5724$, $p=0.5977$, two-tailed paired t-test), beta ($t(4)=0.6657$, $p=0.5420$, two-tailed paired t-test), slow gamma ($t(4)=1.079$, $p=0.3413$, two-

tailed paired t-test), or fast gamma (t(4)=1.101, p=0.3329, two-tailed paired t-test) frequency bands (data not shown). Similarly, no significant effects of CNO were observed in control *Amigo2*-icreERT2- mice during periods of rest for the theta (t(4)=0.3356, p=0.7540, two-tailed paired t-test), beta (t(4)=0.1184, p=0.9115, two-tailed paired t-test), slow gamma (t(4)=0.4089, p=0.7036, two-tailed paired t-test), or fast gamma (t(4)=0.4324, p=0.6878, two-tailed paired t-test) frequency bands (data not shown).

2.4 Discussion

In this study, we used excitatory and inhibitory DREADDs to reversibly modify activity of CA2 pyramidal cells and examined the effects on hippocampal neuronal oscillations in the pyramidal cell layer of CA2/proximal CA1. We found that increasing activity of CA2 pyramidal cells by engaging the Gq-coupled signaling pathway robustly increased hippocampal slow gamma power and reduced beta power. Conversely, inhibiting CA2 pyramidal cell output by engaging the Gi-coupled signaling pathway decreased hippocampal slow gamma power during running by approximately 20% and increased beta power by a similar magnitude. These findings demonstrate that manipulation of the endogenous Gq- and Gi-signaling pathways in CA2 can bidirectionally modulate hippocampal oscillations in the beta and slow gamma frequency ranges, and suggest a role for CA2 in oscillations naturally induced by running.

When recording in the pyramidal cell layer of the hippocampus from actively spiking neurons, increases in gamma power detected in the LFP indicate increases in local network entrainment. Interestingly, the magnitude of the hM3Dq-mediated increase in slow gamma power appears to be attenuated during periods of running. This is apparent in the spectrograms presented in figure 2.4 B, in which periods of running can be identified by a robust increase in theta power (~8 Hz), as well as in the PSDs presented in figure 2.5 E, where the magnitude of the hM3Dq-induced slow gamma power at the 4.0 mg/kg CNO dose is approximately four-fold larger relative to vehicle during periods of rest, but only about 50% larger during periods of running. One possible explanation for this observation is that some portion of the same neurons are recruited for synchronization in the gamma frequency range regardless of the inputs or behavioral demands driving synchronization. The naturally occurring increases in gamma power observed during running may involve the same neurons engaged by the hM3Dq manipulation, resulting in a disruption of the synchronized timing imposed by hM3Dq activation. Because chemogenetic tools are an artificial means of manipulating neuronal activity, it is perhaps not surprising

that activation of cells using this approach could interfere with endogenous synchronization mechanisms. Accordingly, although the robust, long-lasting induction of gamma power through hM3Dq activation reported here does not resemble the short bursts of increased gamma power observed during natural behaviors (Colgin & Moser, 2010), the propensity of the network to readily synchronize in the slow gamma frequency range suggests a role for neural activity in this frequency range in CA2-mediated functions, including social and spatial memory.

Acute inhibition of CA2 through the endogenous Gi-signaling pathway reduced slow gamma power during running by approximately 20%. Slow gamma oscillations observed in CA1 have previously been shown to depend on Schaffer collateral input from CA3 pyramidal cells (Bragin et al., 1995). However, permanent silencing of CA3 neurotransmitter release with a genetically targeted tetanus toxin light chain construct produced only a 30% reduction in slow gamma power recorded in CA1 (Middleton & McHugh, 2016), thereby challenging the notion that CA3 is the sole origin of hippocampal slow gamma oscillations. Our results demonstrate that CA2 innervation also contributes to slow gamma generation and, although the magnitude of reduction was smaller compared to silencing CA3 with tetanus toxin light chain, hM4Di was previously reported to substantially, but not entirely, inhibit synaptic neurotransmitter release (Stachniak, Ghosh, & Sternson, 2014). Thus, complete silencing of CA2 may reduce slow gamma power by greater than the 20% observed here. The most likely scenario is that complete silencing of both CA2 and CA3 is required to abolish endogenous hippocampal slow gamma oscillations during running. Based on these findings, CA2 and CA3 together likely provide the excitatory drive required to generate hippocampal slow gamma oscillations; however, due to the brain's plastic nature and ability to dynamically reassign function following insult, it would not be unexpected that upon inhibiting CA2, CA3 or another source would be capable of compensating for the initial loss following some passage of time. Further, because CA2 and CA3 preferentially innervate the deep and superficial CA1 pyramidal neurons, respectively (Kohara et al., 2014; S. H. Lee et al., 2014), gamma oscillations arising from the two areas may be actively engaging distinct hippocampal circuits and, consequently, serve distinct cognitive functions based on the output of these two populations.

Our findings also revealed a role for CA2 in modulating beta oscillations in that CA2 activation decreased beta power during resting, while CA2 inhibition increased beta power during running. Although

oscillations in the beta frequency band have been studied far less in the hippocampus than the theta and gamma oscillations, they are thought to contribute to hippocampal novelty detection, as beta power is increased upon exposure to a novel environment and decreases with subsequent exposures (Berke, Hetrick, Breck, & Greene, 2008; Grossberg, 2009). A role for CA2 in novelty detection is perhaps unsurprising, given the recent findings that CA2 place fields remap in response to exposure to novel environmental stimuli, social and otherwise (Alexander et al., 2016), as well as other studies demonstrating CA2's responsiveness to novelty (Lu et al., 2015; Wintzer, Boehringer, Polygalov, & McHugh, 2014), even when there is no social component involved in the task.

Here, we have provided evidence that modulation of the endogenous Gq- and Gi- signaling pathways in CA2 pyramidal cells can bi-directionally control hippocampal slow gamma and beta oscillations during periods of running and rest. In line with traditional views of rodent hippocampal function, and prior studies demonstrating CA2 contributions to spatial cognition, these data support the idea that CA2 participates in spatial processing by contributing to the organization of hippocampal oscillations naturally induced by running. One possible role for CA2-dependent gamma oscillations could be aiding the formation and retrieval of spatial representations formed by place cells, either locally in CA2, or downstream in CA1. Further, the propensity of the CA2 network to readily synchronize in the slow gamma frequency range suggests a role for this frequency of neural activity in CA2-dependent functions, including social and spatial memory. Accordingly, we next asked if CA2 activity contributes to the organization of hippocampal oscillations during investigation of social stimuli relative to non-social ones.

2.5 Figures

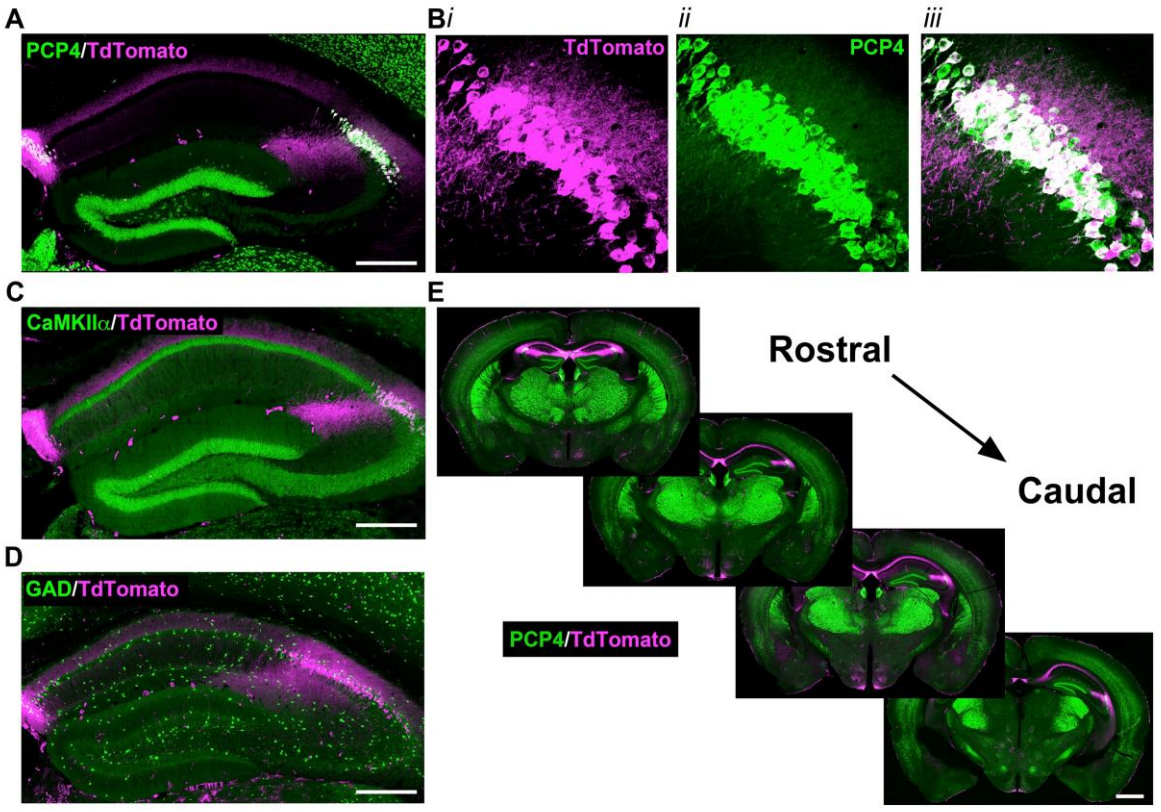

Figure 2.1: Expression of the Cre indicator, tdTomato, in *Amigo2*-icreERT2+; ROSA-tdTomato+ mice. Cre-dependent tdTomato expression colocalized with PCP4 and CaMKIIα but not GAD. (**A**) Coronal sections showing expression of Cre protein from *Amigo2-icreERT2*+ mice crossed to a ROSA-tdTomato+ reporter line and treated with tamoxifen. (**B**) Co-expression of tdTomato and PCP4, a marker for CA2 pyramidal neurons in the hippocampus. (**C**) Co-expression of tdTomato and CaMKIIα, a marker for principal neurons in the hippocampus. (**D**) Expression of tdTomato and GAD, a marker for inhibitory neurons. (**E**) Expression of tdTomato colocalizes with expression of PCP4 across the rostral to caudal extent of CA2. Scale bars = (**A**, **C**, **D**) 200 μm, (**B**) 50 μm, and (**E**) 1 mm.

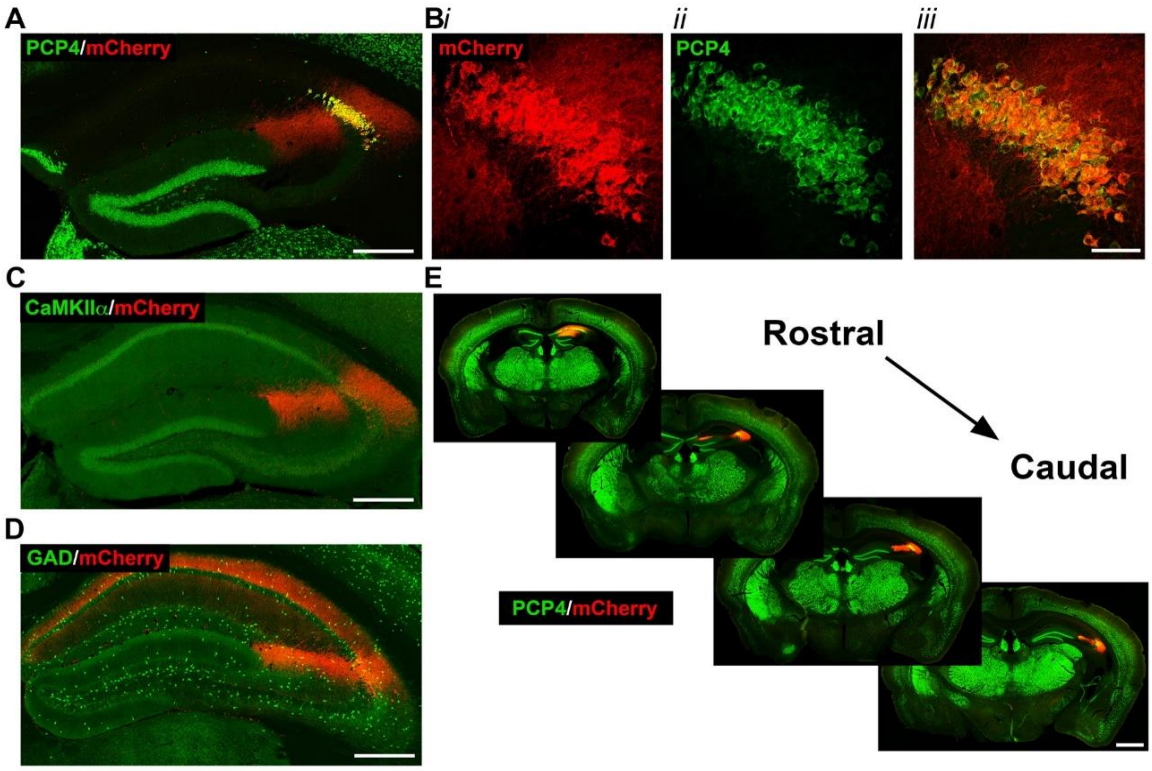

Figure 2.2: Selective expression of hM3Dq-mCherry-tagged DREADD receptors in CA2 pyramidal cells of *Amigo2*-icreERT2+ mice. Coronal sections from *Amigo2-icreERT2+* mice infused unilaterally with AAV-hSyn-DIO-hM3Dq-mCherry and treated with tamoxifen. Cre-dependent expression of mCherry colocalized with PCP4 and CaMKIIα, but not GAD. (**A**) Expression of hM3Dq-mCherry and PCP4, a marker for CA2 pyramidal cells. (**B**) Expression pattern of (*i*) hM3Dq-mCherry, (*ii*) PCP4 and (*iii*) the merged image. No evidence of mCherry expression was found outside of the PCP4 expressing region of the hippocampus. (**C**) Co-expression of hM3Dq-mCherry and CaMKIIα, a marker for hippocampal principal neurons. (**D**) Expression of hM3Dq-mCherry and GAD, a marker for inhibitory neurons. (**E**) Expression of hM3Dq-mCherry co-localizes with PCP4 across the rostral to caudal extent of CA2. Scale bars = (**A**, **C**, **D**) 200 µm, (**B**) 50 µm, and (**E**) 1 mm.

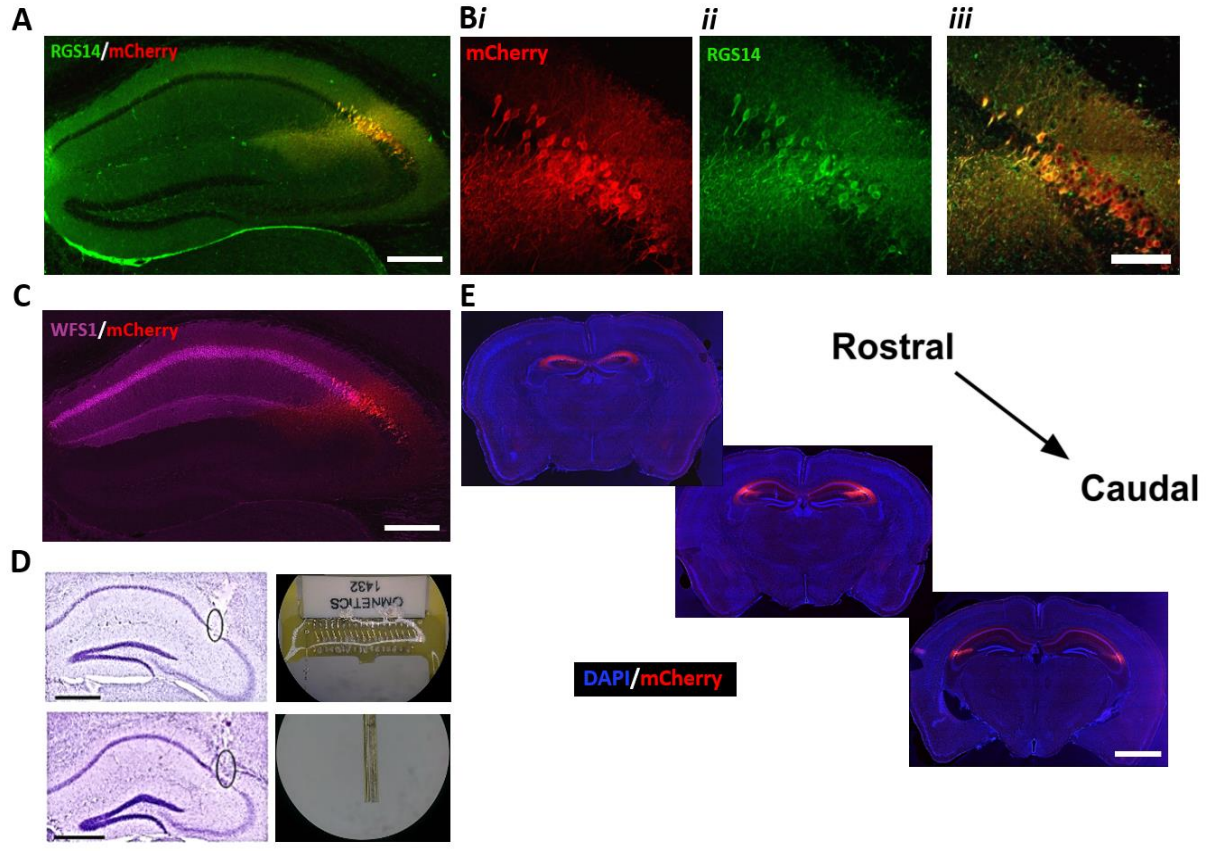

Figure 2.3: Selective expression of hM4Di-mCherry-tagged DREADD receptors in CA2 pyramidal cells of *Amigo2*-icreERT2+ mice. Coronal sections from *Amigo2-icreERT2+* mice infused bilaterally with AAV-hSyn-DIO-hM4Di-mCherry and treated with tamoxifen. (**A**) Co-expression of hM4Di and RGS14, a marker for CA2 pyramidal cells. (**B**) Expression pattern of (*i*) hM4Di, (*ii*) RGS14 and (*iii*) the merged image**.** No evidence of mCherry expression was found outside of the RGS14 expressing region. (**C**) Expression of hM4Di and WFS1, a marker for CA1 principal neurons. Cre-dependent expression of mCherry co-localized with expression of RGS14, but not WFS1. (**D**) Example electrode board (top right) and wire bundles (bottom right) used to acquire in vivo electrophysiology data and representative recording location in CA2/proximal CA1 (Nissl stain; tracks surrounded by black ellipses). (**E**) Expression of hM4Di provides coverage of CA2 across the rostral to caudal extent of the hippocampus. Scale bars = (**A**, **C**, **D**) 200 μm, (**B**) 50 μm, and (**E**) 1 mm.

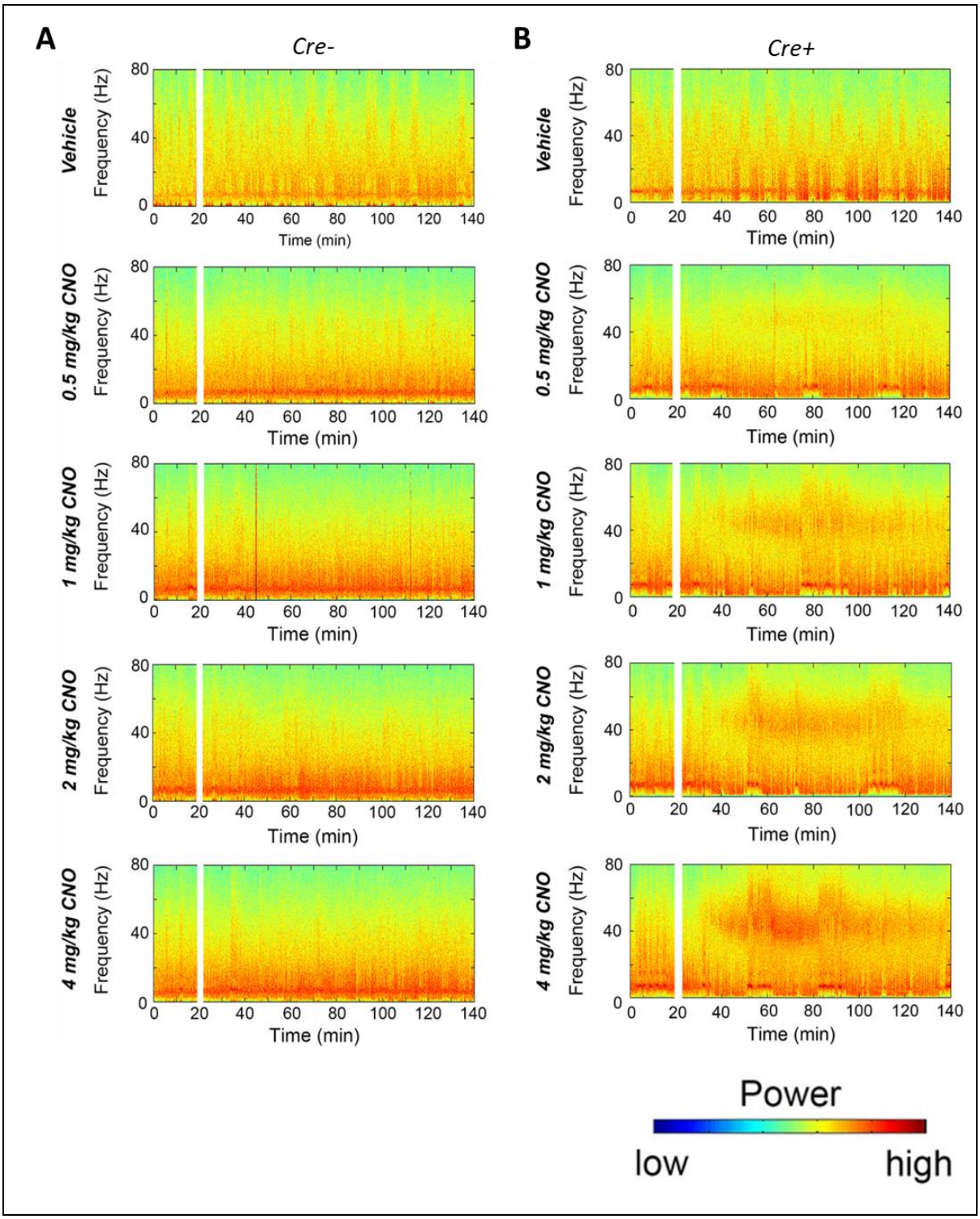
A
Cre-
B
Cre+
Vehicle
0.5 mg/kg CNO
1 mg/kg CNO
2 mg/kg CNO
4 mg/kg CNO
Frequency (Hz)
Time (min)
Power
low
high

Figure 2.4: CNO dose-dependently increases slow gamma power in the pyramidal cell layer of the hippocampus in *Amigo2*-icreERT2+ mice infused with hM3Dq-mCherry. Spectrograms of hippocampal LFP recordings from (**A**) *Amigo2*-icreERT2- and (**B**) *Amigo2*-icreERT2+ mice. Time (minutes) is represented on the X-axis. Frequency is represented on the Y-axis. Vehicle or CNO was administered at the 20-minute time point and is denoted by the white bar. Treatment level is shown to the left of each spectrogram. Spectral analysis was performed using a Fourier transform of the LFP from a 140-minute recording session in which subjects could freely explore an open field arena.

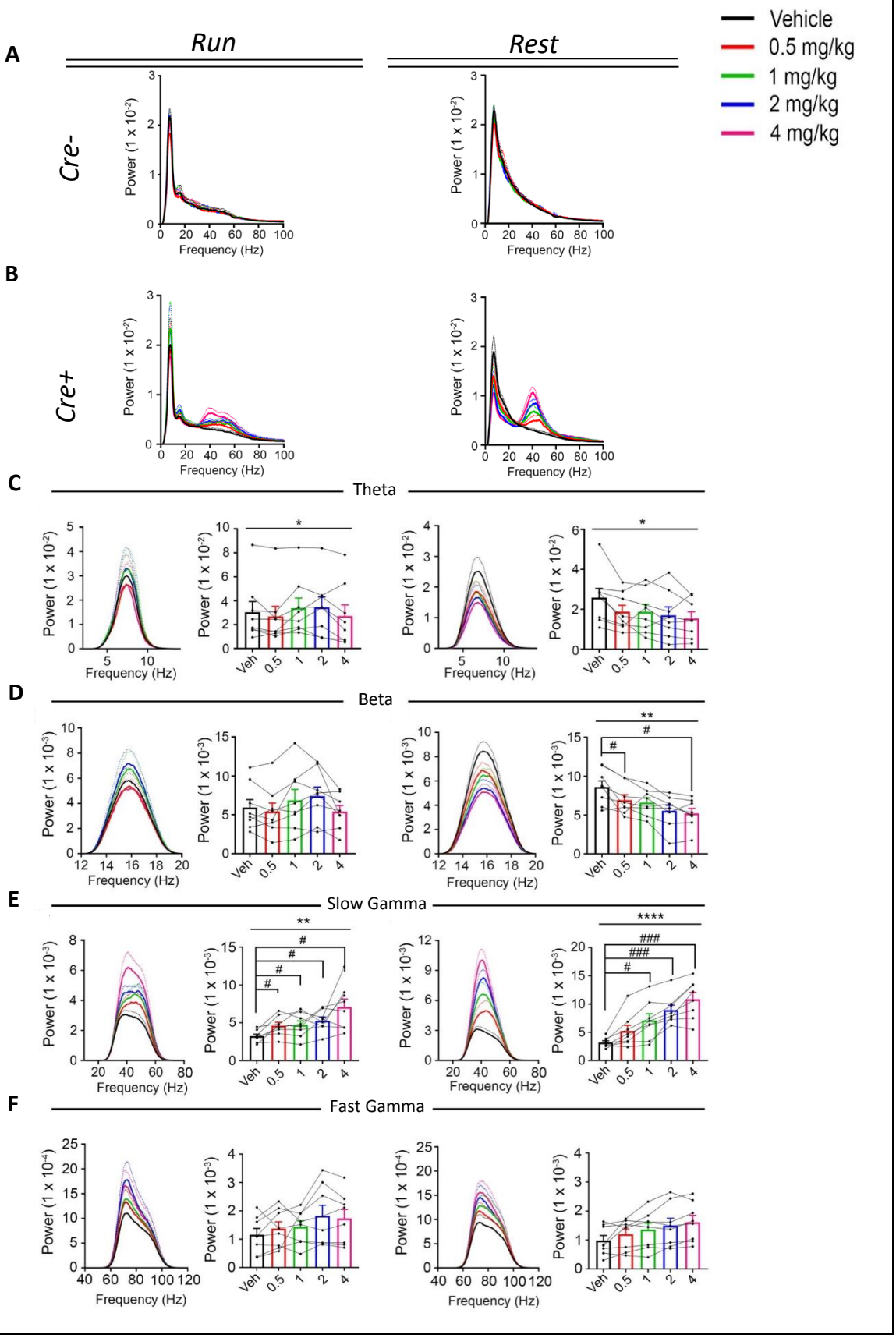
Vehicle
0.5 mg/kg
1 mg/kg
2 mg/kg
4 mg/kg
A
Run
Rest
Cre-
B
Cre+
Power (1 x 10-2)
Frequency (Hz)
C
Theta
Power (1 x 10-2)
Frequency (Hz)
Veh
0.5
1
2
4
D
Beta
Power (1 x 10-3)
E
Slow Gamma
F
Fast Gamma
Power (1 x 10-4)

Figure 2.5: Activation of CA2 pyramidal cells with CNO in hM3Dq-infused *Amigo2*-icreERT2+ mice dose-dependently increases slow gamma power in the hippocampus. Power spectral densities of hippocampal LFP recordings measured 30-60 minutes following treatment with vehicle or CNO from (**A**) *Amigo2*-icreERT2- and (**B**) *Amigo2*-icreERT2+ mice during periods of running (left column) or resting (right column). PSDs were computed using a Fourier transform of the 1-100Hz LFP during periods of exploration of an open field arena. For (**C-F**) all data are from *Amigo2*-icreERT2+ mice during periods of running (left column) and resting (right column). The left sub-panel of each plot show the group average power spectral density with standard error of the mean (dotted line) and the right sub-panel shows the mean peak power for the population of animals in colored bars. Individual subject values are shown as black dots. (**C**) CNO significantly decreased theta (5-10 Hz) power during rest ($F(1.972, 13.81)=4.825$, $p=0.0261$, repeated-measures one-way ANOVA with Geisser-Greenhouse correction) and varied significantly during run (Friedman statistic=11.3; p=0.0234; results of *post hoc* tests not significant). (**D**) CNO produced a significant decrease in beta (14-18 Hz) power during rest ($F(1.408, 9.857)=10.07$, $p=0.0066$, repeated-measures one-way ANOVA with Geisser-Greenhouse correction; results of Holm-Sidak *post hoc* tests are shown by symbols), but did not did not affect beta power during running ($F(2.274, 15.91)=2.91$, $p=0.0784$, repeated-measures one-way ANOVA with Geisser-Greenhouse correction). (**E**) CNO produced a significant, dose-dependent increase in slow gamma (30-60 Hz) power during running ($F(1.904, 13.33)=9.457$, $p=0.0030$, repeated-measures one-way ANOVA with Geisser-Greenhouse correction; results of Holm-Sidak *post hoc* tests are shown by symbols) and during rest ($F(2.306, 16.15)=32.2$), $p<0.0001$, repeated-measures one-way ANOVA with Geisser-Greenhouse correction; results of Holm-Sidak *post hoc* tests are shown by symbols). (**F**) CNO did not significantly affect high gamma (65-100 Hz) power during running ($F(1.384, 9.69)=2.288$, $p=0.1602$, repeated-measures one-way ANOVA with Geisser-Greenhouse correction) or during rest ($F(1.286, 9.003)=4.775$, $p=0.0501$, repeated-measures one-way ANOVA with Geisser-Greenhouse correction for unequal variance). *$p<0.05$, **$p<0.01$, ****$p<0.0001$, one-way ANOVA; #$p<0.05$, ###$p<0.001$, Holm-Sidak *post hoc* test.

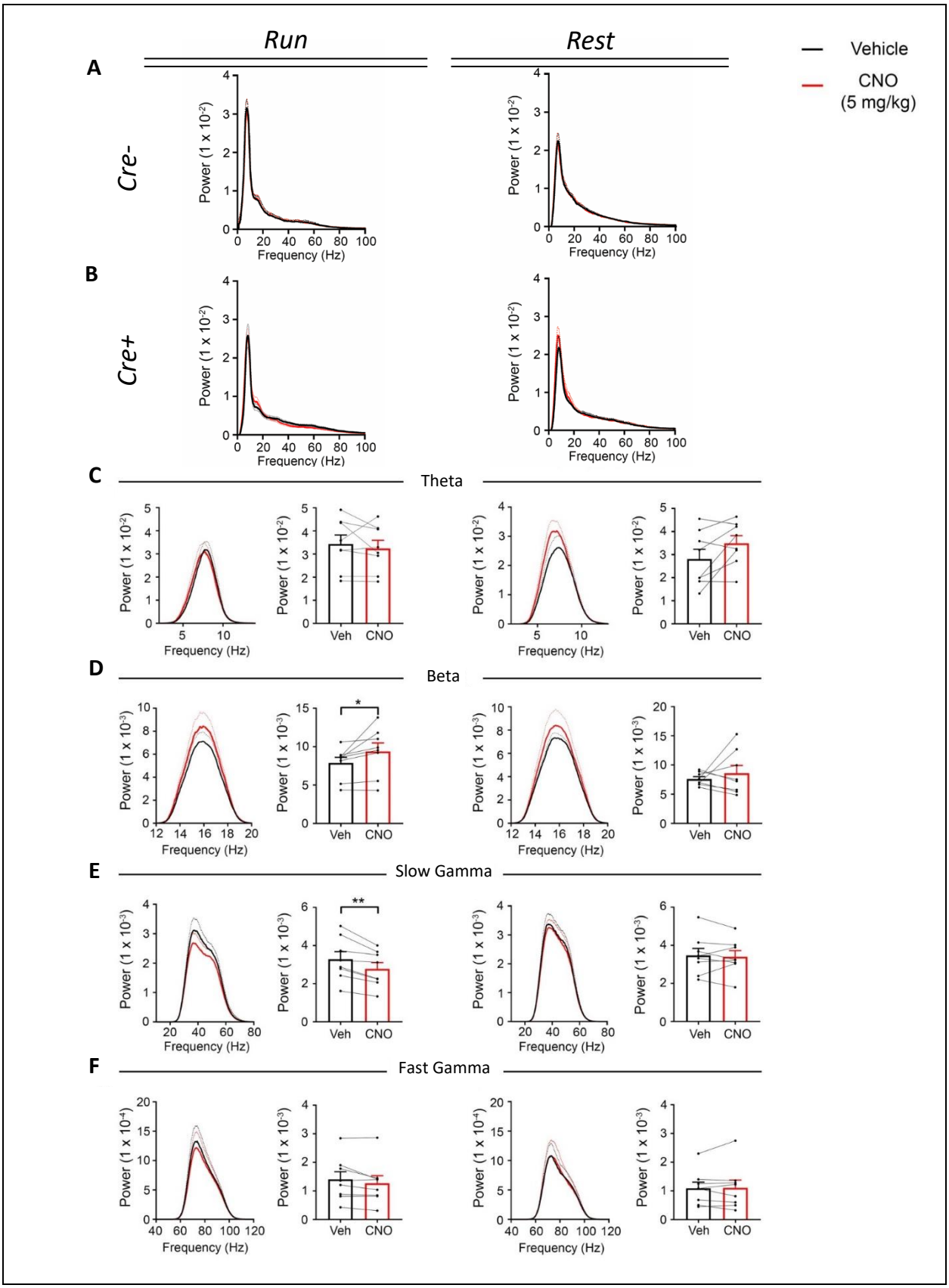
Run
Rest
Vehicle
CNO
(5 mg/kg)
A
Cre-
B
Cre+
C
Theta
D
Beta
E
Slow Gamma
F
Fast Gamma
Power (1 x 10-2)
Power (1 x 10-3)
Power (1 x 10-4)
Frequency (Hz)
Veh
CNO
*
**

Figure 2.6: Inhibition of CA2 pyramidal cells with CNO in hM4Di-infused *Amigo2*-icreERT2+ mice decreases slow gamma power in the hippocampus. Power spectral densities of hippocampal LFP recordings measured 30-60 minutes following treatment with vehicle or CNO (5mg/kg) from (**A**) *Amigo2*-icreERT2- and (**B**) *Amigo2*-icreERT2+ mice during periods of running (left column) or resting (right column). PSDs were computed using a Fourier transform of the 1-100Hz LFP during periods of exploration of an open field arena. For (**C-F**) all data are from *Amigo2*-icreERT2+ mice during periods of running (left column) and resting (right column). The left sub-panel of each plot show the group average power spectral density with standard error of the mean (dotted line) and the right sub-panel shows the mean peak power for the population of animals in colored bars. Individual subject values are shown as black dots. (**C**) CNO did not affect theta band (5-10 Hz) power during running ($t(7)=0.7786$, $p=0.4617$) or periods of rest ($t(7)=2.214$, $p=0.0625$). (**D**) CNO produced a significant increase in beta power during running ($t(7)=2.401$, $p=0.0474$, two-tailed paired t-test), but had no affect during periods of rest ($t(7)=0.7453$, $p=0.0625$). (**E**) CNO produced a significant decrease in hippocampal slow gamma power during running ($t(7)=4.408$, $p=0.0031$, two-tailed paired t-test), but had no affect during periods of rest ($t(7)=0.4522$, $p=0.6648$). (**F**) CNO did not significantly affect high gamma power during running ($t(7)=2.029$, $p=0.0821$) or periods of rest ($t(7)=0.172$, $p=0.8683$).

CHAPTER 3. CHEMOGENETIC MODULATION OF GI-COUPLED GPCR SIGNALING IN CA2 INHIBITS CA1 SLOW AND FAST GAMMA OSCILLATIONS IN A LAYER-SPECIFIC MANNER DURING INVESTIGATION OF NOVEL STIMULI

3.1 Overview of Findings

In this study we used inhibitory DREADDs to reversibly modify CA2 pyramidal cell activity and examine the effects on neuronal oscillations in the different layers of CA1. Given the evidence for CA2's role in social memory (Hitti & Siegelbaum, 2014), our previous evidence demonstrating CA2's ability to bi-directionally modulate hippocampal slow gamma oscillations during running, and evidence that the output of CA3 is reflected in pathway-specific LFPs in CA1 (Fernandez-Ruiz, Makarov, Benito, & Herreras, 2012), we hypothesized that CA2 pyramidal cells may also coordinate activity in the slow gamma frequency range when exposed to a social stimulus. Based on this hypothesis we formed two predictions: 1) Neuronal activity in the gamma frequency range, as measured by increases in LFP power, would increase in stratum oriens and the pyramidal cell layer of CA1 during investigation of a novel animal, but not a novel object and 2) Inhibition of CA2 pyramidal cells with hM4Di during this behavior would cause the observed increase in slow gamma power to be reduced or abolished.

To test our hypothesis and address these predictions, we implanted silicone probes with a linear array of electrode contacts that permitted sampling of LFPs from all layers of CA1 in mice expressing hM4Di in CA2 neurons. We then recorded LFPs while subjects investigated a novel animal or novel object and examined the effects on oscillatory power. To explore possible effects of CA2 inhibition on oscillatory activity in the different layers of CA1, we first ran a series of independent, repeated measures, two-way ANOVAs to analyze each frequency band of interest, in each layer, using all experimental conditions (Vehicle-Animal, Vehicle-Object, CNO-Animal, and CNO-Object). Our analyses were aimed toward identifying effects of drug treatment (vehicle vs. CNO) (**Figures 3.2 - 3.5**) and stimulus type (animal vs. object.) (**Figures 3.6 - 3.9**).

We found that acute, reversible inhibition of CA2 pyramidal cells in awake, behaving mice selectively reduces hippocampal CA1 oscillatory power in a layer- and frequency-specific manner.

Specifically, inhibition of CA2 pyramidal cells caused a significant reduction in slow and fast gamma power in the pyramidal cell layer and stratum oriens, and in fast gamma power in stratum radiatum. No significant changes in power in stratum lacunosum-moleculare were detected. While the magnitude of gamma reduction in the pyramidal cell layer and stratum oriens tended to be larger when the stimulus presented was a novel animal relative to a novel object, with fast gamma in stratum pyramidal being the one exception, CA2 inhibition showed a similar overall effect of reducing gamma power regardless of the stimulus type. Consistent with our hypotheses, these results reveal a role for CA2 output in coordinating hippocampal gamma oscillations during investigation of novel stimuli, and demonstrate that the state- and frequency- dependent organization of gamma oscillations in CA1 in vivo relies on CA2 output. In contrast to our hypothesis, although we found that the magnitude of gamma reduction tended be larger when the stimulus presented was a novel object relative to a novel animal, we did not find a significant difference in gamma power reduction between the stimulus conditions, suggesting that rather than serving exclusively as a social memory hub, CA2 pyramidal cells may serve a more general episodic memory function that signals novelty within the hippocampal circuits.

3.2 Methods

Mice: All animals (>8 weeks old) were maintained on a 12:12 light/dark cycle with *ad libitum* access to food and water. All subjects were male. Mice were naïve to any treatment, procedure or testing at the beginning of the experiments described here. Mice were group-housed until the time of virus infusion, at which point they were singly housed. All procedures were approved by the NIEHS Animal Care and Use Committee and were in accordance with the National Institutes of Health guidelines for care and use of animals.

Viruses: All AAV viruses were produced by the Gene Therapy Center Vector Core at the University of North Carolina at Chapel Hill and had titers of $>10^{12}$ genome copies/mL. For chemogenetic manipulation using hM4Di-mCherry, mice were bilaterally infused with 0.5 µl of AAV5-hsyn-DIO-hM4Di-mCherry into each hemisphere of the brain.

Stereotaxic virus infusions and tamoxifen treatment: For virus-infusion surgery, mice were anesthetized with ketamine (100 mg/kg, IP) and xylazine (7 mg/kg, IP), then placed in a stereotaxic apparatus while on a heated pad. Sedation was maintained with 1.5-2.5% isoflurane during surgery if

animals regained reflex responses at any point during the surgery. Following 3 alternating swabs with betadine and 70% ethanol, an incision was made down the midline of the scalp, a burr hole was drilled above each target region and viruses were microinjected using a 1 µl Neuros Hamilton syringe at a rate of 100 nl/min. Following infusion, the needle was left in place for 5 additional minutes to allow for diffusion of the virus before slowly being withdrawn. Injection coordinates for CA2 were (in mm: -2.30 AP, +/-2.50 ML, -1.90 mm DV from bregma). The scalp was then sutured shut and animals were administered buprenorphine (0.1 mg/kg, SQ) for pain and returned to their cages. Two weeks following AAV infusion, *Amigo2*-icreERT2 mice began daily tamoxifen treatments (100 mg/kg tamoxifen dissolved in warmed corn oil, IP) for a total of seven days. Animals were allowed to recover from tamoxifen treatment for 1 week before undergoing electrode implantation to allow sufficient time for estrogen receptor translocation to the nucleus and subsequent recombination.

Electrode implantation: At least one week after the last tamoxifen treatment, mice for in vivo electrophysiology were implanted with NeuroNexus silicone electrodes. Mice were anesthetized with ketamine (100 mg/kg, IP) and xylazine (7 mg/kg, IP), then placed in a stereotaxic apparatus. An incision was made in the scalp, and the skull was cleaned and dried. One reference wire screw (positioned approximately 4 mm posterior and 2 mm lateral to Bregma over the right hemisphere), one ground screw (positioned in the skull over the cerebellum), and three anchor screws were secured to the skull. Electrodes were then lowered into the hole drilled over dorsal CA1 (in mm: -1.30 AP, -1.40 ML, -1.85 DV from bregma). The NeuroNexus electrode was configured to use a single reference channel and the ground and reference wires were attached to the appropriate screws as designated above. The A1x32 electrode design has 32 recording sites spaced evenly apart (25 µm) along a single, linear shank providing a total coverage range of 775 µm.

Neurophysiological data acquisition and behavioral tracking: Neural activity was transmitted via a 32-channel wireless 10× gain head stage (Triangle BioSystems International, Durham, NC) and was acquired using the Cerebus acquisition system (Blackrock Microsystems, Salt Lake City, UT). Continuous LFP data were band-pass filtered at 0.3–500 Hz and stored at 1,000 Hz. Single unit data were sampled at 30 kHz and high-pass filtered at 250 Hz. For behavioral tracking, videos of recording sessions were acquired with a sampling rate of 30Hz using the Neuromotive Software (Blackrock Microsystems) and

infrared camera. Behavior was analyzed offline using the Ethovision XT (Noldus, Wageningen, Netherlands) behavioral tracking software. Subject's smoothed instantaneous velocity was used to isolate periods of running from periods of relative immobility. Samples in which the animal's smoothed instantaneous velocity exceeded a threshold of ≥ 7 cm/sec were designated as periods of running and excluded from analysis. For isolation of periods in which subjects were investigating stimuli, a virtual 10cm circle was drawn around the area of the cage in which a stimulus were presented and periods in which the subject's body, nose, or tail were located within the circle were considered periods of active investigation. For any analyses presented during which stimuli were present, only samples in which subjects were both immobile and actively investigating the stimulus were used. All indexed tracking information was exported from Ethovision XT to Microsoft Excel files which were then used to select LFP samples from behavioral periods of interest in Matlab.

Experimental paradigm: We recorded one session per day for eight sequential days, with CNO and vehicle treatments alternating across days. All recordings were made during the animal's light phase under red light illumination to encourage exploration. For these experiments, animals were allowed to freely explore a clear plexiglass cage (40.5cm x 24.5cm). Bedding was placed in the bottom of the cage (as in their home cages) to encourage exploration. Curtains surrounded the cage to prevent viewing of the experimental room and limit light exposure. Forty minutes prior to the start of each experiment subjects were administered CNO (3.0mgkg) or an equivalent volume of saline and returned to their home cages outside the recording room. Ten minutes prior to the start of the experiments, subjects were lightly anesthetized to allow attachment of the wireless head stage and were transferred to the recording room where room lights were turned off and red lights were illuminated. Five minutes prior to the start of the experiment subjects were transferred from their home cage to the recording cage and allowed to habituate for 5 minutes before. For the first 5 minutes of each recording session no stimulus was present and this phase was used as a baseline period to assess possible effects of CNO on the subjects' mobility levels. For the last 5 minutes of each session a novel animal or novel object was inserted into the recording cage and only periods in which the subject was actively investigating a stimulus were used for subsequent behavioral and spectral analysis.

Electrophysiology data analysis: All neuronal data analyses were performed with Matlab (MathWorks, Inc., Natick, MA) using the Chronux toolbox (http://chronux.org/, Cold Springs Harbor, Long Island, NY) or custom written scripts for wavelet analysis. Wavelet analysis was performed using a family of 80 Morlet wavelet carrier frequencies which increased logarithmically, had a low frequency cutoff of 0.5Hz, and a high frequency cut off of 128Hz. Prior to spectral analysis noise and muscle artifacts were removed based on a 6 standard deviation rejection threshold; when detected, a 3 second window around the noise threshold crossing was removed. For each recording session, the time-frequency representation of the data was obtained by convolving the LFP with the family of wavelets to produce a vector of the same length as the original LFP data. Behavioral vectors indicating the animal's behavioral state were generated using the tracking data obtained from Ethovision XT and were used to match behaviors of interest to the appropriate LFP samples. We analyzed power for the beta (12-25 Hz), slow gamma (25-55 Hz), and fast gamma (55-100 Hz) frequencies ranges. Mean power for each frequency band of interest was calculated for each recording session. Of the eight recording days, each of the four possible drug and stimulus combinations (Vehicle-Animal, Vehicle-Object, CNO-Animal, CNO-Object) were delivered twice, and the averages from these two repeat sessions were also averaged. For group comparisons of frequency bands, all wavelet-carrier frequencies used to generate the time-frequency representation of that band were averaged together to produce a single value. For example, the slow gamma band (25-55Hz) time-frequency representation was computed with 19 of the 80 carrier wavelets. The 19 values corresponding to the 25-55Hz range were averaged to yield a single power value for the slow gamma band. These values were calculated for each frequency band from each subject and used for group comparisons of power under different behavioral conditions.

Electrode localization & immunohistochemistry: At the end of experiments, a small amount of current was passed through the bottom channel of each electrode (5 μA for 5 s) to create a small lesion that could be used in subsequent immunhistochemical experiments to aid electrode localization. Three hours after creating the lesion, animals were euthanized with Fatal Plus (sodium pentobarbital, 50 mg/mL; >100 mg/kg) and underwent transcardial perfusion with 4% paraformaldehyde. Heads with electrodes remaining implanted were submerged in 4% paraformaldehyde for 72 hours. Electrodes were carefully removed, rinsed in PBS, and sectioned at 40μm on a vibratome. For immunohistochemistry, brain

sections were rinsed in PBS, boiled in deionized water for 3 min, and blocked for at least 1 h in 3-5% normal goat serum/0.01% Tween 20 PBS. Sections were incubated in IBA1 anti-rabbit primary antibody, a marker for activated microglia (Wako, Cat.No.012-26723, 1:500). Antibodies were diluted in blocking solution and sections were incubated for 24 hours. After three rinses in PBS/Tween, sections were incubated in secondary antibody (Alexa 488 goat anti-rabbit, Invitrogen, 1:500) for 2 hours. Finally, sections were washed in PBS/Tween and mounted with Vectashield hardset mounting medium with DAPI. Images of hippocampi were acquired with a slide scanner using the Aperio Scanscope FL Scanner (Leica Biosystems Inc.). The slide scanner uses a monochrome TDI line-scan camera, with a PC-controlled mercury light source to capture high resolution, seamless digital fluorescent images.

Sample size and group assignment: For all experiments presented, 19 *Amigo2*-icreERT2 (10 *Amigo2*-icreERT2+ and 9 *Amigo2*-icreERT2-) mice were used. *Amigo2*-icreERT2 mice were randomly selected from individual litters. No specific method of randomization was used to assign groups. Whenever possible, Cre+ and Cre- mice from the same litter were used. Animals were housed with same-sex littermates following weaning, but before genotyping. Pre-established criteria for excluding mice from analysis included 1) missed electrode implantation 2) equipment failures during testing 3) insufficient investigation of experimental stimuli, with a minimum of 10 seconds required to be included in the analysis. Sample sizes were based on the expected variances from previous behavioral and electrophysiological experiments.

Statistical analysis of power: For some frequency bands and layers, the ANOVA revealed a significant main effect of CNO, but not a main effect of stimulus type, that segregated according to stimulus type in subsequent t-test comparisons. To address the possibility that the lack of significance from t-test comparisons for the object condition could have been due to insufficient statistical power, we used the program G*Power (Heinrich Heine Universität Dusseldorf, Germany) to estimate the sample size that would be required to confirm the t-test results based on our observed effect sizes, chosen level of significance ($\alpha = 0.05$), and power ($1-\beta$ err prob = 0.8). The test family used was t-tests, and the statistical test used was Means: Difference between two dependent means (two-tailed, matched pairs).

Statistical results reporting: For each experiment presented within the Results section and in figures, the number of replicates is presented as "N" when indicating the number of animals that were used for the experiment. Statistical tests used for each experiment are presented in the text. Statistical significance was based on a p-value of 0.05. All error bars in graphs represent standard error of the mean unless otherwise noted. Data are presented as means ± SEM or ± SD. To explore potential layer and frequency specific effects of our experimental manipulation, we first analyzed the data by running a series of independent, repeated measures, 2-way ANOVAs with Geisser-Greenhouse correction for unequal variance on each of the four hippocampal layers and three frequency bands of interest. Each ANOVA was a 2-factorial design and compared the four possible experimental conditions (Vehicle-Animal, Vehicle-Object, CNO-Animal, CNO-Object) for main effects of drug (vehicle vs. CNO) and socialness (animal vs. object). To further explore the relationships between variables, we also performed a series of paired t-tests to make explicit comparisons that were of *a priori* interest. For each layer and frequency band of interest, we performed four paired t-tests to further explore the effects of the drug and stimulus type manipulations. For all comparisons, *p* values were calculated using two-tailed paired *t*-tests. Differences were considered significant at *p* values below 0.05. All statistical analyses were performed using GraphPad Prism version 6 and SPSS version 21 (IBM, Armonk, NY). Figures were assembled using Adobe Illustrator and Microsoft Powerpoint.

3.3 Results

3.3.1 Acute chemogenetic inhibition of CA2 pyramidal cells decreases hippocampal slow and fast gamma power in the pyramidal layer of CA1 during investigation of novel stimuli

We previously demonstrated that engagement of the Gi-coupled signaling pathway in CA2 pyramidal cells of hM4Di-expressing mice decreased synchronized neuronal activity in the slow gamma frequency range in the pyramidal cell layer of the hippocampus during running, a time when physiological gamma power is elevated. Here we infused *Amigo2*-icreERT2+ and control *Amigo2*-icreERT2- mice with AAV-hM4Di-mCherry, treated subjects with tamoxifen, implanted silicone electrodes into CA1, and compared LFP power recorded from the pyramidal cell layer for the the beta, slow gamma, and fast gamma frequency ranges during periods in which subjects actively investigated either a novel animal or novel object.

No significant effects of CNO were observed in control *Amigo2*-icreERT2- for the beta, slow gamma, or fast gamma frequency bands under any experimental condition tested (**Figure 3.2 A**). Inhibition of CA2 pyramidal cells in *Amigo2*-icreERT2+ mice (**Figure 3.2 B**) with CNO did not affect beta power relative to vehicle during investigation of novel stimuli (F(1, 6)=0.329, *p*=0.587, RM two-way ANOVA with Geisser-Greenhouse; animal: (t(7)=0.248, *p*=0.911, two-tailed, paired t-test) (**Figure3.2 C, left**); object: (t(7)=0.813, *p*=0.423, two-tailed, paired t-test) (**Figure 3.2 C, right**). CNO did not significantly affect beta power in control *Amigo2*-icreERT2- mice F(1, 6)=4.435, *p*=0.080, RM two-way ANOVA with Geisser-Greenhouse correction; animal: (t(6)=0.337, two-tailed, paired t-test, *p*=0.748; object: (t(6)=0.341, *p*=0.745, two-tailed, paired t-test) (data not shown). Treatment with CNO revealed a significant reduction in slow gamma power relative to vehicle during investigation of a novel stimulus (F(1, 6)=14.095, *p*=0.009, RM two-way ANOVA with Geisser-Greenhouse correction; animal: (t(7)=2.845, *p*=0.025, two-tailed, paired t-test) (**Figure 3.2 D, left**); object: (t(7)=2.121, *p*=0.072, two-tailed, paired t-test) (**Figure 3.2 D, right**). CNO did not significantly affect slow gamma power in control *Amigo2*-icreERT2- mice F(1, 6)=1.040, *p*=0.347, RM two-way ANOVA with Geisser-Greenhouse correction; animal: (t(6)=0.462, *p*=0.661, two-tailed, paired t-test); object: (t(6)=0.461, *p*=0.661, two-tailed, paired t-test) (data not shown). Treatment with CNO revealed a significant reduction in fast gamma power relative to vehicle during investigation of a novel stimulus (F(1, 6)=22.836, *p*=0.003, RM two-way ANOVA with Geisser-Greenhouse correction; animal: (t(7)=4.163, *p*=0.004, two-tailed, paired t-test) (**Figure 3.2 E, left**); object: (t(7)=5.721, *p*=0.001, two-tailed paired t-test) (**Figure 3.2 E, right**). CNO did not significantly affect fast gamma power in control *Amigo2*-icreERT2- mice (F(1, 6)=3.109, *p*=0.197, RM two-way ANOVA with Geisser-Greenhouse correction; animal: (t(6)=0.348, *p*=0.740, two-tailed, paired t-test); object: (t(6)=1.124, *p*=0.304, two-tailed, paired t-test) (data not shown).

3.3.2 Acute chemogenetic inhibition of CA2 pyramidal cells decreases hippocampal slow and fast gamma power in stratum oriens during investigation of novel stimuli

Because hippocampal gamma oscillations have been shown to be regulated in a layer-specific manner (Fernandez-Ruiz et al., 2012; Lasztoczi & Klausberger, 2014, 2016; Scheffer-Teixeira et al., 2012), and CA2 inputs preferentially target specific layers of CA1 (Kohara et al., 2014; Shinohara et al., 2012; Tamamaki et al., 1988), we hypothesized that if CA2 neurons firing at the gamma frequency is important for facilitating communication between the CA2 and CA1 subfields, then frequency-specific

effects observed at the level of the pyramidal soma should also be observed in the relevant dendritic input domains of CA1. To test our hypothesis, we compared LFP power recorded from stratum oriens in the beta, slow gamma, and fast gamma frequency ranges during periods in which subjects actively investigated either a novel animal or novel object. No significant effects of CNO were observed in control *Amigo2*-icreERT2- for the beta, slow gamma, or fast gamma frequency bands under any experimental condition tested (**Figure 3.3 A**). Inhibition of CA2 pyramidal cells in *Amigo2*-icreERT2+ mice (**Figure 3.3 B**) with CNO did not affect beta power relative to vehicle during investigation of stimuli ($F(1, 6)=1.949$, $p=0.212$, RM two-way ANOVA with Geisser-Greenhouse correction; animal: ($t(7)=1.115$, $p=0.302$, two-tailed, paired t-test) (**Figure3.3 C, left**); object: ($t(7)=1.037$, $p=0.334$, two-tailed, paired t-test) (**Figure3.3 C, right**). CNO did not significantly affect beta power in control *Amigo2*-icreERT2- mice $F(1, 5)=1.814$, $p=0.236$, RM two-way ANOVA with Geisser-Greenhouse correction; animal: ($t(6)=0.625$, two-tailed, paired t-test, $p=0.560$; object: ($t(6)=1.136$, $p=0.307$, two-tailed, paired t-test) (data not shown). Treatment with CNO revealed a significant reduction in slow gamma power relative to vehicle during investigation of a novel stimulus ($F(1, 6)=7.745$, $p=0.032$, RM two-way ANOVA with Geisser-Greenhouse correction; animal: ($t(7)=2.596$, $p=0.036$, two-tailed, paired t-test) (**Figure 3.3 D, left**); object: ($t(7)=0.880$, $p=0.408$, two-tailed, paired t-test) (**Figure 3.3 D, right**). CNO did not significantly affect slow gamma power in control *Amigo2*-icreERT2- mice $F(1, 5)=0.420$, $p=0.545$, RM two-way ANOVA with Geisser-Greenhouse; animal: ($t(6)=0.493$, $p=0.643$, two-tailed, paired t-test); object: ($t(6)=1.045$, $p=0.400$, two-tailed, paired t-test) (data not shown). Treatment with CNO revealed a significant reduction in fast gamma power relative to vehicle during investigation of a novel stimulus ($F(1, 6)=10.568$, $p=0.017$, RM two-way ANOVA with Geisser-Greenhouse; animal: ($t(7)=3.222$, $p=0.015$, two-tailed, paired t-test) (**Figure 3.3 E, left**); object: ($t(7)=1.513$, $p=0.174$, two-tailed paired t-test) (**Figure 3.3 E, right**). CNO did not significantly affect fast gamma power in control *Amigo2*-icreERT2- mice $F(1, 5)=0.382$, $p=0.564$, RM two-way ANOVA with Geisser-Greenhouse correction; animal: ($t(6)=0.116$, $p=0.912$, two-tailed, paired t-test); object: ($t(6)=1.241$, $p=0.270$, two-tailed, paired t-test) (data not shown).

3.3.3 Acute chemogenetic inhibition of CA2 pyramidal cells decreases hippocampal fast gamma power in stratum radiatum during investigation of novel stimuli

We next asked whether inhibition of CA2 pyramidal cells affects oscillatory power in stratum radiatum. We hypothesized that oscillations would not be significantly impacted by this manipulation because a minority of CA2 inputs contact CA1 dendrites in this layer. No significant effects of CNO were observed in control *Amigo2*-icreERT2- for the beta, slow gamma, or fast gamma frequency bands under any experimental condition tested (**Figure 3.4 A**). Inhibition of CA2 pyramidal cells in *Amigo2*-icreERT2+ mice (**Figure 3.4 B**) with CNO did not affect beta power relative to vehicle during investigation of stimuli ($F(1, 6)=0.913$, $p=0.376$, RM two-way ANOVA with Geisser-Greenhouse correction; animal: ($t(7)=0.738$, $p=0.488$, two-tailed, paired t-test) (**Figure3.4 C, left**); object: ($t(7)=1.027$, $p=0.334$, two-tailed, paired t-test) (**Figure3.4 C, right**). CNO did not significantly affect beta power in control *Amigo2*-icreERT2- mice $F(1, 6)=1.123$, $p=0.330$, RM two-way ANOVA with Geisser-Greenhouse correction; animal: ($t(6)=0.075$, $p=0.942$, two-tailed, paired t-test; object: ($t(6)=0.213$, $p=0.839$, two-tailed, paired t-test) (data not shown). Treatment with CNO did not significantly affect slow gamma power relative to vehicle during investigation of a novel stimulus ($F(1, 6)=1.889$, $p=0.218$, RM two-way ANOVA with Geisser-Greenhouse correction; animal: ($t(7)=1.184$, $p=0.281$, two-tailed, paired t-test) (**Figure 3.4 D, left**); object: ($t(7)=1.011$, $p=0.351$, two-tailed, paired t-test) (**Figure 3.4 D, right**). CNO did not significantly affect slow gamma power in control *Amigo2*-icreERT2- mice $F(1, 6)=0.0265$, $p=0.878$, RM two-way ANOVA with Geisser-Greenhouse correction; animal: ($t(6)=0.358$, $p=0.733$, two-tailed, paired t-test) (**Figure 3.4 D, left**); object: ($t(6)=0.582$, $p=0.582$, two-tailed, paired t-test) (data not shown). Treatment with CNO revealed a significant reduction in fast gamma power relative to vehicle during investigation of a novel stimulus ($F(1, 6)=11.054$, $p=0.016$, RM two-way ANOVA with Geisser-Greenhouse correction; animal: ($t(7)=1.778$, $p=0.126$, two-tailed, paired t-test) (**Figure 3.4 E, left**); object: ($t(7)=1.680$, $p=0.144$, two-tailed paired t-test) (**Figure 3.4 E, right**). CNO did not significantly affect fast gamma power in control *Amigo2*-icreERT2- mice $F(1, 6)=1.434$, $p=0.276$, RM two-way ANOVA with Geisser-Greenhouse correction; animal: ($t(6)=0.610$, $p=0.564$, two-tailed, paired t-test); object: ($t(6)=1.786$, $p=0.124$, two-tailed, paired t-test) (data not shown).

3.3.4 Acute chemogenetic inhibition of CA2 pyramidal cells does not affect oscillatory power in stratum lacunosum-moleculare during investigation of novel stimuli

We next asked whether inhibition of CA2 pyramidal cells affects oscillatory power in stratum lacunosum-moleculare. We hypothesized that oscillations would not be significantly impacted by this manipulation because CA2 inputs do not project to CA1 dendrites in this layer. No significant effects of CNO were observed in control *Amigo2*-icreERT2- for the beta, slow gamma, or fast gamma frequency bands under any experimental condition tested (**Figure 3.5 A**). Inhibition of CA2 pyramidal cells in *Amigo2*-icreERT2+ mice (**Figure 3.5 B**) with CNO did not affect beta power relative to vehicle during investigation of stimuli ($F(1, 6)=0.967$, $p=0.363$, RM two-way ANOVA with Geisser-Greenhouse correction; animal: ($t(7)=0.586$, $p=0.579$, two-tailed, paired t-test) (**Figure3.5 C, left**); object: ($t(7)=1.473$, $p=0.191$, two-tailed, paired t-test) (**Figure3.5 C, right**). CNO did not significantly affect beta power in control *Amigo2*-icreERT2- mice $F(1, 6)=0.018$, $p=0.898$, RM two-way ANOVA with Geisser-Greenhouse correction; animal: ($t(6)=0.063$, $p=0.956$, two-tailed, paired t-test; object: ($t(6)=0.224$, $p=0.830$, two-tailed, paired t-test) (data not shown). Treatment with CNO did not significantly affect slow gamma power relative to vehicle during investigation of a novel stimulus ($F(1, 6)=0.159$, $p=0.704$, RM two-way ANOVA with Geisser-Greenhouse; animal: ($t(7)=0.111$, $p=0.915$, two-tailed, paired t-test) (**Figure 3.5 D, left**); object: ($t(7)=0.710$, $p=0.504$, two-tailed, paired t-test) (**Figure 3.5 D, right**). CNO did not significantly affect slow gamma power in control *Amigo2*-icreERT2- mice $F(1, 6)=3.853$, $p=0.097$, RM two-way ANOVA with Geisser-Greenhouse correction; animal: ($t(6)=1.048$, $p=0.335$, two-tailed, paired t-test) (**Figure 3.5 D, left**); object: ($t(6)=1.106$, $p=0.311$, two-tailed, paired t-test) (data not shown). Treatment with CNO did not significant affect fast gamma power relative to vehicle during investigation of a novel stimulus ($F(1, 6)=3.195$, $p=0.124$, RM two-way ANOVA with Geisser-Greenhouse correction; animal: ($t(7)=0.014$, $p=0.989$, two-tailed, paired t-test) (**Figure 3.5 E, left**); object: ($t(7)=2.248$, $p=0.066$, two-tailed paired t-test) (**Figure 3.5 E, right**). CNO did not significantly affect fast gamma power in control *Amigo2*-icreERT2- mice $F(1, 6)=0.565$, $p=0.481$, RM two-way ANOVA with Geisser-Greenhouse correction; animal: ($t(6)=0.079$, $p=0.940$, two-tailed, paired t-test); object: ($t(6)=1.269$, $p=0.252$, two-tailed, paired t-test) (data not shown).

3.3.5 Hippocampal oscillations in the pyramidal cell layer of CA1 do not significantly differ during investigation of a novel animal relative to a novel object

We found that engagement of the Gi-coupled signaling pathway in CA2 pyramidal cells of hM4Di-expressing mice decreased synchronized neuronal activity in the slow and fast gamma frequency ranges in the hippocampus when comparing the effects of vehicle administration to CNO administration while subjects investigated the same type of stimulus. Given these results, we next asked if there was a significant difference in hippocampal slow or fast gamma power when subjects investigated the different stimulus types after receiving the same drug treatment. To explore possible effects of stimulus type, we compared LFP power filtered in the beta, slow gamma, and fast gamma frequency ranges while subjects investigated different stimulus types after receiving the same drug treatment (Vehicle-Animal vs. Vehicle-Object or CNO-Animal vs. CNO-Object). Here we report the results for main effects of stimulus type from the same repeated-measures, 2-way ANOVAs and follow up comparisons using repeated measures, two-tailed, paired t-tests. No significant effects of stimulus type were observed in control *Amigo2*-icreERT2- for the beta, slow gamma, or fast gamma frequency bands under any experimental condition tested (**Figure 3.6 A**). In *Amigo2*-icreERT2+ mice (**Figure 3.6 B**), stimulus type did not affect beta power following administration of vehicle or CNO ($F(1, 6)=0.084$, $p=0.782$, RM two-way ANOVA with Geisser-Greenhouse correction; vehicle: ($t(7)=0.086$, $p=0.934$, two-tailed, paired t-test) (**Figure3.6 C, left**); CNO: ($t(7)=1.121$, $p=0.231$, two-tailed, paired t-test) (**Figure3.6 C, right**). Stimulus type did not significantly affect beta power in control *Amigo2*-icreERT2- mice $F(1, 6)=0.642$, $p=0.454$, RM two-way ANOVA with Geisser-Greenhouse; vehicle: ($t(6)=0.401$, two-tailed, paired t-test, $p=0.703$; CNO: ($t(6)=0.962$, $p=0.373$, two-tailed, paired t-test) (data not shown). Stimulus type did not significantly affect slow gamma power following administration of vehicle or CNO ($F(1, 6)=0.785$, $p=0.410$, RM two-way ANOVA with Geisser-Greenhouse; vehicle: ($t(7)=1.552$, $p=0.167$, two-tailed, paired t-test) (**Figure 3.6d left**); CNO: ($t(7)=1.311$, $p=0.231$, two-tailed, paired t-test) (**Figure 3.6 D, right**). Stimulus type did not significantly affect slow gamma power in control *Amigo2*-icreERT2- mice $F(1, 6)=0.024$, $p=0.881$, RM two-way ANOVA with Geisser-Greenhouse correction; vehicle: ($t(6)=0.338$, $p=0.075$, two-tailed, paired t-test); CNO: ($t(6)=0.386$, $p=0.713$, two-tailed, paired t-test) (data not shown). Stimulus type did not significantly affect fast gamma power following administration of vehicle or CNO ($F(1, 6)=0.320$, $p=0.592$, RM two-way ANOVA with Geisser-Greenhouse correction; vehicle: ($t(7)=0.335$, $p=0.745$, two-tailed, paired t-test)

(**Figure 3.6 E, left**); CNO: (t(7)=0.346, *p*=0.734, two-tailed paired t-test) (**Figure 3.6 E, right**). Stimulus type did not significantly affect fast gamma power in control *Amigo2*-icreERT2- mice F(1, 6)=2.271, *p*=0.183, RM two-way ANOVA with Geisser-Greenhouse correction; vehicle: (t(6)=1.010, *p*=0.352, two-tailed, paired t-test); CNO: (t(6)=0.681, *p*=0.521, two-tailed, paired t-test) (data not shown).

3.3.6 Hippocampal oscillations in CA1 stratum oriens do not significantly differ during investigation of a novel animal relative to a novel object

To explore possible effects of stimulus type in stratum oriens, we compared LFP power filtered in the beta, slow gamma, and fast gamma frequency ranges while subjects investigated different stimulus types after receiving the same drug treatment (Vehicle-Animal vs. Vehicle-Object or CNO-Animal vs. CNO-Object). Here we report the results for effects of stimulus type (socialness) from repeated-measures, 2-way ANOVAs and follow up comparisons using repeated measures, two-tailed, paired t-tests. No significant effects of stimulus type were observed in control *Amigo2*-icreERT2- for the beta, slow gamma, or fast gamma frequency bands under any experimental condition tested (**Figure 3.7 A**). In *Amigo2*-icreERT2+ mice (**Figure 3.7 B**), stimulus type did not affect beta power following administration of vehicle or CNO (F(1, 6)=0.070, *p*=0.800, RM two-way ANOVA with Geisser-Greenhouse correction; vehicle: (t(7)=0.244, *p*=0.814, two-tailed, paired t-test) (**Figure 3.7 C, left**); CNO: (t(7)=0.217, *p*=0.834, two-tailed, paired t-test) (**Figure 3.7 C, right**). Stimulus type did not significantly affect beta power in control *Amigo2*-icreERT2- mice F(1, 5)=1.179, *p*=0.327, RM two-way ANOVA with Geisser-Greenhouse; vehicle: (t(6)=1.164, two-tailed, paired t-test, *p*=0.297; CNO: (t(6)=0.317, *p*=0.764, two-tailed, paired t-test) (data not shown). Stimulus type did not significantly affect slow gamma power following administration of vehicle or CNO (F(1, 6)=0.720, *p*=0.429, RM two-way ANOVA with Geisser-Greenhouse correction; vehicle: (t(7)=0.779, *p*=0.462, two-tailed, paired t-test) (**Figure 3.7 D, left**); CNO: (t(7)=0.252, *p*=0.801, two-tailed, paired t-test) (**Figure 3.7 D, right**). Stimulus type did not significantly affect slow gamma power in control *Amigo2*-icreERT2- mice F(1, 5)=0.292, *p*=0.612, RM two-way ANOVA with Geisser-Greenhouse correction; vehicle: (t(6)=0.804, *p*=0.458, two-tailed, paired t-test); CNO: (t(6)=1.526, *p*=0.188, two-tailed, paired t-test) (data not shown). Stimulus type did not significantly affect fast gamma power following administration of vehicle or CNO (F(1, 6)=0.381, *p*=0.560, RM two-way ANOVA with Geisser-Greenhouse correction; vehicle: (t(7)=0.054, *p*=0.959, two-tailed, paired t-test) (**Figure 3.7 E, left**); CNO: (t(7)=0.206, *p*=0.843, two-tailed paired t-test) (**Figure 3.7 E, right**). Stimulus

type did not significantly affect fast gamma power in control *Amigo2*-icreERT2- mice F(1, 5)=1.533, *p*=0.271, RM two-way ANOVA with Geisser-Greenhouse correction; vehicle: (t(6)=2.203, *p*=0.079, two-tailed, paired t-test); CNO: (t(6)=0.624, *p*=0.624, two-tailed, paired t-test) (data not shown).

3.3.7 Hippocampal oscillations in CA1 stratum radiatum do not significantly differ during investigation of a novel animal relative to a novel object

To explore possible effects of stimulus type in stratum radiatum, we compared LFP power filtered in the beta, slow gamma, and fast gamma frequency ranges while subjects investigated different stimulus types after receiving the same drug treatment (Vehicle-Animal vs. Vehicle-Object or CNO-Animal vs. CNO-Object). Here we report the results for effects of stimulus type (socialness) from repeated-measures, 2-way ANOVAs and follow up comparisons using repeated measures, two-tailed, paired t-tests. No significant effects of stimulus type were observed in control *Amigo2*-icreERT2- for the beta, slow gamma, or fast gamma frequency bands under any experimental condition tested (**Figure 3.8 A**). In *Amigo2*-icreERT2+ mice (**Figure 3.8 B**), stimulus type did not affect beta power following administration of vehicle or CNO (F(1, 6)=0.008, *p*=0.933, RM two-way ANOVA with Geisser-Greenhouse correction; vehicle: (t(7)=0.753, *p*=0.480, two-tailed, paired t-test) (**Figure 3.8 C, left**); CNO: (t(7)=1.874, *p*=0.110, two-tailed, paired t-test) (**Figure 3.8 C, right**). Stimulus type did not significantly affect beta power in control *Amigo2*-icreERT2- mice F(1, 6)=0.149, *p*=0.713, RM two-way ANOVA with Geisser-Greenhouse correction; vehicle: (t(6)=0.210, two-tailed, paired t-test, *p*=0.841; CNO: (t(6)=0.962, *p*=0.373, two-tailed, paired t-test) (data not shown). Stimulus type did not significantly affect slow gamma power following administration of vehicle or CNO (F(1, 6)=0.030, *p*=0.869, RM two-way ANOVA with Geisser-Greenhouse correction; vehicle: (t(7)=0.457, *p*=0.664, two-tailed, paired t-test) (**Figure 3.8 D, left**); CNO: (t(7)=0.249, *p*=0.812, two-tailed, paired t-test) (**Figure 3.8 D, right**). Stimulus type did not significantly affect slow gamma power in control *Amigo2*-icreERT2- mice F(1, 6)=0.012, *p*=0.916, RM two-way ANOVA with Geisser-Greenhouse correction; vehicle: (t(6)=0.350, *p*=0.739, two-tailed, paired t-test); CNO: (t(6)=0.400, *p*=0.703, two-tailed, paired t-test) (data not shown). Stimulus type did not significantly affect fast gamma power following administration of vehicle or CNO (F(1, 6)=0.114, *p*=0.747, RM two-way ANOVA with Geisser-Greenhouse correction; vehicle: (t(7)=0.517, *p*=0.624, two-tailed, paired t-test) (**Figure 3.8 E, left**); CNO: (t(7)=0.281, *p*=0.788, two-tailed paired t-test) (**Figure 3.8 E, right**). Stimulus type did not significantly affect fast gamma power in control *Amigo2*-icreERT2- mice F(1, 6)=0.636,

p=0.455, RM two-way ANOVA with Geisser-Greenhouse correction; vehicle: (t(6)=1.553, *p*=0.471, two-tailed, paired t-test); CNO: (t(6)=0.365, *p*=0.728, two-tailed, paired t-test) (data not shown).

3.3.8 Hippocampal oscillations in CA1 stratum lacunosum-moleculare do not significantly differ during investigation of a novel animal relative to a novel object

To explore possible effects of stimulus type in stratum lacunosum-moleculare, we compared LFP power filtered in the beta, slow gamma, and fast gamma frequency ranges while subjects investigated different stimulus types after receiving the same drug treatment (Vehicle-Animal vs. Vehicle-Object or CNO-Animal vs. CNO-Object). Here we report the results for effects of stimulus type (socialness) from repeated-measures, 2-way ANOVAs and follow up comparisons using repeated measures, two-tailed, paired t-tests. No significant effects of stimulus type were observed in control *Amigo2*-icreERT2- for the beta, slow gamma, or fast gamma frequency bands under any experimental condition tested (**Figure 3.9 A**). In *Amigo2*-icreERT2+ mice (**Figure 3.9 B**), stimulus type did not affect beta power following administration of vehicle or CNO (F(1, 6)=0.002, *p*=0.965, RM two-way ANOVA with Geisser-Greenhouse correction; vehicle: (t(7)=0.270, *p*=0.796, two-tailed, paired t-test) (**Figure 3.9 C, left**); CNO: (t(7)=1.226, *p*=0.266, two-tailed, paired t-test) (**Figure 3.9 C, right**). Stimulus type did not significantly affect beta power in control *Amigo2*-icreERT2- mice F(1, 6)=0.150, *p*=0.712, RM two-way ANOVA with Geisser-Greenhouse correction; vehicle: (t(6)=0.974, two-tailed, paired t-test, *p*=0.368; CNO: (t(6)=0.482, *p*=0.647, two-tailed, paired t-test) (data not shown). Stimulus type did not significantly affect slow gamma power following administration of vehicle or CNO (F(1, 6)=0.000, *p*=0.994, RM two-way ANOVA with Geisser-Greenhouse; vehicle: (t(7)=0.105, *p*=0.920, two-tailed, paired t-test) (**Figure 3.9 D, left**); CNO: (t(7)=0.394, *p*=0.707, two-tailed, paired t-test) (**Figure 3.9 D, right**). Stimulus type did not significantly affect slow gamma power in control *Amigo2*-icreERT2- mice F(1, 6)=0.008, *p*=0.931, RM two-way ANOVA with Geisser-Greenhouse correction; vehicle: (t(6)=0.856, *p*=0.856, two-tailed, paired t-test); CNO: (t(6)=0.728, *p*=0.494, two-tailed, paired t-test) (data not shown). Stimulus type did not significantly affect fast gamma power following administration of vehicle or CNO (F(1, 6)=0.720, *p*=0.429, RM two-way ANOVA with Geisser-Greenhouse correction; vehicle: (t(7)=1.651, *p*=0.150, two-tailed, paired t-test) (**Figure 3.9 E, left**); CNO: (t(7)=0.111, *p*=0.915, two-tailed paired t-test) (**Figure 3.9 E, right**). Stimulus type did not significantly affect fast gamma power in control *Amigo2*-icreERT2- mice F(1, 6)=0.813,

p=0.402, RM two-way ANOVA with Geisser-Greenhouse correction; vehicle: (t(6)=0.013, *p*=0.990, two-tailed, paired t-test); CNO: (t(6)=1.201, *p*=0.275, two-tailed, paired t-test) (data not shown).

3.3.9 Acute chemogenetic inhibition of CA2 pyramidal cells reduces average distance traveled

Based on our findings of reduced gamma power in the hippocampus during acute inhibition of CA2 pyramidal cells in hM4Di-expressing mice during running and investigation of novel stimuli, we asked whether the effects observed on neuronal oscillations correlated with changes in behavior. We assessed hM4Di-infused *Amigo2*-icreERT2+ and control *Amigo2*-icreERT2- mice for differences in average distance traveled and time spent mobile while acutely inhibiting CA2 pyramidal cells with CNO (3.0mg/kg). For analysis of distance traveled and time spent mobile only samples from the baseline phase in which no stimulus was present were used. Periods of mobility were assessed by binning all samples from a given recording session into either the mobile or immobile condition using a 7cm/s threshold of the subject's smoothed instantaneous velocity. The 7cm/s value was chosen based on manual optimization of tracking parameters to separate periods of active exploration from relative immobility while excluding in-place body movements, such as grooming. *Amigo2*-icreERT2+ and control *Amigo2*-icreERT2- did not travel significantly different distances across recording days (Cre positive: F(7)=2.141, *p*=0.115, RM two-way ANOVA with Geisser-Greenhouse correction, blue line; Cre negative: (F(1, 6)=1.772, *p*=0.189, RM two-way ANOVA with Geisser-Greenhouse, red line) (**Figure 3.10 A**). Treatment with CNO revealed a significant reduction in the average distance traveled by *Amigo2*-icreERT2+ mice (t(7)=2.462, *p*=0.043, two-tailed, paired t-test, blue bars) relative to vehicle, but not by *Amigo2*-icreERT2- mice (t(7)=1.242, *p*=0.261, two-tailed, paired t-test, red bars) (**Figure 3.10 B**)**.** *Amigo2*-icreERT2+ and control *Amigo2*-icreERT2- did not spend significantly different amounts of time being mobile across recording days (Cre positive: F(7)=2.082, *p*=0.122, RM two-way ANOVA with Geisser-Greenhouse, blue line; Cre negative: (F(1, 6)=1.528, *p*=0.239, RM two-way ANOVA with Geisser-Greenhouse correction, red line) (**Figure 3.10 C**). CNO did significantly affect the average time spent mobile by *Amigo2*-icreERT2+ mice (t(7)=1.644, *p*=0.144, two-tailed, paired t-test, blue bars) or *Amigo2*-icreERT2- mice (t(7)=1.119, *p*=0.306, two-tailed, paired t-test, red bars) (**Figure 3.10 D**)**.**

3.3.10 Acute chemogenetic inhibition of CA2 pyramidal cells does not affect time spent investigating novel stimuli

We also asked whether the amount of time *Amigo2*-icreERT2+ and control *Amigo2*-icreERT2- mice spent investigating different types of novel stimuli was affected by CNO or stimulus type. CNO did not significantly affect the amount of time *Amigo2*-icreERT2+ mice ($F(1, 6)=0.776$, $p=0.408$, RM two-way ANOVA with Geisser-Greenhouse correction; animal: ($t(7)=1.912$, $p=0.098$, two-tailed, paired t-test); object: ($t(7)=0.025$, $p=0.981$, two-tailed, paired t-test) or *Amigo2*-icreERT2- mice $F(1, 6)=5.741$, $p=0.054$, RM two-way ANOVA with Geisser-Greenhouse; animal: ($t(6)=0.319$, $p=0.761$, two-tailed, paired t-test; object: ($t(6)=1.252$, $p=0.257$, two-tailed, paired t-test) spent investigating stimuli (**Figure 3.10 E**). Stimulus type did significantly affect the amount of time *Amigo2*-icreERT2+ ($F(1, 6)=0.141$, $p=0.719$, RM two-way ANOVA with Geisser-Greenhouse correction; vehicle: ($t(7)=0.285$, $p=0.784$, two-tailed, paired t-test; CNO: ($t(7)=0.675$, $p=0.521$, two-tailed, paired t-test) or *Amigo2*-icreERT2- ($F(1, 6)=0.020$, $p=0.891$, RM two-way ANOVA with Geisser-Greenhouse correction; vehicle: ($t(7)=0.019$, $p=0.985$, two-tailed, paired t-test; CNO: ($t(7)=1.365$, $p=0.221$, two-tailed, paired t-test) mice spent investigating stimuli (**Figure 3.10 F**).

3.4 Discussion

In this study we used inhibitory DREADDs to reversibly modify CA2 pyramidal cell activity and examine the effects on neuronal oscillations in the different layers of CA1. We found that acute, reversible inhibition of CA2 pyramidal cells with hM4Di in awake, behaving mice selectively reduced hippocampal CA1 oscillatory power in a layer- and frequency-specific manner. Specifically, inhibition of CA2 pyramidal cells caused a significant reduction in slow and fast gamma power in the pyramidal cell layer and stratum oriens of CA1, and in fast gamma power in stratum radiatum. No significant changes in power in stratum lacunosum-moleculare were detected. While the magnitude of gamma reduction in the pyramidal cell layer and stratum oriens tended to be larger when the stimulus presented was a novel animal relative to a novel object, with fast gamma in stratum pyramidal being the one exception, CA2 inhibition overall showed a similar effect of reducing gamma power regardless of stimulus type.

These experiments were designed to address two aspects about the role of CA2 in organizing hippocampal network synchronization in vivo. First, despite knowledge that CA2 is required for intact social recognition memory (Hitti & Siegelbaum, 2014), whether CA2 neurons coordinate their activity with

CA1 to integrate social cues into memory remained unexplored. Given our previous evidence demonstrating CA2's role in organizing hippocampal slow gamma oscillations during running, we hypothesized that if CA2 is preferentially involved in processing information about socially relevant stimuli, CA2 pyramidal cells would cause an increase in neuronal activity in CA1 only while investigating a novel animal, and not a novel object. Thus, we sought to extend our investigation of CA2 by examining CA1 activity while subjects could freely explore different types of novel stimuli. Second, although oscillations are most commonly recorded at the level of the pyramidal cell soma, hippocampal gamma oscillations have been shown to be regulated in a layer-specific manner (Fernandez-Ruiz et al., 2012; Lasztoczi & Klausberger, 2014, 2016; Scheffer-Teixeira et al., 2012). In the synaptic layers of the hippocampus, increases in LFP power are thought to represent synchronized input from distal regions into the observed area (Colgin & Moser, 2010). Because CA2 pyramidal cells have been shown to selectively target different dendritic domains of CA1, with the basal dendrites in stratum oriens receiving the densest projections, followed by the apical dendrites in stratum radiatum and, notably, no projections to lacunosum-moleculare, we hypothesized that there would be layer-specific reductions of slow gamma power in CA1 while inhibiting CA2 pyramidal cells.

Consistent with our hypotheses, our results reveal that CA2 is capable of coordinating hippocampal oscillations during investigation of novel stimuli, and demonstrate that the state- and frequency- dependent organization of CA1 gamma oscillations in vivo rely on CA2 output. In contrast to our hypothesis, although the magnitude of slow gamma reduction was larger in stratum oriens and the pyramidal cell layer when the stimulus presented was a novel animal, the significant main effects of drug treatment, in combination with the lack of significant effect for stimulus type, or interaction effects between the two, demonstrate that CA2 inhibition causes a reduction in slow and fast gamma power regardless of the stimulus presented. Interestingly, the magnitude of fast gamma power reduction in stratum radiatum was larger for the novel object condition relative to the novel animal, suggesting that divergent CA2 projections may selectively innervate distinct CA1 populations according to behavioral demands. Further, given that slow and fast gamma oscillations in CA1 are regulated in a layer-specific manner, and that CA1 pyramidal cells form functionally distinct sublayers (Mizuseki, Diba, Pastalkova, & Buzsaki, 2011), CA2 collaterals targeting the apical and basal dendrites of CA1 may engage distinct populations of CA1

pyramidal cells and, consequently, serve distinct cognitive functions based on the output of the two populations.

In some instances, the ANOVA revealed a significant effect of drug that segregated according to stimulus type in the subsequent t-test comparisons. That is, for the five main effects of drug observed, there were three instances in which the follow up t-tests only revealed a significant difference between vehicle and CNO when the stimulus presented was an animal and not an object. This result was observed for the slow and fast gamma bands in stratum oriens, and the slow gamma band in the pyramidal cell layer. This may be due to several factors including too much scatter in the variance, insufficient statistical power due to small sample size, or that CA2 is not the only area involved in the observed effects. Although the possibility that the effects observed in CA1 were mediated by another CA1-projecting region cannot be excluded, the genetically targeted manipulation of CA2 pyramidal cells causally links CA2 activity with the network organization observed in CA1.

To address the possibility that the lack of significance from t-test comparisons for the object condition could have been due to insufficient statistical power, we estimated the sample sizes that would be required to confirm these results, and our original hypothesis, based on our observed effect sizes and chosen level of significance (Faul, Erdfelder, Lang, & Buchner, 2007). For slow gamma in the pyramidal cell layer, the sample size that would be required to confirm the lack of difference in power between the vehicle and CNO conditions when the stimulus presented was an object was 16 animals. For slow gamma in stratum oriens it was 84 animals, and for fast gamma in stratum oriens it was 30 animals. These large sample size estimates can be attributed to the small effect size of the object condition relative to the animal condition. Because the actual sample size in these experiments was 9 animals, these estimates indicate that the lack of significant difference in LFP power between the vehicle and CNO conditions during investigation of a novel object could be due to insufficient statistical power, and that a significant effect could emerge upon increasing the sample size. This interpretation is consistent with the significant main effect of drug in the 2-way, repeated-measures ANOVAs.

For comparison, we also ran the same analysis for the animal condition and found that the sample sizes that would be required to confirm the results of these t-tests were 10 animals for slow gamma in the pyramidal cell layer, 12 animals for slow gamma in statum oriens, and 9 animals for fast

gamma in stratum oriens. With an actual sample size of 9, although a few more animals would be needed to confirm the slow gamma band results, these much smaller sample size requirements are indicative of a real difference in effect size based on stimulus type that was not captured by the ANOVA results. Overall, this analysis supports the results of the ANOVA, which revealed that inhibition of CA2 causes a reduction in slow and fast gamma power regardless of stimulus type; however, the magnitude of the reduction is larger in stratum oriens and the pyramidal cell layer for the animal condition, and larger in stratum radiatum for the object condition.

Overall, these results support our previous finding that slow gamma power is increased and decreased with excitation and inhibition, respectively, of CA2 pyramidal neurons. These results also demonstrate that slow gamma arising from CA2 is transmitted to the primary dendritic input layer of CA2 neurons in CA1, stratum oriens, as well as to stratum radiatum, albeit to a lesser extent. Although we did not observe a state-dependent relationship of CA1 gamma power that supports the idea that CA2 is uniquely involved in social memory, this is consistent with the finding that CA2 place fields remap in response to exposure to novel environmental stimuli, social and otherwise (Alexander et al., 2016), as well as other studies demonstrating CA2's responsiveness to novelty (Lu et al., 2015; Wintzer et al., 2014), even when there is no social component involved in the task. Together, these results suggest that rather than serving as a hippocampal hub exclusively reserved for social memory, CA2 pyramidal cells may be more generally involved in episodic memory function, perhaps by signaling the novelty of environmental stimuli within hippocampal circuits.

3.5 Figures

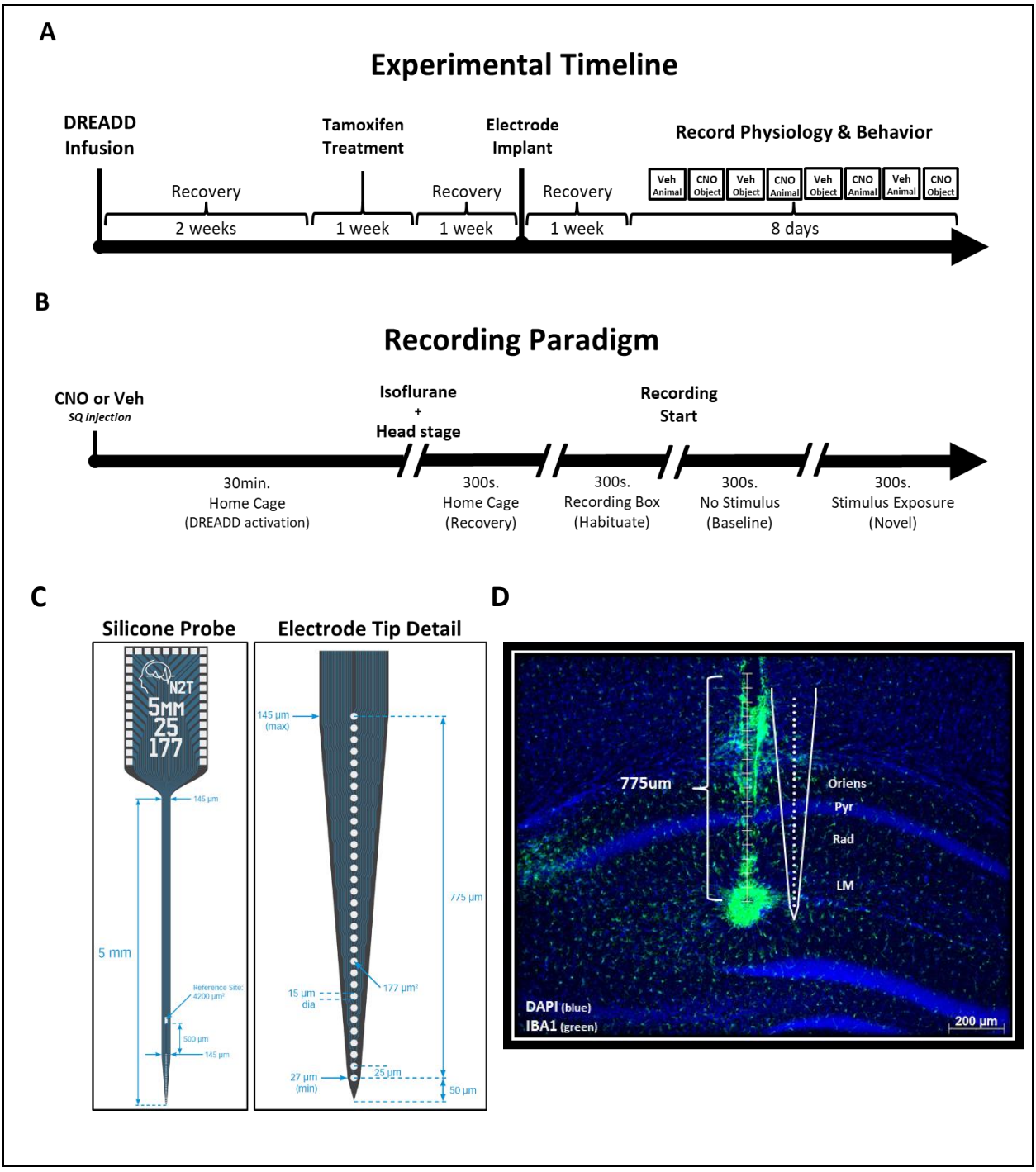
A
Experimental Timeline
DREADD Infusion
Tamoxifen Treatment
Electrode Implant
Record Physiology & Behavior
Recovery
2 weeks
1 week
Recovery
1 week
Recovery
1 week
Veh Animal
CNO Object
Veh Object
CNO Animal
Veh Object
CNO Animal
Veh Animal
CNO Object
8 days
B
Recording Paradigm
CNO or Veh
SQ injection
Isoflurane + Head stage
Recording Start
30min. Home Cage (DREADD activation)
300s. Home Cage (Recovery)
300s. Recording Box (Habituate)
300s. No Stimulus (Baseline)
300s. Stimulus Exposure (Novel)
C
Silicone Probe
Electrode Tip Detail
N2T
5MM
25
177
145 µm
5 mm
Reference Site: 4200 µm²
500 µm
145 µm
145 µm (max)
775 µm
15 µm dia
177 µm²
27 µm (min)
25 µm
50 µm
D
775um
Oriens
Pyr
Rad
LM
DAPI (blue)
IBA1 (green)
200 µm

Figure 3.1: Experimental timeline, recording paradigm, electrodes, and recording location. (**A**) For these experiments *Amigo2-icreERT2* mice were infused bilaterally with 0.5 µl of AAV-hSyn-DIO-hM4Di-mCherry, treated with tamoxifen, and implanted with silicone electrodes. Treatment with vehicle and CNO alternated across the eight days of recording. (**B**) For each daily recording session, animals were administered CNO (3.0mg/kg) or vehicle and returned to their home cage for 30 minutes to allow activation of the DREADD receptor. Ten minutes prior to the start of the experiment, subjects were lightly anesthetized to attach head stages, transferred to the recording room, and then allowed to recover for 300 seconds in their home cage. Subjects were then placed in a new, clean recording box and allowed to habituate for 300 seconds. The recording session consisted of a 300 second baseline phase in which no stimulus was present followed by a 300 second stimulus phase in which a novel animal or object was inserted into the recording arena in a wire-mesh cup. (**C**) For electrophysiology recordings we used NeuroNexus A1x32 silicone electrodes which had 32 recording contacts spaced evenly (25 µm) along a single, linear shank covering a total tissue span of 775 µm. (**D**) Image shows a representative recording location in CA1. At the end of experiments a small amount of electric current was passed through the bottom recording contact of the electrode to create an electrolytic lesion and hippocampal sections were subsequently stained for IBA1, a marker for activated microglia, to aid electrode localization. Electrode implant locations were reconstructed based on IBA1 staining and the presence of hippocampal ripples in the LFP data.

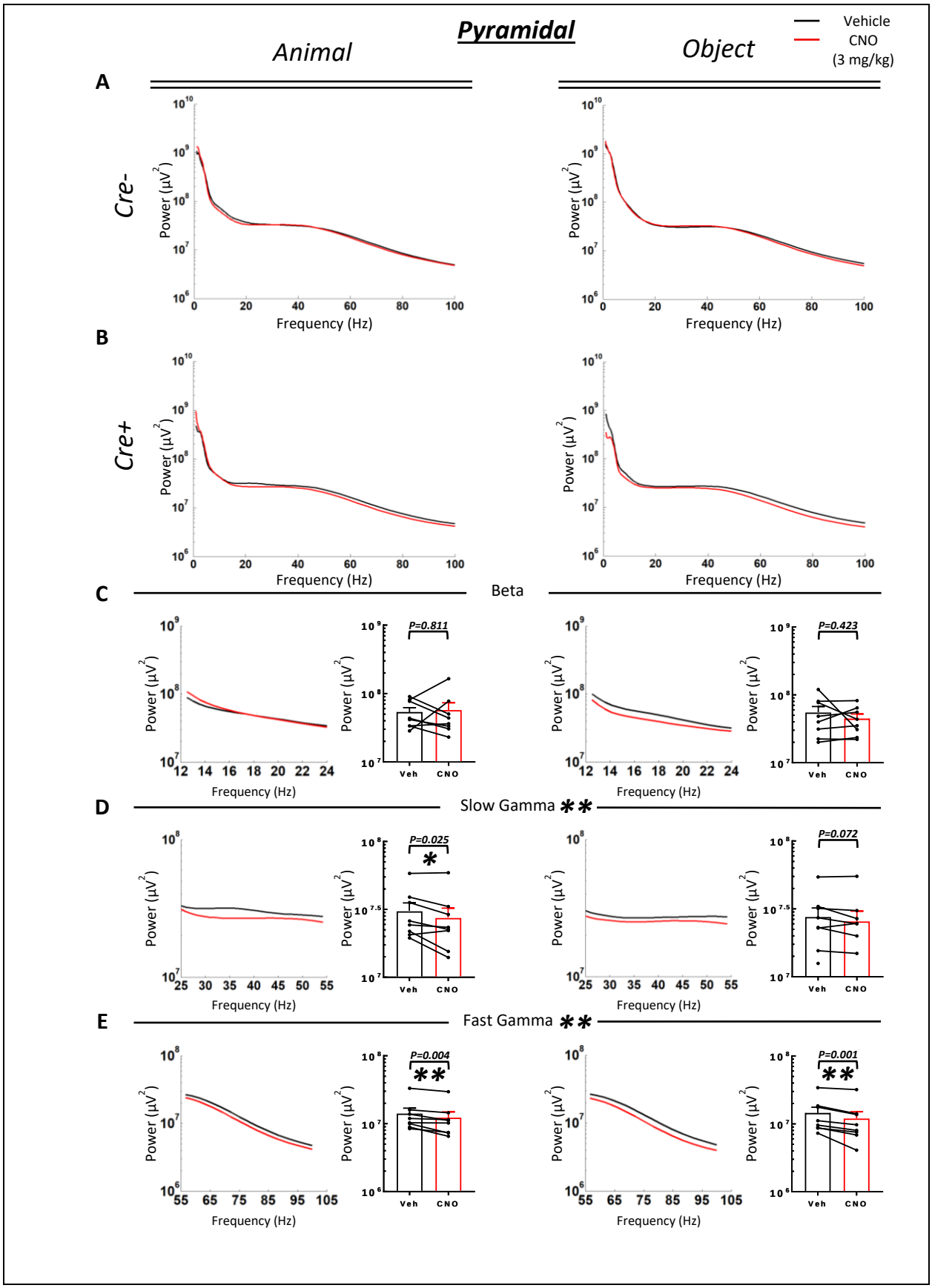
Pyramidal
Animal
Object
Vehicle
CNO
(3 mg/kg)
A
Cre-
B
Cre+
Power (μV²)
Frequency (Hz)
C
Beta
P=0.811
P=0.423
D
Slow Gamma **
P=0.025
P=0.072
E
Fast Gamma **
P=0.004
P=0.001
Veh
CNO

Figure 3.2: Inhibition of CA2 pyramidal cells with CNO in hM4Di-infused *Amigo2*-icreERT2+ mice reduces slow and fast gamma power in the pyramidal cell layer of CA1 during investigation of novel stimuli. Power spectral densities for the 1-100Hz frequency range calculated from LFPs recorded from the pyramidal cell layer of CA1 in *Amigo2*-icreERT2 mice infused with AAV-hM4Di-mCherry, treated with tamoxifen, and challenged with vehicle or CNO (3 mg/kg) while subjects actively investigated a novel animal (left column) or novel object (right column). (**A**) PSDs for *Amigo2*-icreERT2- mice. (**B**) PSDs for *Amigo2*-icreERT2+ mice. Plots (**C-E**) show data only from *Amigo2*-icreERT2+ mice. The left side of each pair of plots shows the group averaged PSD trace for the frequency band of interest. The right side of each pair of plots shows the group averages for each frequency band as colored bars graphs; dots represent data from individual animals. The results of ANOVAs for are indicated by the symbols located next to the heading for each frequency band. The specific p-values from paired t-test comparisons are shown over their respective graphs. (**C**) Treatment with CNO did not affect beta power relative to vehicle during investigation of novel stimuli ($F(1, 6)=0.329$, $p=0.587$, RM two-way ANOVA with Geisser-Greenhouse correction, center heading; animal: ($t(7)=0.248$, $p=0.811$, two-tailed, paired t-test, left; object: ($t(7)=0.813$, $p=0.423$, two-tailed, paired t-test, right). (**D**) Treatment with CNO revealed a significant reduction in slow gamma power relative to vehicle during investigation of novel stimuli ($F(1, 6)=14.095$, $p=0.009$, RM two-way ANOVA with Geisser-Greenhouse correction, center heading; animal: ($t(7)=2.845$, $p=0.025$, two-tailed, paired t-test, left; object: ($t(7)=2.121$, $p=0.072$, two-tailed, paired t-test, right). (**E**) Treatment with CNO revealed a significant reduction in fast gamma power relative to vehicle during investigation of novel stimuli ($F(1, 6)=22.836$, $p=0.003$, RM two-way ANOVA with Geisser-Greenhouse; animal: ($t(7)=4.163$, $p=0.004$, two-tailed, paired t-test, left; object: ($t(7)=5.721$, $p=0.001$, two-tailed paired t-test, right).

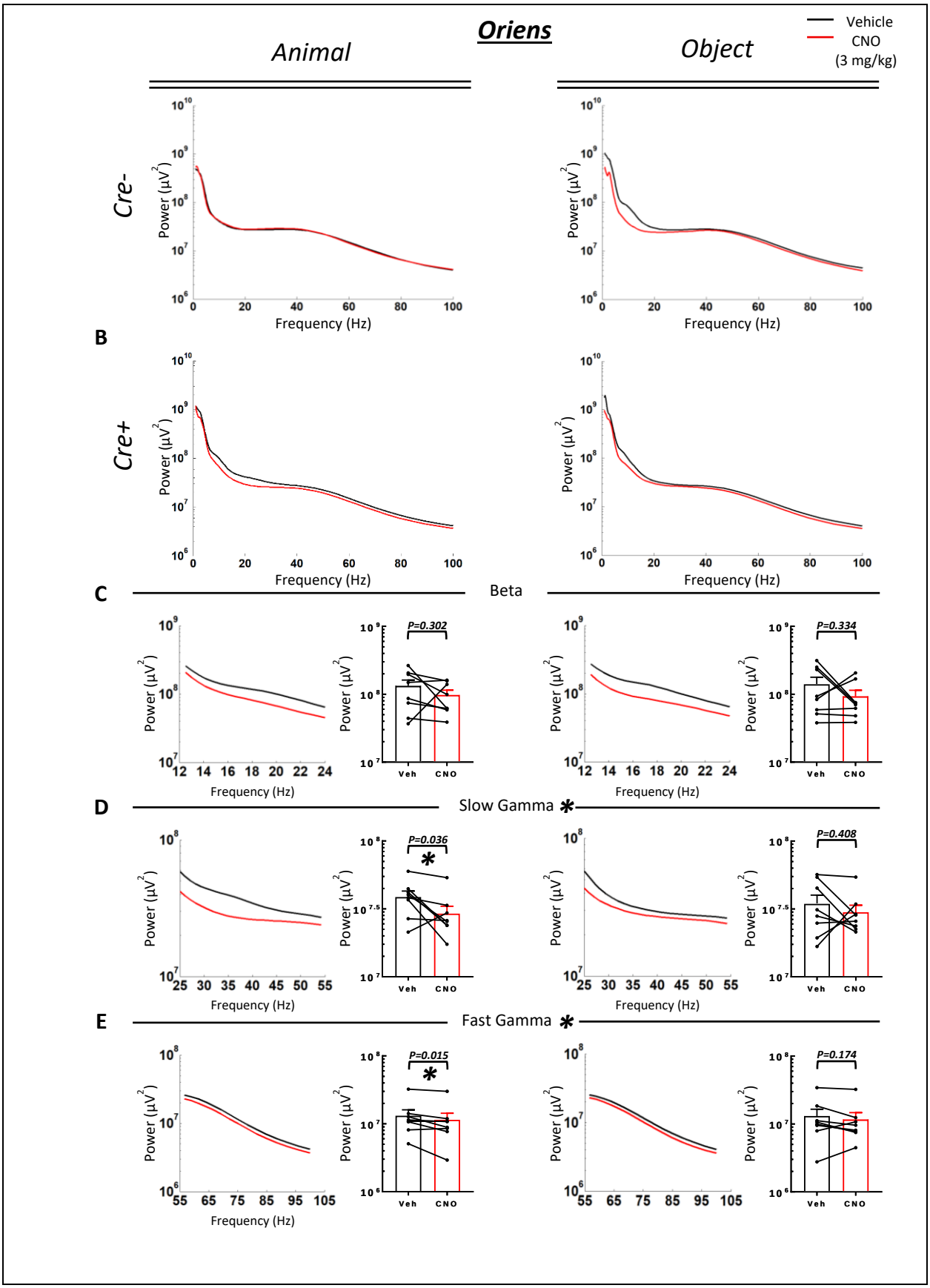
Oriens
Animal
Object
Vehicle
CNO
(3 mg/kg)
Cre-
Cre+
Power (μV²)
Frequency (Hz)
B
C
Beta
D
Slow Gamma
E
Fast Gamma
P=0.302
P=0.334
P=0.036
P=0.408
P=0.015
P=0.174
Veh
CNO

Figure 3.3: Inhibition of CA2 pyramidal cells with CNO in hM4Di-infused *Amigo2*-icreERT2+ mice reduces slow and fast gamma power in stratum oriens of CA1 during investigation of novel stimuli. Power spectral densities for the 1-100Hz frequency range calculated from LFPs recorded from CA1 stratum oriens in *Amigo2*-icreERT2 mice infused with AAV-hM4Di-mCherry, treated with tamoxifen, and challenged with vehicle or CNO (3 mg/kg) while subjects actively investigated a novel animal (left column) or novel object (right column). (**A**) PSDs for *Amigo2*-icreERT2- mice. (**B**) PSDs for *Amigo2*-icreERT2+ mice. Plots (**C-E**) show data only from *Amigo2*-icreERT2+ mice. The left side of each pair of plots shows the group averaged PSD trace for the frequency band of interest. The right side of each pair of plots shows the group averages for each frequency band as colored bars graphs; dots represent data from individual animals. The results of ANOVAs are indicated by symbols located next to the line heading of each frequency band. The specific p-values from paired t-test comparisons are shown over their respective graphs. (**C**) Treatment with CNO did not affect beta power relative to vehicle during investigation of novel stimuli ($F(1, 6)=1.949$, $p=0.212$, RM two-way ANOVA with Geisser-Greenhouse correction, center heading; animal: $t(7)=1.115$, $p=0.302$, two-tailed, paired t-test, left; object: $t(7)=1.037$, $p=0.334$, two-tailed, paired t-test, right). (**D**) Treatment with CNO revealed a significant reduction in slow gamma power relative to vehicle during investigation of novel stimuli ($F(1, 6)=7.745$, $p=0.032$, RM two-way ANOVA with Geisser-Greenhouse correction, center heading; animal: $t(7)=2.596$, $p=0.036$, two-tailed, paired t-test, left; object: $t(7)=0.880$, $p=0.408$, two-tailed, paired t-test, right). (**E**) Treatment with CNO revealed a significant reduction in fast gamma power relative to vehicle during investigation of novel stimuli ($F(1, 6)=10.568$, $p=0.017$, RM two-way ANOVA with Geisser-Greenhouse; animal: $t(7)=3.222$, $p=0.015$, two-tailed, paired t-test, left; object: $t(7)=1.513$, $p=0.174$, two-tailed paired t-test, right).

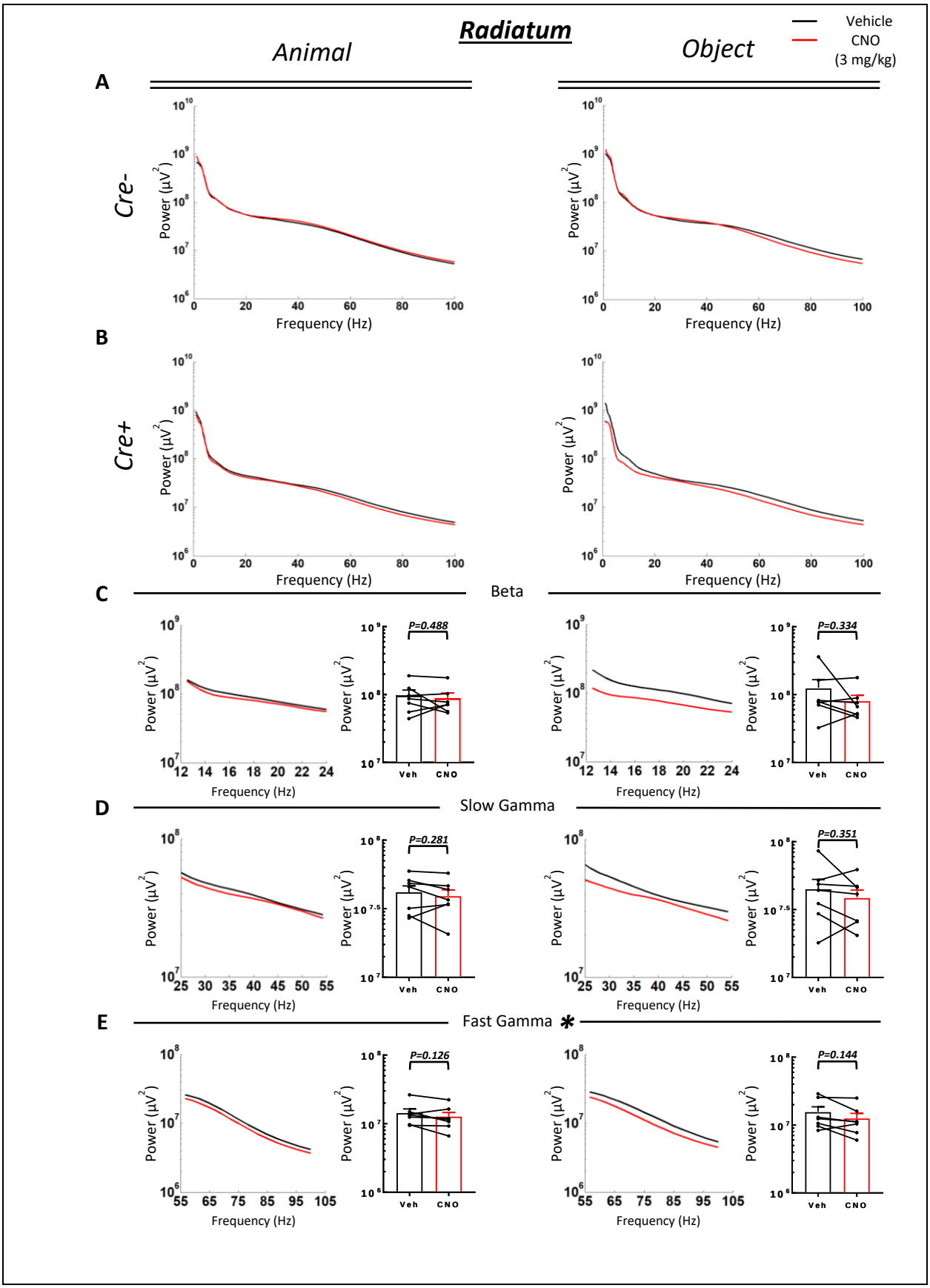
Radiatum
Animal
Object
Vehicle
CNO
(3 mg/kg)
A
Cre-
B
Cre+
Power (μV²)
Frequency (Hz)
C
Beta
P=0.488
P=0.334
D
Slow Gamma
P=0.281
P=0.351
E
Fast Gamma *
P=0.126
P=0.144
Veh
CNO

Figure 3.4: Inhibition of CA2 pyramidal cells with CNO in hM4Di-infused *Amigo2*-icreERT2+ mice reduces fast gamma power in stratum radiatum of CA1 during investigation of novel stimuli. Power spectral densities for the 1-100Hz frequency range calculated from LFPs recorded from the stratum radiatum of CA1 in *Amigo2*-icreERT2 mice infused with AAV-hM4Di-mCherry, treated with tamoxifen, and challenged with vehicle or CNO (3 mg/kg) while subjects actively investigated a novel animal (left column) or novel object (right column). (**A**) PSDs for *Amigo2*-icreERT2- mice. (**B**) PSDs for *Amigo2*-icreERT2+ mice. Plots (**C-E**) show data only from *Amigo2*-icreERT2+ mice. The left side of each pair of plots shows the group averaged PSD trace for the frequency band of interest. The right side of each pair of plots shows the group averages for each frequency band as colored bars graphs; dots represent data from individual animals. The results of ANOVAs for are indicated by the symbols located next to the heading for each frequency band. The specific p-values from paired t-test comparisons are shown over their respective graphs. (**C**) Treatment with CNO did not affect beta power relative to vehicle during investigation of novel stimuli ($F(1, 6)=0.913$, $p=0.376$, RM two-way ANOVA with Geisser-Greenhouse correction, center heading; animal: ($t(7)=0.738$, $p=0.488$, two-tailed, paired t-test, left; object: ($t(7)=1.027$, $p=0.334$, two-tailed, paired t-test, right). (**D**) Treatment with CNO did not affect slow gamma power relative to vehicle during investigation of novel stimuli ($F(1, 6)=1.889$, $p=0.218$, RM two-way ANOVA with Geisser-Greenhouse correction, center heading; animal: ($t(7)=1.184$, $p=0.281$, two-tailed, paired t-test, left; object: ($t(7)=1.011$, $p=0.351$, two-tailed, paired t-test, right). (**E**) Treatment with CNO revealed a significant reduction in fast gamma power relative to vehicle during investigation of novel stimuli ($F(1, 6)=11.054$, $p=0.016$, RM two-way ANOVA with Geisser-Greenhouse; animal: ($t(7)=1.778$, $p=0.126$, two-tailed, paired t-test, left; object: ($t(7)=1.680$, $p=0.144$, two-tailed paired t-test, right).

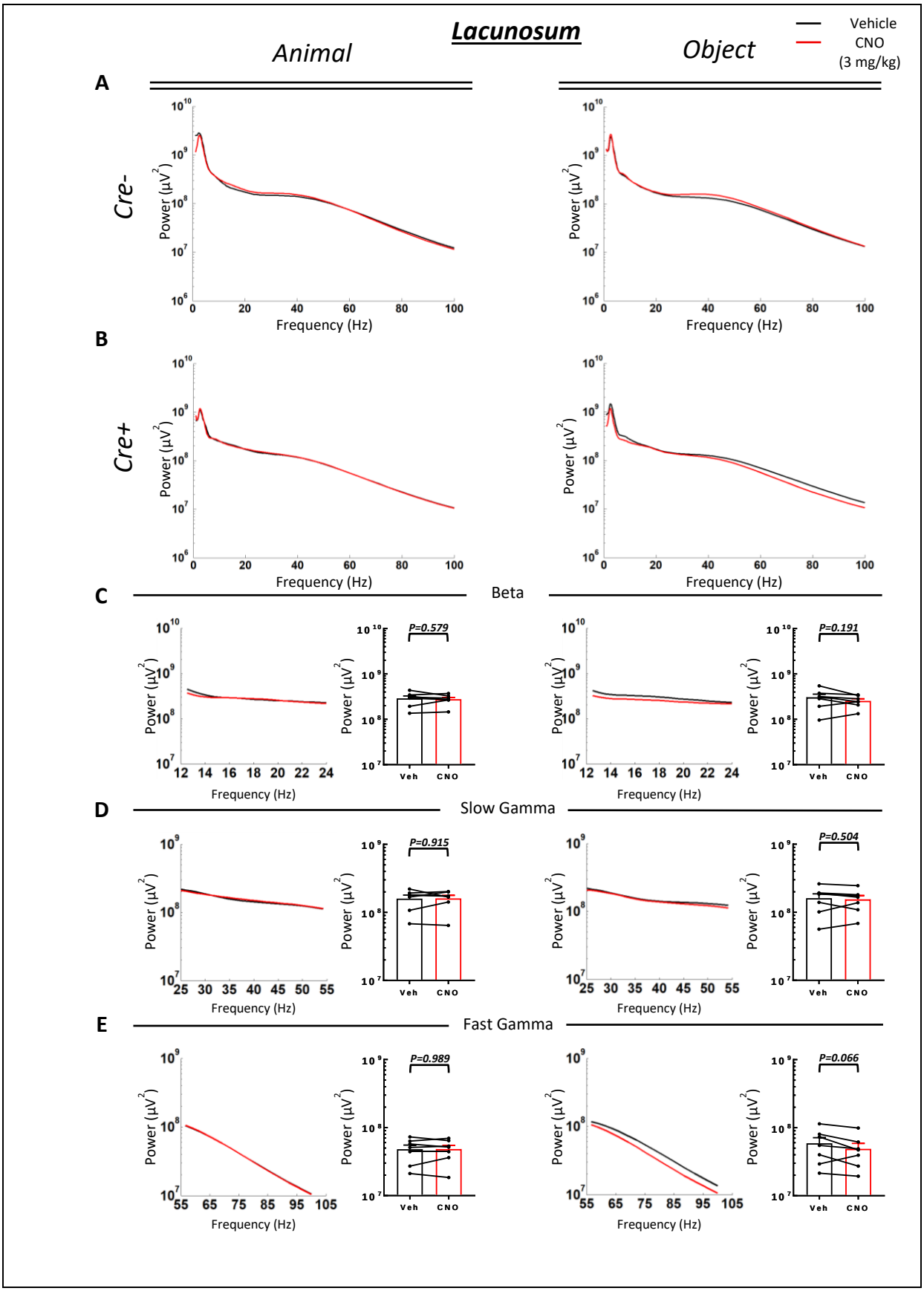
Lacunosum
Animal
Object
Vehicle
CNO
(3 mg/kg)
A
Cre-
B
Cre+
Power (μV²)
Frequency (Hz)
C
Beta
D
Slow Gamma
E
Fast Gamma
P=0.579
P=0.191
P=0.915
P=0.504
P=0.989
P=0.066
Veh
CNO

Figure 3.5: Inhibition of CA2 pyramidal cells with CNO in hM4Di-infused *Amigo2*-icreERT2+ mice does not affect oscillations in stratum lacunosum-moleculare of CA1 during investigation of novel stimuli. Power spectral densit1ies for the 1-100Hz frequency range calculated from LFPs recorded from stratum lacunosum-moleculare of CA1 in *Amigo2*-icreERT2 mice infused with AAV-hM4Di-mCherry, treated with tamoxifen, and challenged with vehicle or CNO (3 mg/kg) while subjects actively investigated a novel animal (left column) or novel object (right column). (**A**) PSDs for *Amigo2*-icreERT2- mice. (**B**) PSDs for *Amigo2*-icreERT2+ mice. Plots (**C-E**) show data only from *Amigo2*-icreERT2+ mice. The left side of each pair of plots shows the group averaged PSD trace for the frequency band of interest. The right side of each pair of plots shows the group averages for each frequency band as colored bars graphs; dots represent data from individual animals. The results of ANOVAs for are indicated by the symbols located next to the heading for each frequency band. The specific p-values from paired t-test comparisons are shown over their respective graphs. (**C**) Treatment with CNO did not affect beta power relative to vehicle during investigation of novel stimuli ($F(1, 6)=0.967$, $p=0.363$, RM two-way ANOVA with Geisser-Greenhouse correction, center heading; animal: $t(7)=0.586$, $p=0.579$, two-tailed, paired t-test, left; object: $t(7)=1.473$, $p=0.191$, two-tailed, paired t-test, right). (**D**) Treatment with CNO did not affect slow gamma power relative to vehicle during investigation of novel stimuli ($F(1, 6)=0.159$, $p=0.704$, RM two-way ANOVA with Geisser-Greenhouse correction, center heading; animal: $t(7)=0.111$, $p=0.915$, two-tailed, paired t-test, left; object: $t(7)=0.710$, $p=0.504$, two-tailed, paired t-test, right). (**E**) Treatment with CNO did not affect fast gamma power relative to vehicle during investigation of novel stimuli ($F(1, 6)=3.195$, $p=0.124$, RM two-way ANOVA with Geisser-Greenhouse; animal: $t(7)=0.014$, $p=0.989$, two-tailed, paired t-test, left; object: $t(7)=2.248$, $p=0.066$, two-tailed paired t-test, right).

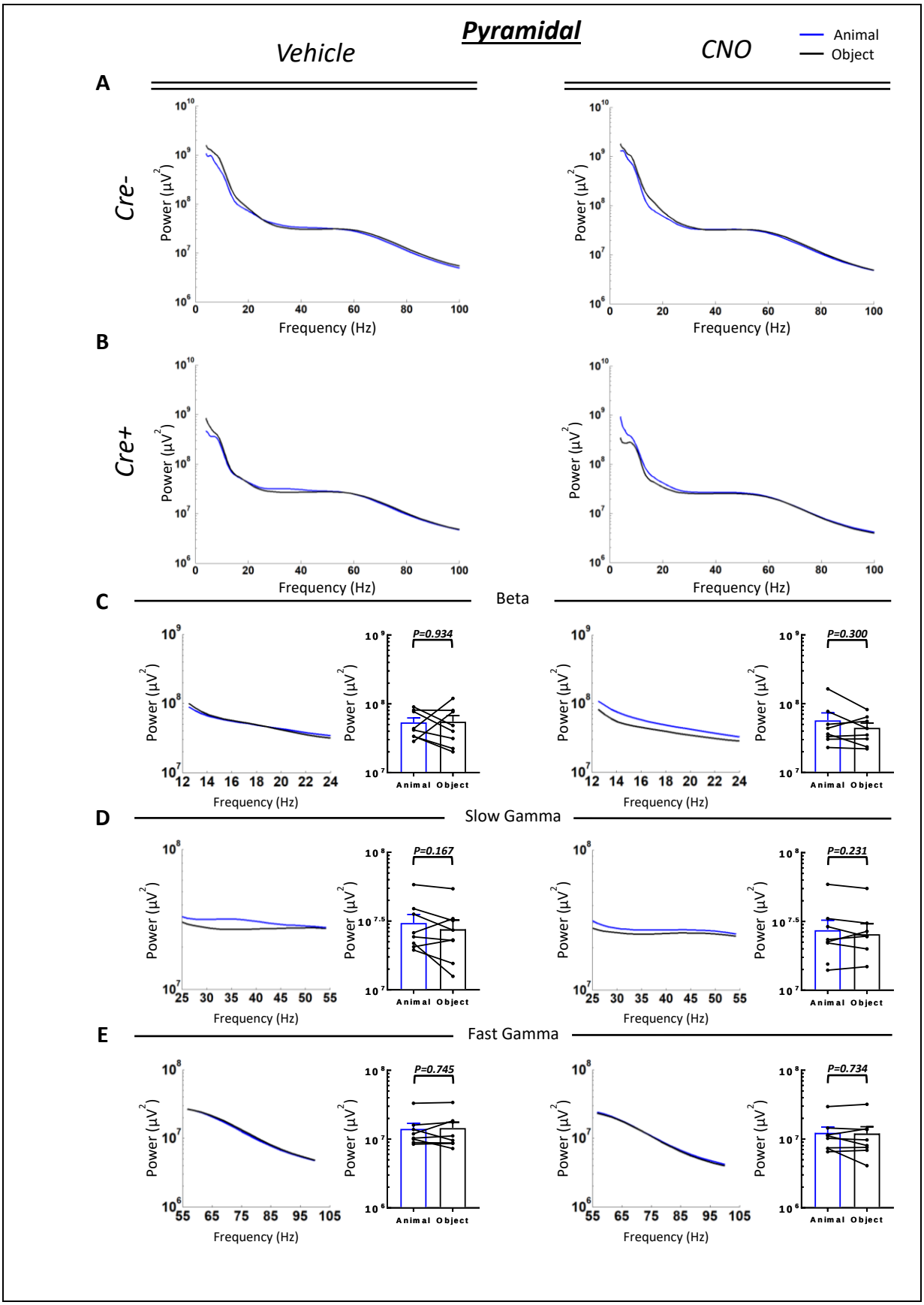
Pyramidal
Vehicle
CNO
Animal
Object
A
Cre-
B
Cre+
Power (μV²)
Frequency (Hz)
C
Beta
D
Slow Gamma
E
Fast Gamma
P=0.934
P=0.300
P=0.167
P=0.231
P=0.745
P=0.734
Animal Object

Figure 3.6: Hippocampal oscillations in the pyramidal cell layer of CA1 do not significantly differ during investigation of a novel animal relative to a novel object following treatment with vehicle or CNO in hM4Di-infused *Amigo2*-icreERT2+ mice. Power spectral densities for the 1-100Hz frequency range calculated from LFPs recorded from the pyramidal cell layer of CA1 in *Amigo2*-icreERT2 mice infused with AAV-hM4Di-mCherry, treated with tamoxifen, and challenged with vehicle or CNO (3 mg/kg) while subjects actively investigated a novel animal (left column) or novel object (right column). (**A**) PSDs for *Amigo2*-icreERT2- mice. (**B**) PSDs for *Amigo2*-icreERT2+ mice. Plots (**C-E**) show data only from *Amigo2*-icreERT2+ mice. The left side of each pair of plots shows the group averaged PSD trace for the frequency band of interest. The right side of each pair of plots shows the group averages for each frequency band as colored bars graphs; dots represent data from individual animals. The results of ANOVAs for are indicated by the symbols located next to the heading for each frequency band. The specific p-values from paired t-test comparisons are shown over their respective graphs. (**C**) Investigation of a novel animal relative to a novel object did not affect beta power following vehicle or CNO administration ($F(1, 6)=0.084$, $p=0.782$, RM two-way ANOVA with Geisser-Greenhouse correction, center heading; vehicle: ($t(7)=0.086$, $p=0.934$, two-tailed, paired t-test, left; CNO: ($t(7)=1.121$, $p=0.231$, two-tailed, paired t-test, right). (**D**) Investigation of a novel animal relative to a novel object did not affect slow gamma power following vehicle or CNO administration ($F(1, 6)=0.785$, $p=0.410$, RM two-way ANOVA with Geisser-Greenhouse correction, center heading; vehicle: ($t(7)=1.552$, $p=0.167$, two-tailed, paired t-test, left; CNO ($t(7)=1.311$, $p=0.231$, two-tailed, paired t-test, right). (**E**) Investigation of a novel animal relative to a novel object did not affect fast gamma power following vehicle or CNO administration ($F(1, 6)=0.320$, $p=0.592$, RM two-way ANOVA with Geisser-Greenhouse correction, center heading; vehicle: ($t(7)=0.335$, $p=0.745$, two-tailed, paired t-test, left; CNO: ($t(7)=0.346$, $p=0.734$, two-tailed, paired t-test, right).

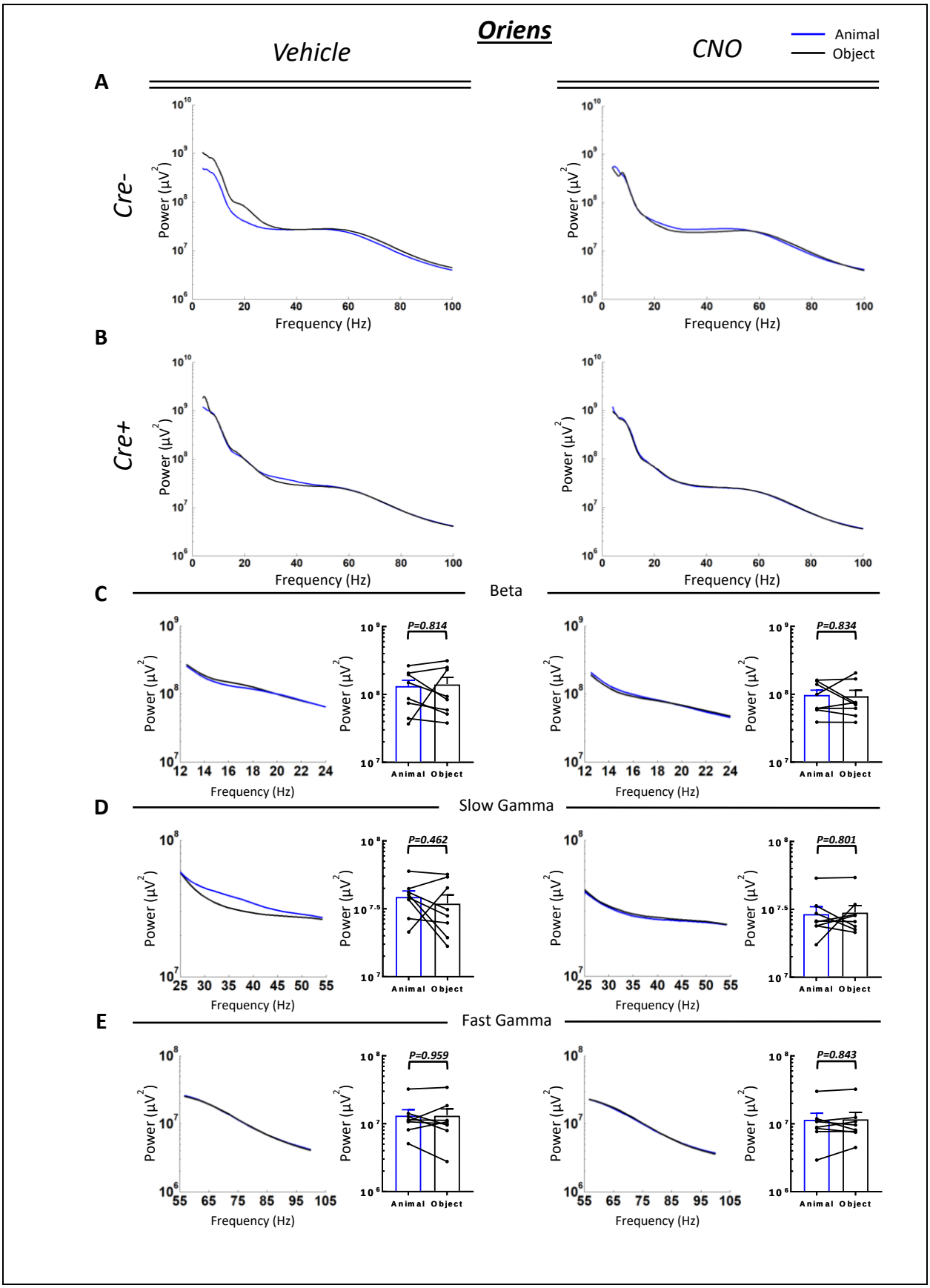
Oriens
Vehicle
CNO
Animal
Object
A
Cre-
B
Cre+
Power (μV²)
Frequency (Hz)
C
Beta
D
Slow Gamma
E
Fast Gamma
P=0.814
P=0.834
P=0.462
P=0.801
P=0.959
P=0.843
Animal Object

Figure 3.7: Hippocampal oscillations in stratum oriens of CA1 do not significantly differ during investigation of a novel animal relative to a novel object following treatment with vehicle or CNO in hM4Di-infused *Amigo2*-icreERT2+ mice. Power spectral densities for the 1-100Hz frequency range calculated from LFPs recorded from stratum oriens of CA1 in *Amigo2*-icreERT2 mice infused with AAV-hM4Di-mCherry, treated with tamoxifen, and challenged with vehicle or CNO (3 mg/kg) while subjects actively investigated a novel animal (left column) or novel object (right column). (**A**) PSDs for *Amigo2*-icreERT2- mice. (**B**) PSDs for *Amigo2*-icreERT2+ mice. Plots (**C-E**) show data only from *Amigo2*-icreERT2+ mice. The left side of each pair of plots shows the group averaged PSD trace for the frequency band of interest. The right side of each pair of plots shows the group averages for each frequency band as colored bars graphs; dots represent data from individual animals. The results of ANOVAs for are indicated by the symbols located next to the heading for each frequency band. The specific p-values from paired t-test comparisons are shown over their respective graphs. (**C**) Investigation of a novel animal relative to a novel object did not affect beta power following vehicle or CNO administration ($F(1, 6)=0.070$, $p=0.800$, RM two-way ANOVA with Geisser-Greenhouse correction, center heading; vehicle: ($t(7)=0.244$, $p=0.814$, two-tailed, paired t-test, left; CNO: ($t(7)=0.217$, $p=0.834$, two-tailed, paired t-test, right). (**D**) Investigation of a novel animal relative to a novel object did not affect slow gamma power following vehicle or CNO administration ($F(1, 6)=0.720$, $p=0.429$, RM two-way ANOVA with Geisser-Greenhouse correction, center heading; vehicle: ($t(7)=0.779$, $p=0.462$, two-tailed, paired t-test, left; CNO ($t(7)=0.252$, $p=0.801$, two-tailed, paired t-test, right). (**E**) Investigation of a novel animal relative to a novel object did not affect fast gamma power following vehicle or CNO administration ($F(1, 6)=0.381$, $p=0.560$, RM two-way ANOVA with Geisser-Greenhouse correction, center heading; vehicle: ($t(7)=0.054$, $p=0.959$, two-tailed, paired t-test, left; CNO: ($t(7)=0.206$, $p=0.843$, two-tailed, paired t-test, right).

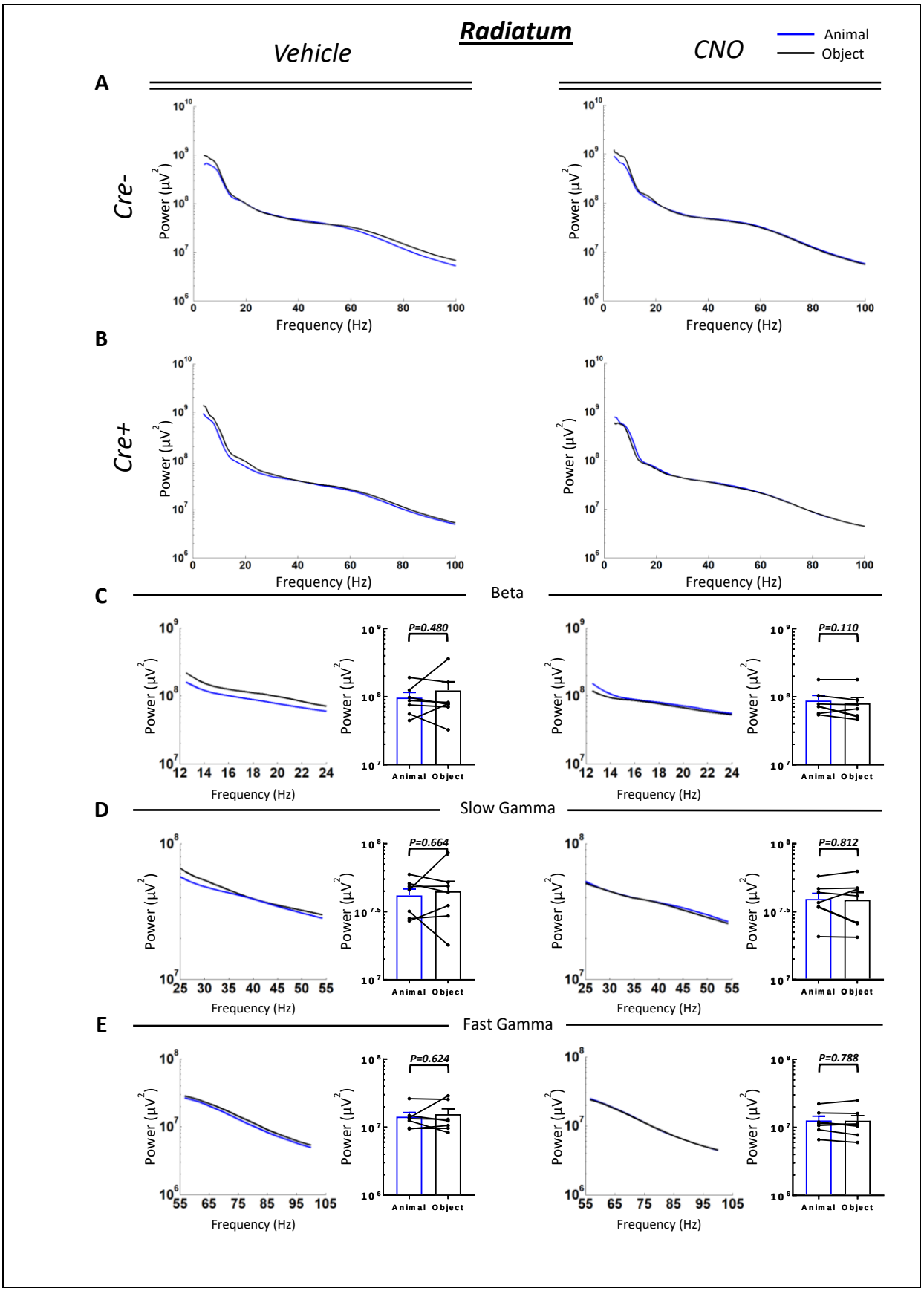
Radiatum
Vehicle
CNO
Animal
Object
A
Cre-
B
Cre+
Power (μV²)
Frequency (Hz)
C
Beta
D
Slow Gamma
E
Fast Gamma
P=0.480
P=0.110
P=0.664
P=0.812
P=0.624
P=0.788
Animal
Object

Figure 3.8: Hippocampal oscillations in stratum radiatum of CA1 do not significantly differ during investigation of a novel animal relative to a novel object following treatment with vehicle or CNO in hM4Di-infused *Amigo2*-icreERT2+ mice. Power spectral densities for the 1-100Hz frequency range calculated from LFPs recorded from stratum radiatum of CA1 in *Amigo2*-icreERT2 mice infused with AAV-hM4Di-mCherry, treated with tamoxifen, and challenged with vehicle or CNO (3 mg/kg) while subjects actively investigated a novel animal (left column) or novel object (right column). (**A**) PSDs for *Amigo2*-icreERT2- mice. (**B**) PSDs for *Amigo2*-icreERT2+ mice. Plots (**C-E**) show data only from *Amigo2*-icreERT2+ mice. The left side of each pair of plots shows the group averaged PSD trace for the frequency band of interest. The right side of each pair of plots shows the group averages for each frequency band as colored bars graphs; dots represent data from individual animals. The results of ANOVAs for are indicated by the symbols located next to the heading for each frequency band. The specific p-values from paired t-test comparisons are shown over their respective graphs. (**C**) Investigation of a novel animal relative to a novel object did not affect beta power following vehicle or CNO administration ($F(1, 6)=0.008$, $p=0.933$, RM two-way ANOVA with Geisser-Greenhouse correction, center heading; vehicle: ($t(7)=0.753$, $p=0.480$, two-tailed, paired t-test, left; CNO: ($t(7)=1.874$, $p=0.110$, two-tailed, paired t-test, right). (**D**) Investigation of a novel animal relative to a novel object did not affect slow gamma power following vehicle or CNO administration ($F(1, 6)=0.030$, $p=0.869$, RM two-way ANOVA with Geisser-Greenhouse correction, center heading; vehicle: ($t(7)=0.457$, $p=0.664$, two-tailed, paired t-test, left; CNO: ($t(7)=0.249$, $p=0.812$, two-tailed, paired t-test, right). (**E**) Investigation of a novel animal relative to a novel object did not affect fast gamma power following vehicle or CNO administration ($F(1, 6)=0.114$, $p=0.747$, RM two-way ANOVA with Geisser-Greenhouse correction, center heading; vehicle: ($t(7)=0.517$, $p=0.624$, two-tailed, paired t-test, left; CNO: ($t(7)=0.281$, $p=0.788$, two-tailed, paired t-test, right).

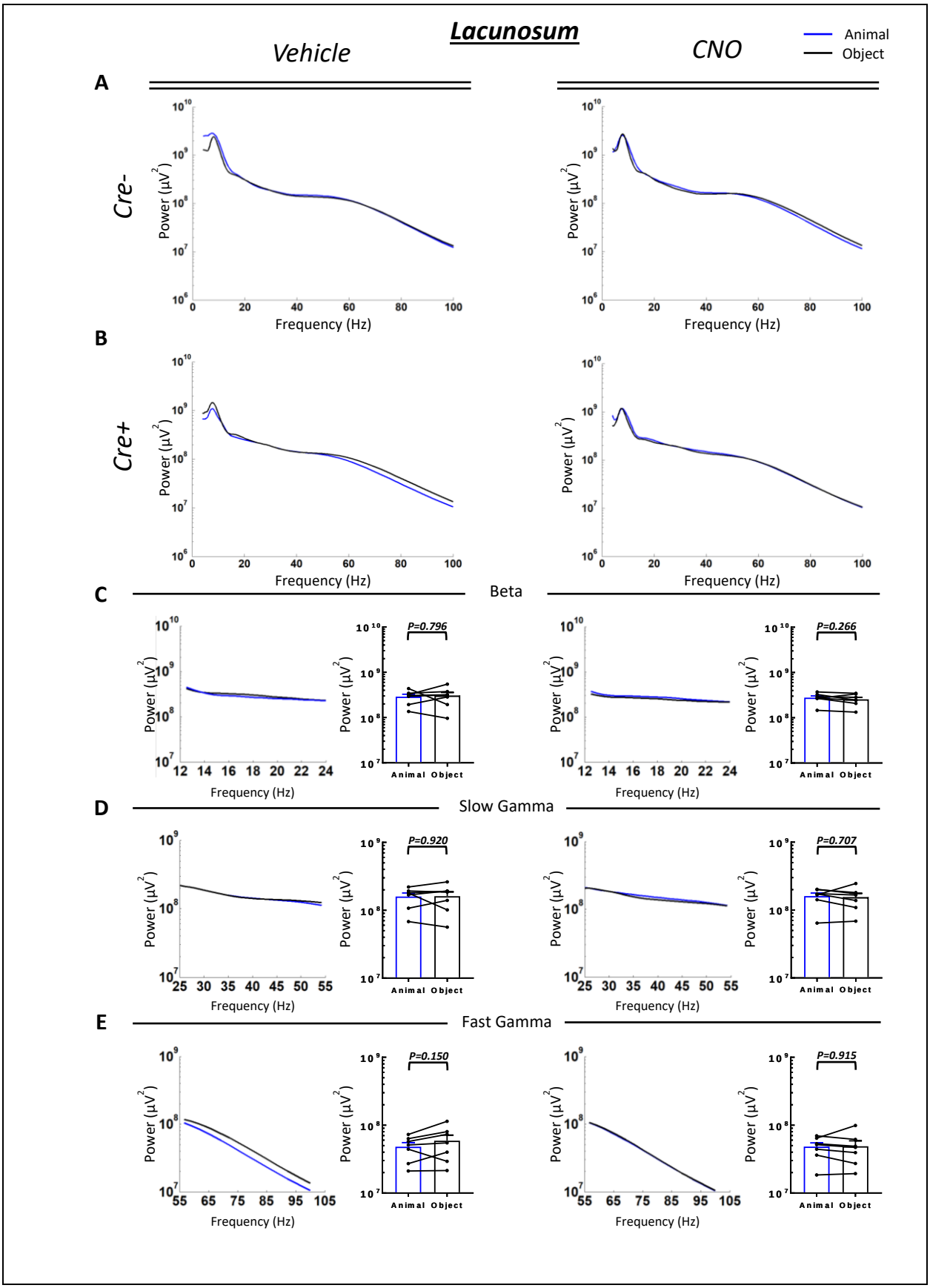
Lacunosum
Vehicle
CNO
Animal
Object
A
Cre-
B
Cre+
Power (μV²)
Frequency (Hz)
C
Beta
D
Slow Gamma
E
Fast Gamma
P=0.796
P=0.266
P=0.920
P=0.707
P=0.150
P=0.915
Animal Object

Figure 3.9: Hippocampal oscillations in stratum lacunosum-moleculare of CA1 do not significantly differ during investigation of a novel animal relative to a novel object following treatment with vehicle or CNO in hM4Di-infused *Amigo2*-icreERT2+ mice. Power spectral densities for the 1-100Hz frequency range calculated from LFPs recorded from stratum lacunosum-moleculare of CA1 in *Amigo2*-icreERT2 mice infused with AAV-hM4Di-mCherry, treated with tamoxifen, and challenged with vehicle or CNO (3 mg/kg) while subjects actively investigated a novel animal (left column) or novel object (right column). (**A**) PSDs for *Amigo2*-icreERT2- mice. (**B**) PSDs for *Amigo2*-icreERT2+ mice. Plots (**C-E**) show data only from *Amigo2*-icreERT2+ mice. The left side of each pair of plots shows the group averaged PSD trace for the frequency band of interest. The right side of each pair of plots shows the group averages for each frequency band as colored bars graphs; dots represent data from individual animals. The results of ANOVAs for are indicated by the symbols located next to the heading for each frequency band. The specific p-values from paired t-test comparisons are shown over their respective graphs. (**C**) Investigation of a novel animal relative to a novel object did not affect beta power following vehicle or CNO administration ($F(1, 6)=0.002$, $p=0.965$, RM two-way ANOVA with Geisser-Greenhouse correction, center heading; vehicle: ($t(7)=0.270$, $p=0.796$, two-tailed, paired t-test, left; CNO: ($t(7)=1.226$, $p=0.266$, two-tailed, paired t-test, right). (**D**) Investigation of a novel animal relative to a novel object did not affect slow gamma power following vehicle or CNO administration ($F(1, 6)=0.000$, $p=0.994$, RM two-way ANOVA with Geisser-Greenhouse correction, center heading; vehicle: ($t(7)=0.105$, $p=0.920$, two-tailed, paired t-test, left; CNO: ($t(7)=0.394$, $p=0.707$, two-tailed, paired t-test, right). (**E**) Investigation of a novel animal relative to a novel object did not affect fast gamma power following vehicle or CNO administration ($F(1, 6)=0.720$, $p=0.429$, RM two-way ANOVA with Geisser-Greenhouse correction, center heading; vehicle: ($t(7)=1.651$, $p=0.150$, two-tailed, paired t-test, left; CNO: ($t(7)=0.111$, $p=0.915$, two-tailed, paired t-test, right).

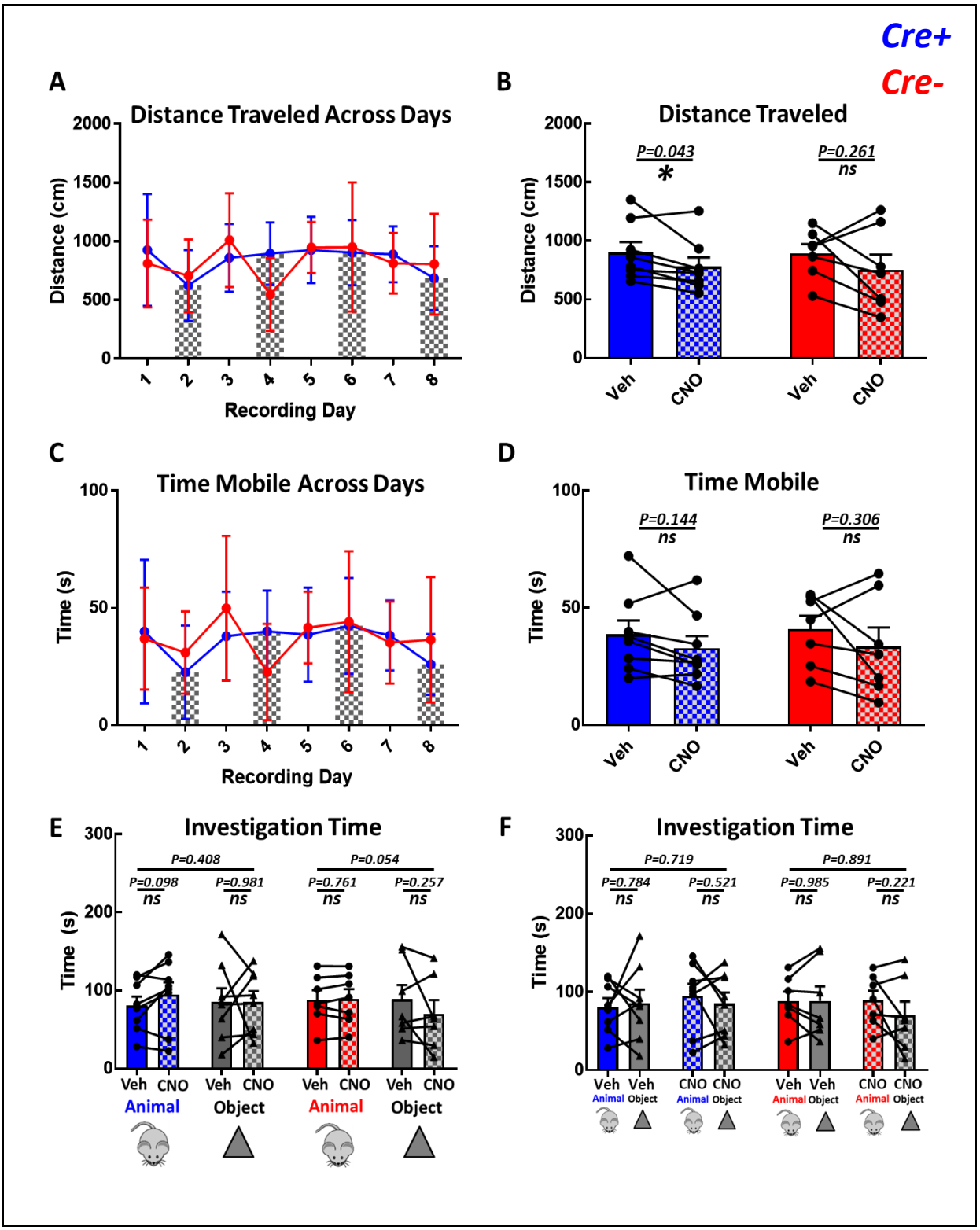
Cre+
Cre-
A
Distance Traveled Across Days
Distance (cm)
Recording Day
B
Distance Traveled
P=0.043
*
P=0.261
ns
Veh
CNO
C
Time Mobile Across Days
Time (s)
D
Time Mobile
P=0.144
ns
P=0.306
E
Investigation Time
P=0.408
P=0.098
ns
P=0.981
P=0.054
P=0.761
P=0.257
Animal
Object
F
P=0.719
P=0.784
P=0.521
P=0.891
P=0.985
P=0.221

Figure 3.10: Acute inhibition of CA2 pyramidal cells with CNO in hM4Di-infused *Amigo2*-icreERT2+ mice reduces the average distance subjects travel. CNO administration is indicated by hash-marked bars. All samples used for analysis of distance traveled and mobility were taken from the baseline phase of recording in which no stimulus was present. (**A**) The average distance traveled across recording sessions did not vary significantly for *Amigo2*-icreERT2+ ($F(1, 6)=2.141$, $p=0.115$, RM two-way ANOVA with Geisser-Greenhouse correction; blue line) or *Amigo2*-icreERT2- ($F(1, 6)=1.772$, $p=0.189$, RM two-way ANOVA with Geisser-Greenhouse; red line) mice. (**B**) CNO revealed a significant reduction in the average distance traveled by *Amigo2*-icreERT2+ mice ($t(7)=2.462$, $p=0.043$, two-tailed, paired t-test; blue bars), but not *Amigo2*-icreERT2- mice ($t(7)=1.242$, $p=0.261$, two-tailed, paired t-test; red bars). (**C**) The average time spent mobile across recording sessions did not vary significantly for *Amigo2*-icreERT2+ ($F(1, 6)=2.082$, $p=0.122$, RM two-way ANOVA with Geisser-Greenhouse correction; blue line) or *Amigo2*-icreERT2- ($F(1, 6)=1.528$, $p=0.239$, RM two-way ANOVA with Geisser-Greenhouse; red line) mice. (**D**) CNO did not significantly affect the average time spent mobile by *Amigo2*-icreERT2+ mice ($t(7)=1.644$, $p=0.144$, two-tailed, paired t-test; blue line) or *Amigo2*-icreERT2- mice ($t(7)=1.119$, $p=0.306$, two-tailed, paired t-test; red line). (**E**) CNO did not significantly affect the amount of time *Amigo2*-icreERT2+ mice ($F(1, 6)=0.776$, $p=0.408$, RM two-way ANOVA with Geisser-Greenhouse correction; animal: $t(7)=1.912$, $p=0.098$, two-tailed, paired t-test); object: ($t(7)=0.025$, $p=0.981$, two-tailed, paired t-test) or *Amigo2*-icreERT2- mice $F(1, 6)=5.741$, $p=0.054$, RM two-way ANOVA with Geisser-Greenhouse; animal: ($t(6)=0.319$, $p=0.761$, two-tailed, paired t-test; object: ($t(6)=1.252$, $p=0.257$, two-tailed, paired t-test) spent investigating stimuli. (**F**) Stimulus type did not significantly affect the time *Amigo2*-icreERT2+ ($F(1, 6)=0.141$, $p=0.719$, RM two-way ANOVA with Geisser-Greenhouse correction; vehicle: ($t(7)=0.285$, $p=0.784$, two-tailed, paired t-test; CNO: ($t(7)=0.675$, $p=0.521$, two-tailed, paired t-test) or *Amigo2*-icreERT2- ($F(1, 6)=0.020$, $p=0.891$, RM two-way ANOVA with Geisser-Greenhouse; vehicle: ($t(7)=0.019$, $p=0.985$, two-tailed, paired t-test; CNO: ($t(7)=1.365$, $p=0.221$, two-tailed, paired t-test) mice spent investigating stimuli.

CHAPTER 4. DISCUSSION

4.1 CA2 as a Generator of Hippocampal Gamma and Beta Oscillations for Spatial Cognition

With the advent of molecular biology has come new tools that enable neurobiologists to selectively target and manipulate genetically defined cell populations to untangle their specific contributions to brain function and behavior. We used an inducible transgenic mouse line in combination with a chemogenetic approach to genetically target and manipulate CA2 pyramidal cells in vivo and explore their role in coordinating hippocampal oscillatory networks during active behaviors. Brain oscillations are periodically fluctuating waves of neuronal activity that represent the synchronous activity of large groups of neurons and different frequencies of oscillatory activity in the hippocampus are thought to support memory acquisition, consolidation, and retrieval. Our findings revealed that engagement of the endogenous GPCR-mediated signaling pathways in CA2 is sufficient to bi-directionally modulate hippocampal oscillations in the beta and slow gamma frequency ranges, and that modulation of the slow and fast gamma bands is coordinated in a layer-specific manner that is reflective of the anatomical connectivity of CA2 pyramidal cells. Together, these results demonstrate that CA2 is an integral node capable of coordinating hippocampal oscillatory networks in the behaving animal.

Acute chemogenetic activation of CA2 pyramidal cells using hM3Dq dose-dependently decreased beta power in the pyramidal cell layer of CA2/proximal CA1 during periods of rest, while acute inhibition using hM4Di increased beta power during running. Although hippocampal oscillations in the beta frequency band have been studied far less than the theta and gamma oscillations, they are thought to contribute to hippocampal novelty detection, as beta power is increased upon exposure to a novel environment and decreases with subsequent, exposures (Berke et al., 2008; Grossberg, 2009). A role for CA2 in novelty detection is consistent with the findings that CA2 place fields remap in response to exposure to novel environmental stimuli (Alexander et al., 2016), social and otherwise, as well as other studies demonstrating CA2's responsiveness to novelty (Lu et al., 2015; Wintzer et al., 2014), even when there is no social component involved in the task. In contrast to the direction of effects in the beta band,

activation of CA2 pyramidal cells dose-dependently increased slow gamma power and acute inhibition decreased it. The inverse relationship between shifts in beta and slow gamma power as a result of CA2 manipulation suggests these oscillations may compete for network dominance in a time-sharing manner, a feature that has also been proposed to describe the relationship between slow and fast gamma oscillations in the hippocampus. Such a relationship may indicate that these oscillations rely on a finite, overlapping pool of neurons, and that at least some portion of the same cells are recruited for synchronization in both frequency bands depending on the behavioral demands driving synchronization. If endogenous mechanisms were competing to entrain some proportion of the same cells, this could explain why increases in slow gamma power co-occur with decreases in beta power, and vice versa. This antagonistic relationship between oscillations in the beta and slow gamma frequency can be contrasted to that of the theta and gamma frequency bands, in which increases and decreases in power occur simultaneously.

Acute chemogenetic activation of CA2 pyramidal cells using the hM3Dq construct dose-dependently increased hippocampal slow gamma power during periods of running and rest, while acute chemogenetic inhibition of CA2 pyramidal cells using the hM4Di construct decreased slow gamma power during periods of running, a time when physiological gamma power is normally elevated. Interestingly, the magnitude of the hM3Dq-mediated increase in slow gamma power appears to be attenuated during periods of running. This is apparent in the spectrograms presented in figure 2.4 B, in which periods of running can be identified by a robust increase in theta power (~8 Hz), as well as in the PSDs presented in figure 2.5 E, where the magnitude of the hM3Dq-induced slow gamma power at the 4.0 mg/kg CNO dose is approximately four-fold larger relative to vehicle during periods of rest, but only about 50% larger during periods of running. These observations indicate that naturally occurring slow gamma driven by running disrupt the synchronized timing imposed by hM3Dq activation. As chemogenetic tools are an artificial means of manipulating neuronal activity, it is perhaps not surprising that activation of cells using this approach interfered with endogenous synchronization mechanisms. Accordingly, although the robust, long-lasting induction of gamma power through hM3Dq activation reported here does not resemble the short bursts of increased gamma power observed during natural behaviors (Colgin & Moser, 2010), the propensity of the network to readily synchronize in the slow gamma frequency range for extended periods

of time suggests a role for neural activity in this frequency range in CA2-mediated functions, including spatial and social memory. Given that the Avpr1b is selectively enriched in CA2 pyramidal cells, and is coupled to the same Gq- signaling pathway manipulated in these experiments, the observation that CA2 mediates slow gamma power suggests this frequency of neural activity may be one mechanism underlying the vasopressin-mediated manipulation of social memory. After observing that acute activation of CA2 pyramidal cells caused a robust increase in slow gamma power, we asked if acute inhibition of CA2 pyramidal cells using the hM4Di construct would reduce endogenous slow gamma driven by natural behaviors, such as running.

Acute chemogenetic inhibition of CA2 pyramidal cells using the hM4Di construct significantly reduced slow gamma power by approximately 20% during periods of running. Although CA3 is the only currently recognized originator of hippocampal slow gamma oscillations, recent work showed that permanent silencing of CA3 output with tetanus toxin light chain only reduced slow gamma power by approximately 30% (Middleton & McHugh, 2016), suggesting another source of hippocampal slow gamma oscillations may exist. Our results indicate that CA2 and CA3 together likely provide the excitatory drive necessary for hippocampal slow gamma oscillations. Thus, to completely abolish endogenous slow gamma oscillations during running would likely require complete silencing of both CA2 and CA3 pyramidal cells. However, due to the brain's plastic nature and ability to dynamically reassign function following insult, it would not be unexpected to find that upon inhibiting either CA2 or CA3, the other subfield would be capable of compensating for the initial loss of input following some passage of time. Further, because CA2 and CA3 axons preferentially target different dendritic domains of CA1 pyramidal cells (Kohara et al., 2014; S. H. Lee et al., 2014), gamma activity arising from CA2 and CA3 may be actively engaging distinct circuits involving the deep and superficial CA1 pyramidal neurons, respectively, which have been shown to form functionally distinct sublayers. These two CA1 populations exhibit unique input responses to stimulation (Mizuseki et al., 2011), are preferentially innervated by CA3 and CA2 Schaffer collateral projections, and may represent functionally divergent output streams. The deep CA1 cells, which are preferentially innervated by CA2, account for the majority of hippocampal projections to the lateral septum, an area implicated in regulating mood and motivation (Sheehan, Chambers, & Russell, 2004). CA1 pyramidal cells can also be differentially regulated by gamma

oscillations (Senior et al., 2008), together suggesting that gamma oscillations arising from CA3 and CA2 may serve distinct cognitive functions.

CA3 and CA2 exhibit several common anatomical features which may account for their shared role in slow gamma generation. Gamma oscillations emerge locally in some cortical regions and propagate to neighboring areas; however, in vivo they have only been observed to occur spontaneously in networks which exhibit a significant recursive collateral system (Hajos & Paulsen, 2009). In brain areas lacking local recurrent connections, such as the DG and CA1, gamma oscillations appear to depend on extrinsic rhythmic inputs (Bragin et al., 1995; Csicsvari, Jamieson, Wise, & Buzsaki, 2003). This is not because these areas are intrinsically unable to maintain rhythmic activity, as gamma oscillations can be evoked in these regions under certain experimental conditions using an acute slice preparation, but appears to depend on the presence of recursive connectivity, which CA2 and CA3 both exhibit (Lorente de No, 1934; Mercer, Trigg, & Thomson, 2007; Tamamaki et al., 1988). Another key component for spontaneous gamma rhythmogenesis is a mutually connected network of fast-spiking, perisomatically-targeting interneurons. During the gamma cycle, such fast-spiking interneurons exert rhythmic inhibition over pyramidal cells which is thought to generate the temporal structure of the gamma oscillation by controlling when, how many, and which pyramidal cells fire during each falling inhibition phase of the cycle (Hajos & Paulsen, 2009). CA2, like CA3, also possesses a robust network of fast-spiking, perisomatically-targeting interneurons (Botcher, Falck, Thomson, & Mercer, 2014; Mercer, Eastlake, Trigg, & Thomson, 2012; Mercer et al., 2007), indicating that CA2 is equipped for spontaneous gamma rhythmogenesis, which could then propagate to CA1.

The finding that CA2 pyramidal cells contribute to the state-dependent organization of hippocampal slow gamma oscillations is consistent with previous knowledge of CA3's role in slow gamma generation, and that CA2 also exhibits morphological and cellular features thought to be necessary for spontaneous gamma rhythmogenesis. However, given that CA3 and CA2 have distinct outputs in CA1, oscillations arising from the two areas may serve distinct aspects of memory formation. Given evidence for CA2's role in social memory, and previous studies demonstrating that slow-gamma synchrony between CA3 and CA1 supports spatial memory, as well as the acquisition of stimulus-context pairings,

we asked if CA2-dependent gamma oscillations in CA1 would show preferential shifts in power when subjects investigated a novel social stimulus relative to a non-social one.

4.2 CA2 as a Generator of Hippocampal Slow and Fast Gamma Oscillations During Investigation of Novel Stimuli

In this study we used inhibitory DREADDs to reversibly modify CA2 pyramidal cell activity and examine the effects on neuronal oscillations in the different layers of CA1. We found that acute, reversible inhibition of CA2 pyramidal cells with hM4Di selectively reduced hippocampal CA1 oscillatory power in a layer- and frequency-specific manner. Inhibition of CA2 pyramidal cells caused a significant reduction in slow and fast gamma power in the pyramidal cell layer and stratum oriens, and in fast gamma power in stratum radiatum of CA1. No significant changes in power in stratum lacunosum-moleculare were observed. While the magnitude of slow gamma reduction in the pyramidal cell layer and stratum oriens was larger when the stimulus presented was a novel animal relative to a novel object, CA2 inhibition overall showed a similar effect of reducing gamma power regardless of the stimulus presented.

These experiments were designed to address two aspects about the role of CA2 in organizing hippocampal networks in vivo. First, despite knowledge that CA2 is required for intact social recognition memory (Hitti & Siegelbaum, 2014), whether CA2 neurons coordinate their activity with CA1 to integrate social cues into memory remained unexplored. Given our previous evidence demonstrating CA2's role in organizing hippocampal slow gamma oscillations during running, we hypothesized that if CA2 is preferentially involved in processing information about socially relevant stimuli, CA2 pyramidal cells would cause an increase in neuronal activity in CA1 only while investigating a novel animal, and not a novel object. Thus, we sought to extend our investigation of CA2 by examining CA1 activity while subjects could freely explore different types of stimuli. Second, although oscillations are most commonly recorded at the level of the pyramidal cell soma, hippocampal gamma oscillations in CA1 have been shown to be regulated in a layer-specific manner (Fernandez-Ruiz et al., 2012; Lasztoczi & Klausberger, 2014, 2016; Scheffer-Teixeira et al., 2012). In the synaptic layers of CA1 increases in LFP power are thought to represent synchronized input from upstream EC and CA3. Because CA2 pyramidal cells also project to CA1 where they selectively target unique dendritic domains, with the basal dendrites in stratum oriens receiving the densest CA2 projections, followed by the apical dendrites in stratum radiatum and, notably, no projections to lacunosum-moleculare (Shinohara et al., 2012; Tamamaki et al., 1988), we

hypothesized that there would be layer-specific reductions of slow gamma power in CA1 while inhibiting CA2 pyramidal cells. Specifically, we predicted that 1) Neuronal activity in the slow gamma frequency range would increase in stratum oriens and the pyramidal cell layer of CA1 during investigation of a novel animal, but not a novel object and 2) Inhibition of CA2 pyramidal cells would cause a reduction in the observed increase in gamma power. To test our hypothesis and address these predictions, we implanted silicone probes with a linear array of electrode contacts that permitted sampling of LFPs from all layers of CA1 in mice expressing hM4Di in CA2 neurons. We then recorded LFPs while subjects investigated a novel animal or novel object and examined the effects on oscillatory power. To explore possible effects, we first ran a series of independent, repeated measures, two-way ANOVAs to analyze each frequency band of interest, in each layer, using all experimental conditions (Vehicle-Animal, Vehicle-Object, CNO-Animal, and CNO-Object). Our analyses were aimed toward identifying effects of drug treatment (vehicle vs. CNO) (**Figures 3.2 - 3.5**) and stimulus type (animal vs. object) (**Figures 3.6 - 3.9**).

Consistent with our hypothesis, we found that inhibition of CA2 pyramidal cells with CNO caused a significant reduction in slow gamma power in the pyramidal cell layer and stratum oriens of CA1 relative to vehicle. We also found a significant reduction in fast gamma power in the pyramidal cell layer, stratum oriens, and stratum radiatum, but no changes in stratum lacunosum-moleculare were observed. These results support our previous finding that slow gamma power in the pyramidal cell layer is increased and decreased with excitation and inhibition of CA2 neurons, respectively. These results extend upon our previous findings in three ways. First, we show that investigation of novel stimuli is another behavior which can be used to probe CA2-dependent shifts in synchronous hippocampal activity. Second, we demonstrate that manipulation of CA2 pyramidal cells can impact activity in both the slow and fast gamma frequency ranges in CA1, in contrast to periods when animals are running or at rest, during which only the slow gamma band was modulated. Third, we found that the manipulation of CA2 pyramidal cells not only influences gamma oscillations measured at the pyramidal cell level, representative of the overall state of entrainment in the local network, but that frequency-specific shifts in oscillatory power also occur in the synaptic layers of CA1. These layer-specific effects reflect the anatomical connectivity of CA2 pyramidal cells, which predominantly form synapses with basal CA1 dendrites in stratum oriens and, to a lesser extent, the apical dendrites in stratum radiatum. Thus, the finding that inhibition of CA2 pyramidal

cells reduces the magnitude of synchronous inputs arriving in CA1 straum oriens and radiatum, the dendritic target domains of CA2 pyramidal cells, suggests that this frequency of neural activity is important for coordinating interactions between CA2 and CA1.

The finding that inhibition of CA2 pyramidal cells reduced fast gamma power in CA1 is particularly surprising given that the EC is currently thought to be the sole originator of this frequency of activity in CA1 and, unlike its shared features with CA3, CA2 does not anatomically of functionally resemble the EC in any immediately apparent way. This observation suggests that 1) CA2 pyramidal cells contribute to the state-dependent organization of fast gamma oscillations in CA1 and 2) frequency specific shifts in CA1 synchrony that depend on CA2 output may be differentially recruited according to specific behavioral demands, with running driving CA2-dependent slow gamma and investigation of stimuli driving CA2-dependent slow and fast gamma.

In contrast to our predictions, we found no significant difference in gamma power based on the type of stimulus presented. Although the ANOVAs did not reveal a significant difference in oscillatory power according to stimulus type, based on *a priori* hypotheses about CA2's role in social memory, we also used a series of two-tailed, paired t-tests to further explore the data and make explicit comparisons that were of interest when designing the study. In some instances, the paired t-tests results segregated according to stimulus type. That is, of the five instances in which the ANOVAs revealed a simple main effect of drug, there were three instances in which the follow up t-tests only revealed a significant difference between vehicle and CNO when the stimulus presented was an animal and not an object. These results suggested a possible difference in slow and fast gamma power caused by stimulus type that was not detected by the ANOVA. This segregation in t-test comparisons was observed for the slow and fast gamma bands in stratum oriens, and the slow gamma band in the pyramidal cell layer. We found the magnitude of slow gamma reduction by CNO was modestly larger in these areas for the animal condition, as indicated by the animal comparisons reaching significance, but not the object-comparisons. This may be due to several factors including too much scatter in the variance, insufficient statistical power due to small sample size, or that CA2 is not the only area involved in the observed effects. Although the possibility that the effects observed in CA1 were mediated by another CA1-projecting brain region cannot

be excluded, the genetically targeted manipulation of CA2 pyramidal cells causally links CA2 activity with the network organization observed in CA1.

To address the possibility that the lack of significance from t-test comparisons for the object condition could have been due to insufficient statistical power, we estimated the sample sizes that would be required to confirm these results, and our original hypothesis, based on our observed effect sizes and chosen level of significance. For slow gamma in the pyramidal cell layer, the sample size that would be required to confirm the lack of difference in power between the vehicle and CNO conditions when the stimulus presented was an object was 16 animals. For slow gamma in stratum oriens it was 84 animals, and for fast gamma in stratum oriens it was 30 animals. Because the actual sample size in these experiments was 9 animals, these results indicate that the lack of significant difference in LFP power between the vehicle and CNO conditions during investigation of a novel object could be due to insufficient statistical power caused by too small a sample. Similar to the animal condition, a significant effect for the object condition could be revealed upon increasing the sample size. However, these large sample size estimates are attributable to the small effect size of the object condition relative to the animal. These results are consistent with the results of the 2-way, repeated-measures ANOVA which revealed a simple main effect of drug, regardless of the stimulus presented, and no interaction effects. For comparison, we also ran the same analysis for the animal condition and found that the sample sizes that would be required to confirm these results were 10 animals for slow gamma in the pyramidal cell layer, 12 animals for slow gamma in statum oriens, and 9 animals for fast gamma in stratum oriens. Again, with an actual sample size of 9, a few more animals would be needed to confirm the slow gamma band results, but relative to the object condition, the much smaller sample size requirements for the animal condition is attributable to a real difference in effect size. Together, these results indicate that inhibition of CA2 causes a reduction in gamma power regardless of stimulus presented, but the magnitude of reduction is larger when the stimulus is an animal, relative to an object.

Given the results of this analysis, we asked if there were inherent differences in CA1 power when subjects were investigating a novel animal relative to a novel object. That is, can the modestly larger reduction in hM4Di-mediated gamma power observed during investigation of a novel animal be explained by the existence of a higher basal gamma power during investigation of an animal relative to an object.

To address our question, we ran a series of independent, paired t-tests to compare power during investigation of the different stimulus types following the same drug treatment, rather than comparing power for the same stimulus type following different drug treatments. Contrary to our hypothesis, no significant differences in power were observed for any frequency band when subjects investigated the novel animal or novel object following the same drug treatment.

Although the magnitude of slow gamma reduction was greater in stratum oriens and the pyramidal cell layer when the stimulus was a novel animal, the significant main effects of drug treatment, in combination with the lack of differences for stimulus type, or interaction effects between drug condition and stimulus type, together demonstrate that CA2 inhibition causes a reduction in slow and fast gamma power regardless of stimulus type. Although these findings do not support the idea that CA2 is exclusively involved in social memory, it is consistent with studies demonstrating CA2 places cells remap in response to both conspecifics and novel objects (Alexander et al., 2016). Given the importance of social cognition in promoting the survival of many species, it is not difficult to construct a narrative in which CA2 function has been refined through natural-selection to serve as a social-memory hub. Given that we did not find evidence for an effect of stimulus type, as well as the finding that CA2 manipulation modulated beta oscillations during running, a frequency thought to be important for novelty detection in the hippocampus, such a narrative may be an overly-simplistic view of CA2 function. An alternative explanation that is consistent with our findings is that CA2 serves as a more general memory platform that is specialized to respond to any novel stimulus deemed salient. Such stimuli could be social in nature, which are likely frequently salient, but could also be anything important for guiding subsequent behavior, such as the location of a novel food source. It is also possible that CA2 is, in fact, a social-memory hub, but that shifts in oscillatory power are not reflective of its functional specialization. The neural code for social information could, for example, take the form of non-periodic spike trains.

Here we provided evidence that CA2 neurons provide part of the excitatory drive required for generation of slow gamma oscillations in the hippocampus during periods of rest and running, and slow and fast gamma oscillations during investigation of novel stimuli. Although we did not observe a differential effect of CA2 inhibition on oscillations according to the type of stimulus presented, we did observe a frequency-specific difference between running and investigation of stimuli. These results 1.

Confirm previous observations that CA1 gamma oscillations are coordinated in a layer- and frequency-specific manner 2. Demonstrate a causal role for CA2 output in structuring this organization, and 3. Indicate that the primary function of CA2 neurons may be processing memories of novel experiences rather than exclusively social ones. Together, these findings support the idea that CA2 is an integral hippocampal node involved in coordinating neuronal synchronization during active behaviors.

4.3 Behavioral Correlates of Chemogenetic Manipulation of CA2 Pyramidal Cells

Based on our findings of reduced gamma power during acute inhibition of CA2 pyramidal cells during running and investigation of novel stimuli, we asked whether the effects observed on neuronal oscillations correlated with changes in behavior. We assessed hM4Di-infused *Amigo2*-icreERT2 mice for differences in average distance traveled and time spent mobile while acutely inhibiting CA2 and found that treatment with CNO significantly reduced the average distance traveled by *Amigo2*-icreERT2+ mice, but did not affect the amount of time animals spent mobile. One possible explanation for the reduction in average distance traveled is that some component of CNO administration, either the compound or the physical act of subcutaneous injection, may have produced an anxiogenic effect. Another possibility is that by disrupting gamma oscillations we also disrupted the spatial representations generated by place cells. This could have resulted in animals becoming disoriented during exploration of the recording box, which itself could have been anxiogenic. Another possible explanation is that if CA2 is truly signaling the novelty of an environment, CA2 activity may promote investigation of previously unexplored environments which was disrupted by our experimental manipulation.

We also assessed subjects for the differences in time spent investigating stimuli. CNO did not cause a significant difference in the amount of time subjects spent investigating novel animals or novel objects, and subjects did not show an inherent preference for the novel animal or novel object based on time spent investigating the different stimulus types. Because we were interested in CA2's role in hippocampal oscillatory networks and the electrophysiological effects of targeted CA2 manipulation, we selected behaviors that naturally increased hippocampal oscillatory power (running and investigation of novel stimuli), but did not require behavioral training. For these reasons, the lack of a significant effect on stimulus investigation times is not surprising, as we used a passive exposure paradigm in which subjects could freely explore the environment of their own volition, with each session separated by 24 hours. In

contrast, social recognition paradigms typically measure the decrease in investigation time of stimuli following repeated exposures that take place over the course of minutes to hours. This does not mean that the electrophysiological effects described here are not relevant to behavior, but that a more refined behavioral paradigm explicitly designed to assess changes in memory-based performance would be required to reveal their behavioral relevance.

4.4 Future Experiments

The results presented here reveal that CA2 is an integral node capable of organizing hippocampal oscillatory networks during active behaviors; however, it also raised several questions regarding the relationship between CA3 and CA2 in the generation of hippocampal slow gamma oscillations, their role in the larger hippocampal network, and the behavioral significance of CA2-mediated gamma oscillations.

Because previous studies have demonstrated that silencing CA3 synaptic output reduces CA1 slow gamma power by about 30% (Middleton & McHugh, 2016), and we show here that inhibiting CA2 reduced gamma power by approximately 10-25% depending on the layer and behavior, whether these two regions are the exclusive originators of slow gamma in CA1 remains unclear. To address this question would require simultaneous silencing of output from both regions to observe whether hippocampal slow gamma oscillations are abolished. Grik4 is a gene which is selectively expressed in CA3 and CA2 pyramidal cells and the Grik4 Cre mouse line provides genetic access to both populations of cells (Nakazawa et al., 2002). This mouse line could be used in a manner similar to the approach we used here to silence the output of both CA2 and CA3 and observe whether slow gamma oscillations in CA1 are abolished.

In our experiments we were limited to recording LFPs from CA1 using a 32-channel recording system. Although we utilized a chemogenetic approach to selectively manipulate our primary brain region of interest, CA2, and observe the effects on its primary output region, CA1, simultaneous recording from CA2 would have allowed additional questions regarding the state of coherence between CA2 and CA1 to be addressed. Recording systems of 256+ channels are commercially available which, when combined with a probe of appropriate geometry, would enable simultaneous sampling from all hippocampal sub-regions in the rodent. This approach would provide a more comprehensive picture of the state of

oscillatory organization in the hippocampus, allowing for a more contextualized understanding of the significance of region-specific changes in synchronization during active behaviors. For example, shifts in gamma coherence between CA3 and CA1 have been shown to support hippocampal-dependent spatial memory, but whether the shifts in CA1 gamma power reported here are accompanied by coherent shifts with gamma power in CA2 remains unknown. It is conceivable, for example, that CA2 might influence gamma oscillations in CA1 without exhibiting coherent rhythmic activity itself. Being able to examine not only the state-dependence of shifts in synchrony between regions, but also the magnitude of shifts, would help to elucidate whether the CA2-CA1 interface operates in a manner similar to the CA3-CA1 interface.

Another question raised by our experiments is the nature of the relationship between vasopressin, CA2-mediated gamma oscillations, and social memory. The Avpr1b receptor is selectively enriched in CA2 pyramidal cells and is coupled to the Gq-signaling pathway. Bath application of a Avpr1b agonist paired with SC stimulation reveals synaptic potentiation at the CA3 → CA2 Schaffer collateral synapses which are otherwise resistant to changes in synaptic strength (Pagani et al., 2015), and in vivo optogenetic stimulation of the vasopressinergic expressing fibers in CA2 extends the duration of social recognition memory (A. S. Smith et al., 2016). Given our finding that activation of the endogenous Gq-coupled pathway in CA2 pyramidal cells dose-dependently increases hippocampal slow gamma oscillations, one possible explanation is that when CA3 input occurs simultaneously with endogenous vasopressin release in CA2 in response to a social stimulus, potentiation is enabled at the CA3→CA2 synapses which concomitantly enables local gamma rhythmogenesis. This CA2-generated gamma oscillation could then propagate to CA1, facilitating inter-regional synchronization, and allowing successful storage of a memory containing socially relevant information. To address the nature of the relationship between vasopressin, gamma oscillations, and memory, genetic control over vasopressin release in the hippocampus is needed. Directly recording from CA2 in vivo while optogenetically invoking vasopressinergic release there would reveal whether this manipulation is sufficient for local, spontaneous gamma rhythmogenesis in CA2. As is the case for induction of synaptic potentiation, concurrent SC innervation from CA3 may also be required for induction of gamma oscillations, and to test this one could perform the same experiment while the animal is engaged in an active behavior that drives CA3 output, such as running. Complimentary experiments using optogenetic inhibition of vasopressinergic release

during behaviors that naturally increase gamma power would further help elucidate the criticality of vasopressin in state-dependent oscillations in CA2. Together these experiments would build upon the work outlined here and potentially provide answers to remaining questions regarding CA2's role in hippocampal oscillatory networks and its relationship with social memory.

REFERENCES

Ahmed, O. J., & Mehta, M. R. (2012). Running speed alters the frequency of hippocampal gamma oscillations. *J Neurosci, 32*(21), 7373-7383. doi: 10.1523/jneurosci.5110-11.2012

Alexander, G. M., Farris, S., Pirone, J. R., Zheng, C., Colgin, L. L., & Dudek, S. M. (2016). Social and novel contexts modify hippocampal CA2 representations of space. *Nat Commun, 7*, 10300. doi: 10.1038/ncomms10300

Alexander, G. M., Rogan, S. C., Abbas, A. I., Armbruster, B. N., Pei, Y., Allen, J. A., . . . Roth, B. L. (2009). Remote control of neuronal activity in transgenic mice expressing evolved G protein-coupled receptors. *Neuron, 63*(1), 27-39. doi: 10.1016/j.neuron.2009.06.014

Amaral, D. G., & Witter, M. P. (1989). The three-dimensional organization of the hippocampal formation: a review of anatomical data. *Neuroscience, 31*(3), 571-591.

Andersen, P., Bliss, T. V., & Skrede, K. K. (1971). Lamellar organization of hippocampal pathways. *Exp Brain Res, 13*(2), 222-238.

Anderson, P. M., R.; Amaral, D.; Bliss, T.; O'Keefe, J. (2007). *The Hippocampus Book*: Oxford University Press.

Armbruster, B. N., Li, X., Pausch, M. H., Herlitze, S., & Roth, B. L. (2007). Evolving the lock to fit the key to create a family of G protein-coupled receptors potently activated by an inert ligand. *Proc Natl Acad Sci U S A, 104*(12), 5163-5168. doi: 10.1073/pnas.0700293104

Aronov, D., Nevers, R., & Tank, D. W. (2017). Mapping of a non-spatial dimension by the hippocampal-entorhinal circuit. *Nature, 543*(7647), 719-722. doi: 10.1038/nature21692

Bartos, M., Vida, I., Frotscher, M., Meyer, A., Monyer, H., Geiger, J. R., & Jonas, P. (2002). Fast synaptic inhibition promotes synchronized gamma oscillations in hippocampal interneuron networks. *Proc Natl Acad Sci U S A, 99*(20), 13222-13227. doi: 10.1073/pnas.192233099

Bartos, M., Vida, I., & Jonas, P. (2007). Synaptic mechanisms of synchronized gamma oscillations in inhibitory interneuron networks. *Nat Rev Neurosci, 8*(1), 45-56. doi: 10.1038/nrn2044

Basu, J., & Siegelbaum, S. A. (2015). The Corticohippocampal Circuit, Synaptic Plasticity, and Memory. *Cold Spring Harb Perspect Biol, 7*(11). doi: 10.1101/cshperspect.a021733

Berke, J. D., Hetrick, V., Breck, J., & Greene, R. W. (2008). Transient 23-30 Hz oscillations in mouse hippocampus during exploration of novel environments. *Hippocampus, 18*(5), 519-529. doi: 10.1002/hipo.20435

Bliss, T. V., & Collingridge, G. L. (1993). A synaptic model of memory: long-term potentiation in the hippocampus. *Nature, 361*(6407), 31-39. doi: 10.1038/361031a0

Bliss, T. V., & Lomo, T. (1973). Long-lasting potentiation of synaptic transmission in the dentate area of the anaesthetized rabbit following stimulation of the perforant path. *J Physiol, 232*(2), 331-356.

Botcher, N. A., Falck, J. E., Thomson, A. M., & Mercer, A. (2014). Distribution of interneurons in the CA2 region of the rat hippocampus. *Front Neuroanat, 8*, 104. doi: 10.3389/fnana.2014.00104

Bragin, A., Jando, G., Nadasdy, Z., Hetke, J., Wise, K., & Buzsaki, G. (1995). Gamma (40-100 Hz) oscillation in the hippocampus of the behaving rat. *J Neurosci, 15*(1 Pt 1), 47-60.

Buzsaki, G., Anastassiou, C. A., & Koch, C. (2012). The origin of extracellular fields and currents--EEG, ECoG, LFP and spikes. *Nat Rev Neurosci, 13*(6), 407-420. doi: 10.1038/nrn3241

Buzsaki, G., Buhl, D. L., Harris, K. D., Csicsvari, J., Czeh, B., & Morozov, A. (2003). Hippocampal network patterns of activity in the mouse. *Neuroscience, 116*(1), 201-211.

Buzsaki, G., & Draguhn, A. (2004). Neuronal oscillations in cortical networks. *Science, 304*(5679), 1926-1929. doi: 10.1126/science.1099745

Buzsaki, G., Leung, L. W., & Vanderwolf, C. H. (1983). Cellular bases of hippocampal EEG in the behaving rat. *Brain Res, 287*(2), 139-171.

Buzsaki, G., & Schomburg, E. W. (2015). What does gamma coherence tell us about inter-regional neural communication? *Nat Neurosci, 18*(4), 484-489. doi: 10.1038/nn.3952

Buzsaki, G., & Wang, X. J. (2012). Mechanisms of gamma oscillations. *Annu Rev Neurosci, 35*, 203-225. doi: 10.1146/annurev-neuro-062111-150444

Caldwell, H. K., Wersinger, S. R., & Young, W. S., 3rd. (2008). The role of the vasopressin 1b receptor in aggression and other social behaviours. *Prog Brain Res, 170*, 65-72. doi: 10.1016/s0079-6123(08)00406-8

Carter, M. S., J. (2010). *Guide to Research Techniques in Neuroscience*: Elsevier.

Chen, Z., Resnik, E., McFarland, J. M., Sakmann, B., & Mehta, M. R. (2011). Speed controls the amplitude and timing of the hippocampal gamma rhythm. *PLoS One, 6*(6), e21408. doi: 10.1371/journal.pone.0021408

Chevaleyre, V., & Siegelbaum, S. A. (2010). Strong CA2 pyramidal neuron synapses define a powerful disynaptic cortico-hippocampal loop. *Neuron, 66*(4), 560-572. doi: 10.1016/j.neuron.2010.04.013

Colgin, L. L. (2015). Do slow and fast gamma rhythms correspond to distinct functional states in the hippocampal network? *Brain Res, 1621*, 309-315. doi: 10.1016/j.brainres.2015.01.005

Colgin, L. L. (2016). Rhythms of the hippocampal network. *Nat Rev Neurosci, 17*(4), 239-249. doi: 10.1038/nrn.2016.21

Colgin, L. L., Denninger, T., Fyhn, M., Hafting, T., Bonnevie, T., Jensen, O., . . . Moser, E. I. (2009). Frequency of gamma oscillations routes flow of information in the hippocampus. *Nature, 462*(7271), 353-357. doi: 10.1038/nature08573

Colgin, L. L., & Moser, E. I. (2010). Gamma oscillations in the hippocampus. *Physiology (Bethesda), 25*(5), 319-329. doi: 10.1152/physiol.00021.2010

Csicsvari, J., Jamieson, B., Wise, K. D., & Buzsaki, G. (2003). Mechanisms of gamma oscillations in the hippocampus of the behaving rat. *Neuron, 37*(2), 311-322.

Cui, Z., Gerfen, C. R., & Young, W. S., 3rd. (2013). Hypothalamic and other connections with dorsal CA2 area of the mouse hippocampus. *J Comp Neurol, 521*(8), 1844-1866. doi: 10.1002/cne.23263

Eichenbaum, H. (2018). What Versus Where: Non-spatial Aspects of Memory Representation by the Hippocampus. *Curr Top Behav Neurosci, 37*, 101-117. doi: 10.1007/7854_2016_450

Eichenbaum, H., & Cohen, N. J. (2014). Can we reconcile the declarative memory and spatial navigation views on hippocampal function? *Neuron, 83*(4), 764-770. doi: 10.1016/j.neuron.2014.07.032

Eichenbaum, H., Dudchenko, P., Wood, E., Shapiro, M., & Tanila, H. (1999). The hippocampus, memory, and place cells: is it spatial memory or a memory space? *Neuron, 23*(2), 209-226.

Engel, A. K., Fries, P., & Singer, W. (2001). Dynamic predictions: oscillations and synchrony in top-down processing. *Nat Rev Neurosci, 2*(10), 704-716. doi: 10.1038/35094565

Faul, F., Erdfelder, E., Lang, A. G., & Buchner, A. (2007). G*Power 3: a flexible statistical power analysis program for the social, behavioral, and biomedical sciences. *Behav Res Methods, 39*(2), 175-191.

Fell, J., & Axmacher, N. (2011). The role of phase synchronization in memory processes. *Nat Rev Neurosci, 12*(2), 105-118. doi: 10.1038/nrn2979

Fernandez-Ruiz, A., Makarov, V. A., Benito, N., & Herreras, O. (2012). Schaffer-specific local field potentials reflect discrete excitatory events at gamma frequency that may fire postsynaptic hippocampal CA1 units. *J Neurosci, 32*(15), 5165-5176. doi: 10.1523/jneurosci.4499-11.2012

Fries, P. (2005). A mechanism for cognitive dynamics: neuronal communication through neuronal coherence. *Trends Cogn Sci, 9*(10), 474-480. doi: 10.1016/j.tics.2005.08.011

Fries, P. (2015). Rhythms for Cognition: Communication through Coherence. *Neuron, 88*(1), 220-235. doi: 10.1016/j.neuron.2015.09.034

Fries, P., Nikolic, D., & Singer, W. (2007). The gamma cycle. *Trends Neurosci, 30*(7), 309-316. doi: 10.1016/j.tins.2007.05.005

Garcia-Lopez, P., Garcia-Marin, V., & Freire, M. (2006). Three-dimensional reconstruction and quantitative study of a pyramidal cell of a Cajal histological preparation. *J Neurosci, 26*(44), 11249-11252. doi: 10.1523/jneurosci.3543-06.2006

Grossberg, S. (2009). Beta oscillations and hippocampal place cell learning during exploration of novel environments. *Hippocampus, 19*(9), 881-885. doi: 10.1002/hipo.20602

Hainer, C., Mosienko, V., Koutsikou, S., Crook, J. J., Gloss, B., Kasparov, S., . . . Alenina, N. (2015). Beyond Gene Inactivation: Evolution of Tools for Analysis of Serotonergic Circuitry. *ACS Chem Neurosci, 6*(7), 1116-1129. doi: 10.1021/acschemneuro.5b00045

Hajos, N., & Paulsen, O. (2009). Network mechanisms of gamma oscillations in the CA3 region of the hippocampus. *Neural Netw, 22*(8), 1113-1119. doi: 10.1016/j.neunet.2009.07.024

Hitti, F. L., & Siegelbaum, S. A. (2014). The hippocampal CA2 region is essential for social memory. *Nature, 508*(7494), 88-92. doi: 10.1038/nature13028

Insel, T. R. (2010). The challenge of translation in social neuroscience: a review of oxytocin, vasopressin, and affiliative behavior. *Neuron, 65*(6), 768-779. doi: 10.1016/j.neuron.2010.03.005

Ishizuka, N., Weber, J., & Amaral, D. G. (1990). Organization of intrahippocampal projections originating from CA3 pyramidal cells in the rat. *J Comp Neurol, 295*(4), 580-623. doi: 10.1002/cne.902950407

Jutras, M. J., & Buffalo, E. A. (2010). Synchronous neural activity and memory formation. *Curr Opin Neurobiol, 20*(2), 150-155. doi: 10.1016/j.conb.2010.02.006

Kay, K., Sosa, M., Chung, J. E., Karlsson, M. P., Larkin, M. C., & Frank, L. M. (2016). A hippocampal network for spatial coding during immobility and sleep. *Nature, 531*(7593), 185-190. doi: 10.1038/nature17144

Klausberger, T., & Somogyi, P. (2008). Neuronal diversity and temporal dynamics: the unity of hippocampal circuit operations. *Science, 321*(5885), 53-57. doi: 10.1126/science.1149381

Kleinfeld, D., Deschenes, M., & Ulanovsky, N. (2016). Whisking, Sniffing, and the Hippocampal theta-Rhythm: A Tale of Two Oscillators. *PLoS Biol, 14*(2), e1002385. doi: 10.1371/journal.pbio.1002385

Kohara, K., Pignatelli, M., Rivest, A. J., Jung, H. Y., Kitamura, T., Suh, J., . . . Tonegawa, S. (2014). Cell type-specific genetic and optogenetic tools reveal hippocampal CA2 circuits. *Nat Neurosci, 17*(2), 269-279. doi: 10.1038/nn.3614

Lasztoczi, B., & Klausberger, T. (2014). Layer-specific GABAergic control of distinct gamma oscillations in the CA1 hippocampus. *Neuron, 81*(5), 1126-1139. doi: 10.1016/j.neuron.2014.01.021

Lasztoczi, B., & Klausberger, T. (2016). Hippocampal Place Cells Couple to Three Different Gamma Oscillations during Place Field Traversal. *Neuron, 91*(1), 34-40. doi: 10.1016/j.neuron.2016.05.036

Lee, E. C., Yu, D., Martinez de Velasco, J., Tessarollo, L., Swing, D. A., Court, D. L., . . . Copeland, N. G. (2001). A highly efficient Escherichia coli-based chromosome engineering system adapted for recombinogenic targeting and subcloning of BAC DNA. *Genomics, 73*(1), 56-65. doi: 10.1006/geno.2000.6451

Lee, S. H., Marchionni, I., Bezaire, M., Varga, C., Danielson, N., Lovett-Barron, M., . . . Soltesz, I. (2014). Parvalbumin-positive basket cells differentiate among hippocampal pyramidal cells. *Neuron, 82*(5), 1129-1144. doi: 10.1016/j.neuron.2014.03.034

Lein, E. S., Callaway, E. M., Albright, T. D., & Gage, F. H. (2005). Redefining the boundaries of the hippocampal CA2 subfield in the mouse using gene expression and 3-dimensional reconstruction. *J Comp Neurol, 485*(1), 1-10. doi: 10.1002/cne.20426

Leung, L. S. (1998). Generation of theta and gamma rhythms in the hippocampus. *Neurosci Biobehav Rev, 22*(2), 275-290.

Lorente de No, R. (1934). Studies of the Structure of the Cerebral Cortex II. Continuation of the Study of the Ammonic System. *Journal f. Psychologie und Neurologie*, 113-174.

Lu, L., Igarashi, K. M., Witter, M. P., Moser, E. I., & Moser, M. B. (2015). Topography of Place Maps along the CA3-to-CA2 Axis of the Hippocampus. *Neuron, 87*(5), 1078-1092. doi: 10.1016/j.neuron.2015.07.007

Madisen, L., Zwingman, T. A., Sunkin, S. M., Oh, S. W., Zariwala, H. A., Gu, H., . . . Zeng, H. (2010). A robust and high-throughput Cre reporting and characterization system for the whole mouse brain. *Nat Neurosci, 13*(1), 133-140. doi: 10.1038/nn.2467

Mankin, E. A., Diehl, G. W., Sparks, F. T., Leutgeb, S., & Leutgeb, J. K. (2015). Hippocampal CA2 activity patterns change over time to a larger extent than between spatial contexts. *Neuron, 85*(1), 190-201. doi: 10.1016/j.neuron.2014.12.001

Mercer, A., Eastlake, K., Trigg, H. L., & Thomson, A. M. (2012). Local circuitry involving parvalbumin-positive basket cells in the CA2 region of the hippocampus. *Hippocampus, 22*(1), 43-56. doi: 10.1002/hipo.20841

Mercer, A., Trigg, H. L., & Thomson, A. M. (2007). Characterization of neurons in the CA2 subfield of the adult rat hippocampus. *J Neurosci, 27*(27), 7329-7338. doi: 10.1523/jneurosci.1829-07.2007

Middleton, S. J., & McHugh, T. J. (2016). Silencing CA3 disrupts temporal coding in the CA1 ensemble. *Nat Neurosci, 19*(7), 945-951. doi: 10.1038/nn.4311

Mizuseki, K., Diba, K., Pastalkova, E., & Buzsaki, G. (2011). Hippocampal CA1 pyramidal cells form functionally distinct sublayers. *Nat Neurosci, 14*(9), 1174-1181. doi: 10.1038/nn.2894

Montgomery, S. M., & Buzsaki, G. (2007). Gamma oscillations dynamically couple hippocampal CA3 and CA1 regions during memory task performance. *Proc Natl Acad Sci U S A, 104*(36), 14495-14500. doi: 10.1073/pnas.0701826104

Muller, R. U., & Kubie, J. L. (1987). The effects of changes in the environment on the spatial firing of hippocampal complex-spike cells. *J Neurosci, 7*(7), 1951-1968.

Nakazawa, K., Quirk, M. C., Chitwood, R. A., Watanabe, M., Yeckel, M. F., Sun, L. D., . . . Tonegawa, S. (2002). Requirement for hippocampal CA3 NMDA receptors in associative memory recall. *Science, 297*(5579), 211-218. doi: 10.1126/science.1071795

O'Keefe, J. (1999). Do hippocampal pyramidal cells signal non-spatial as well as spatial information? *Hippocampus, 9*(4), 352-364. doi: 10.1002/(sici)1098-1063(1999)9:4<352::aid-hipo3>3.0.co;2-1

O'Keefe, J., Burgess, N., Donnett, J. G., Jeffery, K. J., & Maguire, E. A. (1998). Place cells, navigational accuracy, and the human hippocampus. *Philos Trans R Soc Lond B Biol Sci, 353*(1373), 1333-1340. doi: 10.1098/rstb.1998.0287

O'Keefe, J., & Dostrovsky, J. (1971). The hippocampus as a spatial map. Preliminary evidence from unit activity in the freely-moving rat. *Brain Res, 34*(1), 171-175.

O'Keefe, J., & Recce, M. L. (1993). Phase relationship between hippocampal place units and the EEG theta rhythm. *Hippocampus, 3*(3), 317-330. doi: 10.1002/hipo.450030307

Oliva, A., Fernandez-Ruiz, A., Buzsaki, G., & Berenyi, A. (2016). Role of Hippocampal CA2 Region in Triggering Sharp-Wave Ripples. *Neuron, 91*(6), 1342-1355. doi: 10.1016/j.neuron.2016.08.008

Pagani, J. H., Zhao, M., Cui, Z., Avram, S. K., Caruana, D. A., Dudek, S. M., & Young, W. S. (2015). Role of the vasopressin 1b receptor in rodent aggressive behavior and synaptic plasticity in hippocampal area CA2. *Mol Psychiatry, 20*(4), 490-499. doi: 10.1038/mp.2014.47

Redish, A. D. (2001). The hippocampal debate: are we asking the right questions? *Behav Brain Res, 127*(1-2), 81-98.

Roth, B. L. (2016). DREADDs for Neuroscientists. *Neuron, 89*(4), 683-694. doi: 10.1016/j.neuron.2016.01.040

Scheffer-Teixeira, R., Belchior, H., Caixeta, F. V., Souza, B. C., Ribeiro, S., & Tort, A. B. (2012). Theta phase modulates multiple layer-specific oscillations in the CA1 region. *Cereb Cortex, 22*(10), 2404-2414. doi: 10.1093/cercor/bhr319

Schomburg, E. W., Fernandez-Ruiz, A., Mizuseki, K., Berenyi, A., Anastassiou, C. A., Koch, C., & Buzsaki, G. (2014). Theta phase segregation of input-specific gamma patterns in entorhinal-hippocampal networks. *Neuron, 84*(2), 470-485. doi: 10.1016/j.neuron.2014.08.051

Scoville, W. B., & Milner, B. (1957). Loss of recent memory after bilateral hippocampal lesions. *J Neurol Neurosurg Psychiatry, 20*(1), 11-21.

Senior, T. J., Huxter, J. R., Allen, K., O'Neill, J., & Csicsvari, J. (2008). Gamma oscillatory firing reveals distinct populations of pyramidal cells in the CA1 region of the hippocampus. *J Neurosci, 28*(9), 2274-2286. doi: 10.1523/jneurosci.4669-07.2008

Sheehan, T. P., Chambers, R. A., & Russell, D. S. (2004). Regulation of affect by the lateral septum: implications for neuropsychiatry. *Brain Res Brain Res Rev, 46*(1), 71-117. doi: 10.1016/j.brainresrev.2004.04.009

Shinohara, Y., Hosoya, A., Yahagi, K., Ferecsko, A. S., Yaguchi, K., Sik, A., . . . Hirase, H. (2012). Hippocampal CA3 and CA2 have distinct bilateral innervation patterns to CA1 in rodents. *Eur J Neurosci, 35*(5), 702-710. doi: 10.1111/j.1460-9568.2012.07993.x

Shirvalkar, P. R., Rapp, P. R., & Shapiro, M. L. (2010). Bidirectional changes to hippocampal theta-gamma comodulation predict memory for recent spatial episodes. *Proc Natl Acad Sci U S A, 107*(15), 7054-7059. doi: 10.1073/pnas.0911184107

Skaggs, W. E., McNaughton, B. L., Wilson, M. A., & Barnes, C. A. (1996). Theta phase precession in hippocampal neuronal populations and the compression of temporal sequences. *Hippocampus, 6*(2), 149-172. doi: 10.1002/(SICI)1098-1063(1996)6:2<149::AID-HIPO6>3.0.CO;2-K

Smith, A. S., Williams Avram, S. K., Cymerblit-Sabba, A., Song, J., & Young, W. S. (2016). Targeted activation of the hippocampal CA2 area strongly enhances social memory. *Mol Psychiatry, 21*(8), 1137-1144. doi: 10.1038/mp.2015.189

Smith, D. M., & Mizumori, S. J. (2006). Hippocampal place cells, context, and episodic memory. *Hippocampus, 16*(9), 716-729. doi: 10.1002/hipo.20208

Squire, L. R. (1992). Declarative and nondeclarative memory: multiple brain systems supporting learning and memory. *J Cogn Neurosci, 4*(3), 232-243. doi: 10.1162/jocn.1992.4.3.232

Squire, L. R. (2004). Memory systems of the brain: a brief history and current perspective. *Neurobiol Learn Mem, 82*(3), 171-177. doi: 10.1016/j.nlm.2004.06.005

Stachniak, T. J., Ghosh, A., & Sternson, S. M. (2014). Chemogenetic synaptic silencing of neural circuits localizes a hypothalamus-->midbrain pathway for feeding behavior. *Neuron, 82*(4), 797-808. doi: 10.1016/j.neuron.2014.04.008

Stevenson, E. L., & Caldwell, H. K. (2012). The vasopressin 1b receptor and the neural regulation of social behavior. *Horm Behav, 61*(3), 277-282. doi: 10.1016/j.yhbeh.2011.11.009

Strange, B. A., Witter, M. P., Lein, E. S., & Moser, E. I. (2014). Functional organization of the hippocampal longitudinal axis. *Nat Rev Neurosci, 15*(10), 655-669. doi: 10.1038/nrn3785

Tamamaki, N., Abe, K., & Nojyo, Y. (1988). Three-dimensional analysis of the whole axonal arbors originating from single CA2 pyramidal neurons in the rat hippocampus with the aid of a computer graphic technique. *Brain Res, 452*(1-2), 255-272.

Tort, A. B., Komorowski, R. W., Manns, J. R., Kopell, N. J., & Eichenbaum, H. (2009). Theta-gamma coupling increases during the learning of item-context associations. *Proc Natl Acad Sci U S A, 106*(49), 20942-20947. doi: 10.1073/pnas.0911331106

Traub, R. D., Whittington, M. A., Stanford, I. M., & Jefferys, J. G. (1996). A mechanism for generation of long-range synchronous fast oscillations in the cortex. *Nature, 383*(6601), 621-624. doi: 10.1038/383621a0

Tulving, E. (1984). Precis of Elements of Epidsocid Memory. *The Behavioral and Brain Sciences, 7*, 223-268.

van Groen, T., Miettinen, P., & Kadish, I. (2003). The entorhinal cortex of the mouse: organization of the projection to the hippocampal formation. *Hippocampus, 13*(1), 133-149. doi: 10.1002/hipo.10037

Vanderwolf, C. H. (1969). Hippocampal electrical activity and voluntary movement in the rat. *Electroencephalogr Clin Neurophysiol, 26*(4), 407-418.

Wintzer, M. E., Boehringer, R., Polygalov, D., & McHugh, T. J. (2014). The hippocampal CA2 ensemble is sensitive to contextual change. *J Neurosci, 34*(8), 3056-3066. doi: 10.1523/jneurosci.2563-13.2014

Womelsdorf, T., Schoffelen, J. M., Oostenveld, R., Singer, W., Desimone, R., Engel, A. K., & Fries, P. (2007). Modulation of neuronal interactions through neuronal synchronization. *Science, 316*(5831), 1609-1612. doi: 10.1126/science.1139597

Yamamoto, A., Hen, R., & Dauer, W. T. (2001). The ons and offs of inducible transgenic technology: a review. *Neurobiol Dis, 8*(6), 923-932. doi: 10.1006/nbdi.2001.0452

Yamamoto, J., Suh, J., Takeuchi, D., & Tonegawa, S. (2014). Successful execution of working memory linked to synchronized high-frequency gamma oscillations. *Cell, 157*(4), 845-857. doi: 10.1016/j.cell.2014.04.009

Young, W. S., Li, J., Wersinger, S. R., & Palkovits, M. (2006). The vasopressin 1b receptor is prominent in the hippocampal area CA2 where it is unaffected by restraint stress or adrenalectomy. *Neuroscience, 143*(4), 1031-1039. doi: 10.1016/j.neuroscience.2006.08.040

Zhao, M., Choi, Y. S., Obrietan, K., & Dudek, S. M. (2007). Synaptic plasticity (and the lack thereof) in hippocampal CA2 neurons. *J Neurosci, 27*(44), 12025-12032. doi: 10.1523/jneurosci.4094-07.2007

Zheng, C., Bieri, K. W., Hwaun, E., & Colgin, L. L. (2016). Fast Gamma Rhythms in the Hippocampus Promote Encoding of Novel Object-Place Pairings. *eNeuro, 3*(2). doi: 10.1523/eneuro.0001-16.2016